Implied Impermanent Loss for Concentrated Liquidity*

L. Alberici,† A. Papanicolaou,‡ L. Schönleber§

20th March 2026

Abstract

Providing liquidity on decentralized exchanges earns fees but exposes liquidity providers (LPs) to impermanent loss from price movements. With concentrated liquidity, LPs control this risk by choosing how narrowly to deploy capital around the price. Using option prices, we quantify the cost of liquidity provision by developing measures of implied and realized impermanent loss for concentrated liquidity and define the associated impermanent loss risk premium. Empirically, higher expected impermanent loss widens liquidity ranges, while higher risk premia re-center liquidity around the spot price, highlighting opposing effects of risk and compensation.

Keywords: Decentralized Exchanges, Decentralized Finance, Impermanent Loss, Derivatives, Risk-Neutral Pricing, Risk Premium, Staking, Yield Farming.

JEL Classification Codes: G10, G11, G13, G20

*We received helpful comments and suggestions from XXX. We thank Mariia Aksenova for helping us access on-chain data. We also thank the participants of the ALGODEFI25, Seminars in Statistics at the Collegio Carlo Alberto, the Stanford Applied Math Seminar, the 2026 Joint Mathematics Meetings (JMM), and the Decentralized Finance & Crypto Workshop @ Scuola Normale Superiore.

†Bayes Business School, City St George's, University of London, Northampton Square, London, EC1V 0HB, United Kingdom. *luca-luigi.alberici@bayes.city.ac.uk*.

‡Department of Mathematics, North Carolina State University, 2311 Stinson Drive, Raleigh, North Carolina 27695, United States. *apapani@ncsu.edu*.

§Collegio Carlo Alberto and University of Turin, Piazza Vincenzo Arbarello 8, 10122 Turin, Italy. *lorenzo.schoenleber@carloalberto.org*.

Implied Impermanent Loss for Concentrated Liquidity

20th March 2026

Abstract

Providing liquidity on decentralized exchanges earns fees but exposes liquidity providers (LPs) to impermanent loss from price movements. With concentrated liquidity, LPs control this risk by choosing how narrowly to deploy capital around the price. Using option prices, we quantify the cost of liquidity provision by developing measures of implied and realized impermanent loss for concentrated liquidity and define the associated impermanent loss risk premium. Empirically, higher expected impermanent loss widens liquidity ranges, while higher risk premia re-center liquidity around the spot price, highlighting opposing effects of risk and compensation.

Keywords: Decentralized Exchanges, Decentralized Finance, Impermanent Loss, Derivatives, Risk-Neutral Pricing, Risk Premium, Staking, Yield Farming.

JEL: G10, G11, G13, G20

1 Introduction

In equity markets, selling volatility is risky but, on average, profitable. Investors who take the short side of variance—through options or variance swaps—earn a premium for bearing exposure to large price fluctuations. This compensation is summarized by the *variance risk premium (VRP)*, the wedge between option-implied and realized market variance (Bollerslev et al., 2009, Carr and Wu, 2009, Bekaert and Hoerova, 2014).

In this paper, we adapt the logic of variance risk premia to *decentralized finance (DeFi)*, where *liquidity providers (LPs)* on *decentralized exchanges (DEXs)* supply capital to automated market makers (AMMs) and earn fees from token exchanges. In Uniswap-style AMMs, providing liquidity exposes LPs to *impermanent loss*: when relative prices move, arbitrage trades rebalance the pool, leaving LPs with a less favorable token composition and a lower portfolio value than if they had simply held the underlying assets (Capponi and Jia, 2025; Harvey et al., 2024; Heimbach et al., 2022b; Milionis et al., 2024; Papanicolaou et al., 2025). This mechanism makes liquidity provision economically akin to holding a short position in relative price variance: fee income accrues when prices are stable, while large relative price movements generate losses that increase with volatility.

Our contribution is to bring this short-variance interpretation to *concentrated liquidity*, where LPs endogenously choose a finite price interval over which their capital is active. LPs directly control their exposure to impermanent loss by selecting how tightly to concentrate their liquidity around the prevailing price. Narrow ranges generate high fee intensity near the spot price but expose LPs to large losses when prices move out of range. Wider ranges reduce the likelihood and severity of impermanent loss by providing insurance against large price moves, at the cost of lower fee capture. Concentrated liquidity, therefore, transforms variance exposure into a *choice variable*: LPs actively trade off expected fee income against downside risk.

This trade-off motivates measuring both (i) the *level of impermanent loss risk* faced

by LPs and (ii) the *compensation* the market provides for bearing that risk. We construct an *implied impermanent loss* (IIL) measure for concentrated liquidity as the risk-neutral expectation of impermanent loss integrated over a given price band, and pair it with a realized counterpart (RIL) computed from spot data under the same band geometry. The *impermanent loss risk premium* (ILRP) is defined as the difference between implied and realized impermanent loss, capturing the ex-ante compensation associated with short-variance exposure in concentrated liquidity.

Empirically, distinguishing risk from risk compensation is essential for understanding LP behavior. Using daily pool-level liquidity distributions across price bands, we show that higher expected impermanent loss predicts a precautionary reallocation of liquidity from the innermost band to intermediate bands. This pattern is consistent with LPs widening their effective ranges when the likelihood or severity of adverse price movements increases. In contrast, higher compensation for bearing impermanent loss risk predicts a re-centering of liquidity toward the prevailing price, accompanied by a sharp reduction in liquidity allocated to the most distant tail bands. At the LP level, we further show that higher expected impermanent loss reduces the probability that liquidity positioned above or below the market price is moved into the active range, consistent with LPs becoming more cautious about activating liquidity near the spot price. These findings indicate that expected risk and risk premia have qualitatively different effects on liquidity allocation.

We confirm these pool-level patterns using a novel panel of LP actions reconstructed from on-chain mint and burn events. In forward-looking regressions at the LP–pool level, higher expected impermanent loss predicts subsequent moves away from the most concentrated liquidity configurations, while higher impermanent loss risk premia predict adjustments that concentrate liquidity closer to the prevailing price rather than widening ranges. We further show that higher expected impermanent loss reduces the probability that liquidity positioned above or below the market price is moved into the active range,

consistent with LPs managing risk by delaying liquidity activation near the spot price. Taken together, our results show that in concentrated liquidity markets, *risk widens liquidity provision and discourages activation near the spot, while risk premia re-center it.*

Our approach is closely related in spirit to the demand-based option pricing framework of Gârleanu et al. (2009), who show that option prices reflect compensation for unhedgeable variance risk borne by intermediaries. While their setting treats variance exposure as an exogenous feature of market structure, concentrated liquidity allows LPs to endogenously choose how much variance risk to supply by adjusting their range. This distinction highlights how decentralized market design transforms short-variance exposure from a passive consequence of intermediation into an active portfolio choice.

2 Concentrated Liquidity

This section formalizes impermanent loss in AMMs and highlights how the introduction of concentrated liquidity in Uniswap v3 alters the LP's exposure relative to the constant-product benchmark. We begin by briefly reviewing the v2 mechanism, where liquidity is provided over the full price support and portfolio rebalancing is entirely driven by the constant-product invariant. We then extend the discussion to v3, where LPs choose a finite active price interval, and the position's composition changes endogenously as the market price moves within the range. The key implication is that narrower ranges increase capital efficiency but also make LP payoffs more path- and direction-dependent, since positions can become fully invested in a single asset once the price leaves the chosen bounds. We use this framework to motivate our range parameterization, discuss directional (one-sided) allocations, and provide an illustrative example of impermanent loss under concentrated liquidity.

Impermanent Loss for v2

On a DEX, trades are executed against an automated market maker (AMM) that sets prices according to a constant product rule. For a pool with token inventories N_1 and N_2, liquidity is summarized by $L = \sqrt{N_1 N_2}$, which remains unchanged after each trade. Hence, whenever traders buy one asset from the pool, the AMM adjusts the price by changing the inventory ratio, decreasing one reserve as the other increases. Arbitrage ensures that, after external price changes, the pool is rebalanced until the on-chain price aligns with the market price. Impermanent loss arises because this endogenous rebalancing causes the LP's portfolio value to differ from the value of simply holding the initial token quantities.

To illustrate, suppose Token A trades at 100 USD and Token B is a USD stablecoin. The pool initially contains 900 Token A and 90,000 USDT. An LP with 100 Token A and 11,000 USDT adds 100 Token A and 10,000 USDT to the pool (keeping 1,000 USDT idle), obtaining a 10% share of a 200,000 USD pool. If the market price of Token A increases to 121 USD, arbitrage trades adjust the pool to approximately 909.1 Token A and 110,000 USDT. Withdrawing the LP's 10% share yields roughly 90.9 Token A and 11,000 USDT, worth about 22,000 USD at the new price; including the idle 1,000 USDT, the total portfolio value is approximately 23,000 USD. Under buy-and-hold, the LP would instead hold 100 Token A and 11,000 USDT, worth 23,100 USD. The difference, about 100 USD, is the impermanent loss.

2.1 Impermanent Loss for v3

2.1.1 Range Concentrations

We parameterize the LP's active price interval using a concentration parameter (α). The key idea is that a Uniswap v3 position provides liquidity only within its chosen

bounds, and its token composition changes endogenously as prices move inside this interval. As the relative price moves within its range, the LP's inventory is continuously rebalanced by arbitrage: when the relative price increases, the position gradually converts from the first asset in the pair to the second, whereas when the relative price decreases, the conversion occurs in the opposite direction. If the price leaves the interval, the position becomes fully invested in only one of the two assets and stops earning fees until the price re-enters the range. Hence, narrower (more concentrated) ranges amplify the mechanical rebalancing effect of the AMM and can lead to larger deviations from the value of simply holding the initial token quantities, especially when prices trend strongly in one direction or frequently cross the bounds. In Uniswap v3, price ranges are implemented on a discrete grid of *ticks*, so the chosen bounds are effectively rounded to the nearest admissible price levels. As a result, liquidity and fee accrual change discretely when the market price crosses tick boundaries, implying that outcomes may depend not only on the range width but also on how the interval aligns with the tick grid.

2.1.2 Up and Down Ranges

Consider a liquidity position with a one-sided liquidity range. If liquidity is provided only above the current price (an upward-only range), then at inception the position is predominantly held in the asset that will be sold as the price moves upward through the range. As the price rises, the AMM progressively converts the position into the other asset, and once the upper bound is reached, the position becomes fully invested in a single asset and remains inactive until the price re-enters the range. Relative to a hold benchmark that keeps the initial exposure constant, this structure can generate a large impermanent loss during sufficiently strong upward moves, because the benchmark continues to benefit from price appreciation while the LP's exposure effectively caps out after leaving the range. Conversely, downward price movements immediately push the

position out of range, leaving the LP fully invested in the initial asset; in this case, the deviation from the hold benchmark is smaller, and the impermanent loss tends to be comparatively muted. The opposite logic applies to a downward-only range, where the position starts out concentrated in the other asset: upward moves push the LP out of range, with limited rebalancing, while downward moves trigger progressive conversion across assets and can lead to larger losses than holding the initial portfolio.

2.1.3 Numerical Example

To illustrate impermanent loss in a concentrated liquidity setting, Consider an LP supplying liquidity to a Uniswap v3 pool with Token A and a USD stablecoin (USDT). Token A is initially priced at $S_0 = 100$ USD (with USDT as the stablecoin), and the LP supplies liquidity over the price range $[S_l, S_u] = [81, 121]$ USD. Define

$$p = \sqrt{S} = 10, \qquad a = \sqrt{S_l} = 9, \qquad b = \sqrt{S_u} = 11,$$

Assume the LP initially owns $x_0 = 100$ Token A worth 10,000 USD at the prevailing price $S_0 = 100$. The amount of USDT that can be paired with these tokens inside the Uniswap v3 position is determined endogenously by the liquidity constraint. For a position with liquidity L and price $S \in [S_l, S_u]$, the token balances are

$$x(S) = L\frac{b-p}{pb},$$
$$y(S) = L(p-a),$$

where $x(S)$ denotes Token A and $y(S)$ denotes USDT. Imposing that the position contains exactly $x_0 = 100$ Token A at S_0 yields

$$100 = L\frac{b-p_0}{p_0 \cdot b} = L\frac{11-10}{10 \cdot 11} = \frac{L}{110},$$

which implies $L = 11,000$. Hence, the corresponding USDT position at S_0 is therefore

$$y_0 = L(p - a) = 11,000 \times (10 - 9) = 11,000 \text{ USDT}.$$

Thus, the LP's total initial portfolio value is $V_0 = x_0 S_0 + y_0 = 100 \times 100 + 11,000 = 21,000$ USD. Now suppose that the market price of Token A increases from 100 USD to 121 USD. Once the price reaches the upper bound S_u, the position is entirely converted into USDT. The amount held inside the AMM is

$$y_{\text{pos}}(S_u) = L(b - a) = 11,000 \times (11 - 9) = 22,000. \text{ USDT}.$$

Since no Token A is present, the LP's total portfolio value at S_1 is $V_{\text{LP}}(S_1) = 0 \times 121 + 22,000$ USDT. Had the LP instead followed a buy-and-hold strategy, their portfolio at $S_1 = 121$ would consist of 100 Token A $\times 121 = 12,100$ USD, plus the initially held 11,000 USDT, yielding $V_{\text{hold}}(S_1) = 23,100$ USD. The impermanent loss is therefore $V_{\text{hold}}(S_1) - V_{\text{LP}}(S_1) = 23,100 - 22,000 = 1,100$ USD.

3 Mathematical Formulation for Impermanent Loss

We formulate the mathematical framework from the perspective of an LP. Considering a liquidity pool governed by a constant product AMM rule. We consider pools with *concentrated liquidity*, a concept that is introduced by Uniswap v3, enabling LPs to consolidate their pool liquidity within a defined range and earn fees when the spot price enters their specified *active zone*. For a detailed exploration of concentrated liquidity, refer to Heimbach et al. (2022a). We assume that the underlying token prices follow a stochastic volatility model. These assumptions allow us to characterize impermanent loss as a function of the variance of the relative price. Prior to presenting the mathem-

atical derivations, we provide an overview of DEX operations and a specific example of impermanent loss.

3.1 Tokens Prices Under the Constant Product Rule

Let $N_1(t)$ and $N_2(t)$ denote the amounts of two respective tokens that are paired for trading in a liquidity pool, hereafter referred to as the *pool*. The constant product rule for this pool is defined as follows:

$$L = \sqrt{N_1(t)\, N_2(t)}, \tag{3.1}$$

where $L > 0$ is a constant. The relative price of Token 1 in terms of Token 2 is

$$R(t) = \frac{N_2(t)}{N_1(t)} = \text{Token 2 per Token 1.}$$

Combining this relative price with the constant product rule (3.1), we can deduce the amount of each token in the pool,

$$N_1(t) = \frac{L}{\sqrt{R(t)}}, \qquad N_2(t) = L\sqrt{R(t)}.$$

We formalize the relationship between the relative price within a pool and external market prices with the following assumption.

Assumption 3.1. *The relative token price in a pool is equal to the ratio of the market prices of the tokens,*

$$R(t) = \frac{P_1(t)}{P_2(t)} = \frac{\textit{dollar per Token 1}}{\textit{dollar per Token 2}} = \textit{Token 2 per Token 1}, \tag{3.2}$$

where $P_i(t)$ for $i = 1,\ 2$ are the market prices of tokens outside of the pool.

The rationale for equation (3.2) is that if it were not true, then arbitrageurs would enter the pool and exploit the price discrepancy until this parity is restored, thereby ensuring the pool's ratio of $N_1(t)$ to $N_2(t)$ maintains a relative price equal to the relative price of the greater market external of the pool. This assumption is essentially the law of one price, which is a standard assumption in derivative pricing (Black and Scholes (1973)), but in practice, there can be temporary violations, as shown in Makarov and Schoar (2022) for cryptocurrencies or in Van Tassel (2020) for VIX derivatives.

We further assume that token prices evolve according to the following stochastic volatility model,

$$dP_i(t) = \mu_i P_i(t)\, dt + \sigma_i(t)\, P_i(t)\, dB_i(t), \quad i = 1,\ 2, \tag{3.3}$$

where $B_i(t)$ are two correlated standard Brownian motions (SBMs) defined on a filtered probability space $\left(\Omega,\ \mathcal{F},\ (\mathcal{F}_t)_{t\geqslant 0},\ \mathbb{P}\right)$, $dB_1(t)\, dB_2(t) = \rho dt$, $\rho \in [-1,\ 1]$ is the correlation between them, and $\sigma_i(t) > 0$ is the $\mathcal{F}_t$-adapted stochastic volatility process. We apply Itô's lemma to the ratio of $P_1(t)$ and $P_2(t)$ to get the stochastic differential equation (SDE) for the relative price $R(t)$,

$$dR(t) = d\left(\frac{P_1(t)}{P_2(t)}\right) = \mu_R(t)\, R(t)\, dt + \sigma_R(t)\, R(t)\, dB_R(t), \tag{3.4}$$

where the drift and variance terms are $\mu_R(t) = \mu_1 - \mu_2 + \sigma_2^2(t) - \rho\sigma_1(t)\,\sigma_2(t)$, $\sigma_R^2(t) = \sigma_1^2(t) - 2\rho\sigma_1(t)\,\sigma_2(t) + \sigma_2^2(t)$, respectively, and $dB_R(t) = \frac{\sigma_1(t)}{\sigma_R(t)} dB_1(t) - \frac{\sigma_2(t)}{\sigma_R(t)} dB_2(t)$ is a SBM under the physical probability measure $\mathbb{P}$.

3.2 Impermanent Loss

The impermanent loss (IL) is the difference between the value of a staked position and an equivalent un-staked position, relative to the value of the un-staked position. The

total IL over time interval $[0, t]$ is

$$IL_t = \int_0^t \frac{d(N_s^1 P_s^1 + N_s^2 P_s^2) - N_s^1 dP_s^1 - N_s^2 dP_s^2}{N_s^1 P_s^1 + N_s^2 P_s^2} \ . \tag{3.5}$$

Using Ito's lemma and a few other things, the total impermanent loss I_t in (3.5) has a differential that is equal to $-\frac{1}{8}$ times the variance of the relative price times the length of time increment,

$$dIL_t = -\frac{\sigma_R^2(t)}{8} dt, \tag{3.6}$$

where $\sigma_R(t) = \sqrt{\sigma_1^2(t) - 2\rho\sigma_1(t)\sigma_2(t) + \sigma_2^2(t)}$ is the volatility of the relative price R_t given by equation (3.4). From equation (3.6), it is clear that $dIL_t \leqslant 0$ for all $t \geqslant 0$.

Remark 3.1. *Equation* (3.6) *is the continuous-time equivalent to the definition of the impermanent loss given in Heimbach et al. (2022a).*

4 Model-Free Valuation

Equation (3.6) implies that a variance swap with a multiplier of one-eighth serves as an effective instrument for hedging impermanent loss. This swap is a theoretical instrument that we design for valuation, and therefore, we can choose terms such that the swap is settled in units of Token 2. Over the time interval $[0,\ T]$ the realized variance of $R\,(t)$ is $\int_0^T \sigma_R^2\,(t)\,dt$. Given that the USD price of Token 2 is $P_2\,(T)$, the USD value of the floating leg is defined as

$$\text{USD-value of swap's floating leg} = \frac{P_2\,(T)}{8} \int_0^T \sigma_R^2\,(t)\,dt. \tag{4.1}$$

In this section, we develop a methodology for valuing equation (4.1) using market

options data. This approach is model-free in the sense that it requires no parametric specifications for $\sigma_1(t)$ or $\sigma_2(t)$, assuming only their $\mathcal{F}_t$ measurability. We design this framework specifically to address the constraints of the current crypto-derivatives market, where traded options are restricted to calls and puts on the individual tokens, Token 1 and Token 2. Valuing equation (4.1) necessitates a joint risk-neutral distribution for $P_1(T)$ and $P_2(T)$, a quantity that is not directly observable since no options are traded on the relative price $R(T)$. Consequently, a central contribution of our methodology is the extraction of a joint density utilizing only the marginal distributions of $P_1(T)$ and $P_2(T)$. The remainder of this section proceeds as follows: Section 4.1 provides the valuation of equation (4.1), Section 4.3 details the computation of the joint density, and Section 4.4 demonstrates the utility of this approach for LP hedging.

4.1 Risk-Neutral Valuation

Let us consider a risk-neutral probability measure $\mathbb{Q}$ that is equivalent to the physical probability measure $\mathbb{P}$ used in Section 3. Under $\mathbb{Q}$, similar to equation (3.3), over a finite time interval $t \in [0,\, T]$, the SDEs for token prices become

$$dP_i(t) = rP_i(t)\,dt + \sigma_i(t)\,P_i(t)\,dB_i^Q(t), \quad i = 1,\, 2,$$

where $B_1^Q(t)$ and $B_2^Q(t)$ are $\mathcal{F}_t$-adapted SBMs under $\mathbb{Q}$ with correlation $dB_1^Q(t)\,dB_2^Q(t) = \rho dt$, and r denotes the risk-free interest rate. Henceforth, $\mathbb{E}^Q$ denotes the expectation operator under $\mathbb{Q}$.

Following standard variance swap decomposition (Carr and Madan (1998), Demeterfi et al. (1999), and Carr and Wu (2009)), IL can be expressed as the difference between a

total return component and a log contract,

$$\frac{1}{8}\int_0^T \sigma_R^2(t)\,dt = \frac{1}{4}\int_0^T \frac{dR(t)}{R(t)} - \frac{1}{4}\ln\left(\frac{R(T)}{R(0)}\right), \tag{4.2}$$

where $-\frac{1}{4}\ln\left(\frac{R(T)}{R(0)}\right)$ represents the log contract on the relative price, as discussed in Carr and Lee (2008).

4.1.1 USD Stablecoins

If $R(t)$ represented a USD-denominated token price, then the $\mathbb{Q}$-measure expectation of equation (4.2) would correspond to the standard valuation used in equity markets. For instance, if Token 2 is a USD stable coin, then $P_2(t) = P_2(0)$ and $R(t)$ follows a martingale process under $\mathbb{Q}$. Consequently, the expected return component vanishes, $\mathbb{E}^Q\left[\int_0^T \frac{dR(t)}{R(t)}\right] = 0$, and the IL valuation reduces to the expectation of the log contract. This value can be replicated utilizing a portfolio of European options on $R(T)$ through the model proposed by Carr and Madan (1998); or an equivalent log-contract valuation can be obtained utilizing the risk-neutral density formula of $R(T)$ derived from Breeden and Litzenberger (1978).

4.1.2 Pairs of Non-Stablcoins

For token pairs with neither being a stablecoin, the computation of a $\mathbb{Q}$-measure expectation of (4.2) does not have analytic tractability. The reason is that $e^{-rt}R(t)$ is not a martingale under $\mathbb{Q}$. Analogous to SDE (3.4), by applying Itô's lemma, the relative price $R(t)$ under the same risk-neutral measure has the following SDE:

$$dR(t) = \mu_R^Q(t)\,R(t)\,dt + \sigma_R(t)\,R(t)\,dB_R^Q(t), \tag{4.3}$$

where $\mu_R^Q(t) = \sigma_2^2(t) - \rho\sigma_1(t)\sigma_2(t)$, and $dB_R^Q(t) = \frac{\sigma_1(t)}{\sigma_R(t)}dB_1^Q(t) - \frac{\sigma_2(t)}{\sigma_R(t)}dB_2^Q(t)$ is an SBM under $\mathbb{Q}$. Equation (4.3) shows that $R(t)$ is not a martingale under $\mathbb{Q}$. From (4.3) we can see that $R(t)$ has risk-neutral drift $\mu_R^Q(t)$ that depends non-trivially on the volatility processes, which means that neglecting the valuation of $\int_0^T \frac{dR(t)}{R(t)}$ will lead to an erroneous valuation of IL.

This analytic intractability is the reason why we chose the variance swap to be settled in units of Token 2. For the floating leg shown in (4.1) the numéraire is $P_2(t)$. If we consider a Girsanov change-of-measure,

$$\left.\frac{d\widetilde{\mathbb{Q}}}{d\mathbb{Q}}\right|_T := \frac{P_2(T)}{e^{rT}P_2(0)}, \tag{4.4}$$

then $\widetilde{\mathbb{Q}}$ is a pricing measure under which $P_2(t)$ is the numéraire and $R(t)$ is a martingale. Moreover, under $\widetilde{\mathbb{Q}}$ the total return in equation (4.2) is zero, $\widetilde{\mathbb{E}}^Q\left[\int_0^T \frac{dR(t)}{R(t)}\right] = 0$ where $\widetilde{\mathbb{E}}^Q$ denotes expectation under $\widetilde{\mathbb{Q}}$. Using equation (3.6) to write $IL(T) = \frac{1}{8}\int_0^T \sigma_R^2(t)\,dt$, we have an equation for a valuation IL in terms of the $\widetilde{\mathbb{Q}}$-measure valuation of the log contract divided by the forward price of $P_2(T)$,

$$\widetilde{\mathbb{E}}^Q[IL(T)] = -\frac{\mathbb{E}^Q\left[P_2(T)\ln\left(\frac{R(T)}{R(0)}\right)\right]}{4e^{rT}P_2(0)}\,. \tag{4.5}$$

4.2 Implied Impermanent Loss for Uniswap v3

The valuation formula in (4.5) applies to the Uniswap V2 protocol, but many pools now operate under the Uniswap v3 protocol, where LPs allocate tokens within a specific price range. Consider the ticks $(r_i)_{i=1,2,\ldots,m}$ where $r_{i+1} = r_i \times 1.0001$, and let $C_i = [r_i,\ r_{i+1})$ denote the band. If $R(t) \in C_i$ then the LP earns a reward but is also exposed to impermanent loss, in particular, it can be shown that the v3 analog to equation (3.6)

is

$$dIL_i(t) = \frac{\sigma_R^2(t)\sqrt{R(t)}}{4\left(2\sqrt{R(t)} - \sqrt{r_i} - \frac{R(t)}{\sqrt{r_{i+1}}}\right)}\mathbf{1}_{\{R(t)\in C_i\}}dt.$$

This increment of impermanent loss can be derived using Itô's lemma as done in deriving equation (3.6). Integrating over time yields the total impermanent loss, which is equivalent to a corridor variance swap (Lee (2010a) and Lee (2010b)),

$$\begin{aligned}\widetilde{\mathbb{E}}^Q\left[IL_i(T)\right] &= \frac{1}{4}\widetilde{\mathbb{E}}^Q\left[\int_0^T \frac{\sigma_R^2(t)\sqrt{R(t)}}{2\sqrt{R(t)} - \sqrt{r_i} - \frac{R(t)}{\sqrt{r_{i+1}}}}\mathbf{1}_{\{R(t)\in C_i\}}(t)\,dt\right], \qquad (4.6)\\ &= \frac{1}{2}\int_{K\in C_i} \frac{\widetilde{\mathbb{E}}^Q\left[(K - R(T))^+\right]\mathbf{1}_{\{K<R(0)\}} + \widetilde{\mathbb{E}}^Q\left[(R(T) - K)^+\right]\mathbf{1}_{\{K\geqslant R(0)\}}}{\sqrt{K^3}\left(2\sqrt{K} - \sqrt{r_i} - \frac{K}{\sqrt{r_{i+1}}}\right)}dK.\end{aligned}$$

4.3 Optimal Joint Density

Centralized exchanges offer European options on individual tokens, such as BTC and ETH, which are cash-settled and have margins settled in their respective underlying. Using the risk-neutral density formula proposed in Breeden and Litzenberger (1978), options with a fixed maturity date and a continuum of strikes provide the risk-neutral distribution (RND) on the future states of the underlying token. For a token pair, the risk-neutral density formula provides the two marginal densities, and then a further step must be taken to estimate the dependency structure for their joint RND. This joint distribution is exactly what we would need to value the log contract in (4.5).

For $i = 1, 2$, let $Call_i(T,\ K)$ denote European call option prices of tokens on their prices $P_i(T)$ with maturity T and strike price of K. The marginal densities under $\mathbb{Q}$ are

$$f_i(T,\ K) = e^{rT}\frac{\partial^2}{\partial K^2}Call_i(T,\ K), \quad \text{for } i = 1,\ 2.$$

We assume that we are given the joint density under $\mathbb{P}$. Then we estimate the joint pricing kernel using an optimization objective based on arbitrage theory.

A suitable objective is to minimize the HJ upper bound, which states that the Sharpe ratio of a portfolio cannot exceed the standard deviation of any pricing kernel. This is expressed as

$$\sup_{\Pi:\mathrm{std}(\Pi)>0} \frac{\mathbb{E}\left[\Pi\right]}{\mathrm{std}\left(\Pi\right)} \leqslant \inf_{M\in\mathcal{M}(f_1,f_2)} \frac{\mathrm{std}\left(M\right)}{\mathbb{E}\left[M\right]} \tag{4.7}$$

where Π is the excess return on a portfolio, $\mathcal{M}\left(f_1,\ f_2\right)$ is the family of pricing kernels with marginal densities f_1 and f_2, $\mathbb{E}\left[M\right] = e^{-rT}$, and where $\mathrm{std}\left(\cdot\right)$ represents the standard deviation. The left-hand side of equation (4.7) represents a portfolio optimization, our primal problem, while the right-hand side represents an optimal pricing problem, our dual problem. If there are Π and M such that $\frac{\mathbb{E}[\Pi]}{\mathrm{std}(\Pi)} = \frac{\mathrm{std}(M)}{\mathbb{E}[M]}$, then there is no duality gap. Equation (4.7) is derived from the Cauchy-Schwartz inequality for the covariance, denoted by $\mathrm{cov}\left(\cdot\right)$, between Π and M, $\mathrm{cov}\left(\Pi,\ M\right) \geqslant -\mathrm{std}\left(\Pi\right)\mathrm{std}\left(M\right)$. The Cauchy-Schwartz is an equality if and only if Π is a (deterministic) scalar multiple of M. For complete markets, $\mathcal{M}\left(f_1,\ f_2\right)$ is a singleton set with a unique M that is replicated by a portfolio of Arrow-Debreu securities, and hence there is no duality gap. For incomplete markets, there is no duality gap if the optimal M is in the span of investible portfolios, which is, in general, not the case, but when the individual assets each have a complete set of options, then the pricing kernel can be replicated, and thus there is no duality gap.

For simplicity, let us work with probability densities. Denote with $p\left(x,\ y\right)$ the joint density for measure $\mathbb{P}$ and assume $p\left(x,\ y\right) > 0$ for almost everywhere $\left(x,\ y\right)$. Let $q\left(x,\ y\right)$ be a joint density for measure $\mathbb{Q}$ such that $M\left(x,\ y\right) = e^{-rT}\frac{q(x,\,y)}{p(x,\,y)}$ is a pricing kernel. Computing the HJ upper bound is a quadratic programming problem:

$$\begin{aligned}
\underset{q:q\sim p}{\text{minimize}} \quad & \int\int \left(\frac{q\left(x,\ y\right)}{p\left(x,\ y\right)}\right)^2 p\left(x,\ y\right) dxdy, \\
\text{subject to} \quad & \int q\left(x,\ y\right) dy = f_1\left(T,\ x\right), \\
& \int q\left(x,\ y\right) dx = f_2\left(T,\ y\right),
\end{aligned}$$

where $p\,(x,\ y)$ is the joint density under $\mathbb{P}$, and $q \sim p$ denotes the set of joint densities such that $q\,(x,\ y) > 0$ if and only if $p\,(x,\ y) > 0$ for all $(x,\ y)$. The existence and uniqueness of solutions of a Sharpe-optimal portfolio are proven in Guasoni and Mayerhofer (2020).

4.4 Hedging Losses with the Variance Swap

Although we do not aim to replicate or hedge LVR itself, analyzing LVR reveals why the $\widetilde{\mathbb{Q}}$-based valuation of impermanent loss is the natural object for the LP's risk management. To justify the choice of the variance-swap contract with floating-leg given by (4.1), we now show its usefulness for LPs. In line with Fukasawa et al. (2023) and Milionis et al. (2024), let us consider a valuation of the LP's loss-versus-rebalancing (LVR). LVR is essentially the numerator of (3.5). In terms of risk management, LVR is the USD value of losses to the LP, and therefore, it is sensible to hedge against it. In continuous time, the differential of LVR is (more detailed calculations are given in A.2)

$$dLVR(t) = \frac{1}{8} TVL(t)\sigma_R^2(t)dt\ ,$$

where $TVL(t)$ is the total value locked. For a constant product rule with parameter L it is easy to show that $TVL(t) = 2L\sqrt{P_1(t)P_2(t)}$, and then it follows that

$$\mathbb{E}^Q\left[LVR\,(T)\right] = -2L\left(\mathbb{E}^Q\sqrt{P_1\,(T)\,P_2\,(T)} - e^{rT}\sqrt{P_1\,(0)\,P_2\,(0)}\right)\ .$$

This is a useful formula because it shows that an LP can hedge losses by shorting a contract on the square root of the product of prices, for which a valuation can be computed using the joint density from Section 4.3. Using the change of measure defined in (4.4) we have $\mathbb{E}^Q\sqrt{P_1(T)P_2(T)} = e^{rT}P_2(0)\widetilde{\mathbb{E}}^Q\sqrt{R(T)} = e^{rT}P_2(0)\widetilde{\mathbb{E}}^Q e^{-\frac{1}{8}\int_0^T \sigma_R^2(t)dt}$, and then we

re-arrange the LVR valuation to obtain

$$\frac{\mathbb{E}^Q LVR(T)}{e^{rT} TVL(0)} = 1 - \widetilde{\mathbb{E}}^Q e^{-\frac{1}{8}\int_0^T \sigma_R^2(t)dt} < \frac{1}{8}\widetilde{\mathbb{E}}^Q \int_0^T \sigma_R^2(t)dt \ , \tag{4.8}$$

where we have used the inequality $1 - e^{-x} < x$ for $x > 0$. Equation (4.8) is important for two reasons. First, it shows us that the change of numéraire given by (4.4) appears if we consider a natural quantity such as LVR. In fact, the quantity $\frac{\mathbb{E}^Q LVR(T)}{e^{rT} TVL(0)}$ is in units of IL and is equal to the $\widetilde{\mathbb{Q}}$ measure's forward valuation of LP losses. In **?** it is discussion to show that estimated $\frac{\mathbb{E}^Q LVR(T)}{e^{rT} TVL(0)}$ is close to estimated $\widetilde{\mathbb{E}}^Q IL(T)$. Second, the inequality in (4.8) shows that the valuation of IL settled in units of $P_2(T)$ is higher than $\frac{\mathbb{E}^Q LVR(T)}{e^{rT} TVL(0)}$, indicating that an LP accounting for profit and loss in units of $P_2(T)$ does not underestimate IL.

5 Data Description and Empirical Measurements

This section provides a general description of data sources, the construction of the option-implied variables, and the variables for pools.

5.1 Option Data and Risk-Neutral Moments

Activity in cryptocurrency options markets has grown substantially in recent years. Since 2020, Bitcoin (BTC) options have dominated the market, with trading volumes consistently exceeding those of Ethereum (ETH). In both markets, Deribit has remained the leading exchange. After expanding through 2021, options activity declined in 2022 and rebounded strongly from 2023 onward. Options on other tokens, including Solana (SOL), Ripple (XRP), and Binance Coin (BNB), emerged only in 2024.[1]

[1]Figure I.1 plots monthly option volume on Deribit in notional U.S. dollars. Bitcoin (BTC) dominates throughout, with volume often above $100 billion and peaking above $150 billion in 2025, while Ethereum (ETH) remains a distant second at roughly 20˜30 billion in 2024–2025. Activity in Solana (SOL), Ripple

The options dataset is sourced from Amberdata[2], which provides hourly observations of implied volatility surfaces. These surfaces are constructed for standardized maturities of 7 and 30 days and span multiple levels of moneyness. The underlying quotes originate from Deribit, the leading marketplace for cryptocurrency options. Contracts traded on Deribit are cash-settled and denominated in the underlying cryptocurrency rather than U.S. dollars. For each maturity, the implied volatility surface includes five delta-based moneyness points for both call and put options.

Our analysis focuses on Uniswap v3 pools that actually exist and exhibit non-trivial liquidity. We study pools formed by pairs of major volatile tokens (BTC, ETH, BNB, SOL, XRP) as well as pools pairing each of these assets with a stablecoin. While other token combinations could in principle be constructed, such pools are not deployed or lack liquidity on Uniswap v3 and are therefore not included.

We examine two classes of liquidity pools. The first comprises pools formed by pairs of volatile cryptoassets. For the major tokens in our sample—BTC, ETH, BNB, SOL, and XRP—there are ten possible unordered pairs. Only four, however, appear as actively traded Uniswap v3 pools in our sample: BTC–ETH, ETH–SOL, ETH–XRP, and ETH–BNB. The remaining volatile–volatile combinations are excluded because they are either not deployed on Uniswap v3 or lack sufficient liquidity. The second class comprises pools that match a volatile token with a stablecoin, including BTC–USD, ETH–USD, and SOL–USD.

Table 5.1 reports the start and end dates of the implied-volatility options dataset for each volatile cryptocurrency token included in our analysis. BTC and ETH feature the longest data availability, spanning from April 5, 2019, to December 15, 2025. SOL and XRP were included in the sample only in mid-March 2024. Finally, BNB is observed

(XRP), and Binance Coin (BNB) options is much smaller, with SOL growing only from mid-2024, XRP remaining sporadic, and BNB the least active.

[2]https://www.amberdata.io/

from October 5, 2024, with data ending earlier on July 18, 2025. These coverage periods determine the effective sample window for constructing volatility-based measures and for analyzing pools involving the corresponding tokens.

Token	Start Date	End Date
BTC	2019-04-01	2025-12-16
ETH	2019-04-01	2025-12-16
XRP	2024-03-12	2025-12-16
SOL	2024-03-11	2025-12-16
BNB	2024-10-01	2025-07-18

Table 5.1: Sample Coverage of Options Data. This table reports the start and end dates of IV surfaces for each token included in the analysis.

5.1.1 Risk-Neutral Densities (RND)

The IV surface is used to compute the RND. Specifically, we interpolate IV across moneyness to obtain a smooth curve and apply a generalized version of the Breeden and Litzenberger (1978). Specifically, we extract the RND using

$$f_i\left(T,\ K;\ \theta\right) = e^{rT}\frac{\partial^2}{\partial K^2} Call_i\left(T,\ K,\ \widehat{\sigma}_i\left(T,\ K;\ \theta\right)\right), \quad \text{for } i = 1,\ 2,$$

where $\widehat{\sigma}_i(T, K; \theta)$ is the interpolated IV surface. Figlewski (2018) shows that improved estimation of the risk-neutral density is obtained by parametrically fitting the IV smile and then differentiating the option price. Hence, we first fit a quadratic polynomial to the IVs $\sigma(K)$ observed across different strike prices K, i.e., $\sigma(K) \approx aK^2 + bK + c$. We then compute the first and second derivatives of the fitted volatility curve, denoted by $\sigma'(K)$ and $\sigma''(K)$, respectively. Using this smoothed and differentiable representation, we evaluate IVs and their derivatives on a dense grid of strikes $\{k_i\}$. The RND at each grid

point k_i is then computed using the extended Breeden and Litzenberger (1978) formula:

$$p(k_i) = \frac{\partial^2 C(k_i)}{\partial K^2} + \text{Vega}(k_i) \cdot \sigma''(k_i) + \text{Volga}(k_i) \cdot (\sigma'(k_i))^2 + 2 \cdot \frac{\partial^2 C(k_i)}{\partial K \, \partial \sigma} \cdot \sigma'(k_i),$$

where the first term corresponds to the classical second derivative of the call price w.r.t strike, while the remaining terms correct for the slope and curvature of the IV-surface. Specifically, $\text{Vega}(k_i)$ is the option's sensitivity to volatility, $\text{Volga}(k_i)$ captures the curvature of this sensitivity, and $\frac{\partial^2 C(k_i)}{\partial K \, \partial \sigma}$ is the cross-partial derivative with respect to strike and volatility. These adjustments improve the robustness of the density estimate in the presence of a non-flat volatility smile. We extend the estimated density beyond the observed strike range by appending log-normal tails on both sides; Appendix D provides the construction details.

5.1.2 Liquidity Ranges

Let $P_{1,t}$ and $P_{2,t}$ denote the prices of tokens 1 and 2 at time t, and define the price ratio

$$S_t = \frac{P_{1,t}}{P_{2,t}}.$$

The price bounds $[S_{\ell,t}, S_{u,t}]$ are parameterized by a concentration parameter α. Specifically, we consider the following cases: i) For $\alpha \in (0, 1)$, we consider symmetric ranges

$$S_{\ell,t} = (1 - \alpha) S_{t-1}, \qquad S_{u,t} = (1 + \alpha) S_{t-1}.$$

To benchmark against directional allocations, we also consider: (ii) an upward-only range (up) with $S_{\ell,t} = S_{t-1}(1 - 0.01)$ and $S_{u,t} = (1 + 10)S_{t-1}$; (iii) a downward-only range (dn) with $S_{\ell,t} = S_{t-1}10^{-4}$ and $S_{u,t} = S_{t-1}(1 + 0.01)$.

5.1.3 Implied Impermanent Loss for Concentrated Liquidity

For each pool and maturity T, we compute an integrated measure of impermanent loss for Uniswap v3 pools across alternative liquidity ranges (5.1.2). The object of interest captures the implied impermanent loss associated with a given price band, conditional on the current price ratio and the risk-neutral distribution of future price movements.

For a given liquidity range $[S_\ell, S_u]$ and normalized liquidity $\tilde{L} = 1$, we discretize the admissible price support using n grid points, $K \in [S_\ell, S_u]$ and compute impermanent loss payoffs for deviations of the future price ratio R from each grid point. Specifically, the payoff at (K, S) is defined as

$$\Pi(K, S) = \mathbb{1}_{\{K<S_0\}} \max(K - S, 0) + \mathbb{1}_{\{K\geqslant S_0\}} \max(S - K, 0),$$

where the indicator determines whether liquidity is effectively positioned below or above the current price. Let $\tilde{q}(R)$ denote the estimated pricing kernel (or state-price density) of the future price ratio. For each grid point K, the impermanent loss price is computed as

$$\mathrm{IL}(K) = \frac{\int \Pi(K, S)\, \tilde{q}(S)\, dS}{K^{3/2}\left(2\sqrt{K} - \sqrt{S_\ell} - \frac{K}{\sqrt{S_u}}\right)},$$

where the denominator accounts for the Uniswap v3 liquidity geometry. Integrated impermanent loss over the range $[S_\ell, S_u]$ is then obtained by numerical integration,

$$\mathrm{IIL}^{\mathrm{v3}} = \frac{1}{T/365} \int_{S_\ell}^{S_u} \mathrm{IL}(K)\, dK.$$

If not stated otherwise, this variable will be called IIL. For the IIL of v2, we follow Papanicolaou et al. (2025), calculating equation (4.5).

Pool	Start date	End date	N
BTC-ETH	2019-04-05	2025-12-15	2396
ETH-SOL	2024-03-16	2025-12-15	640
ETH-XRP	2024-03-17	2025-12-15	639
ETH-BNB	2024-10-05	2025-07-18	278
BTC-USD	2019-04-01	2025-12-16	2450
ETH-USD	2019-04-01	2025-12-16	2450
SOL-USD	2024-03-13	2025-12-16	644

Table 5.2: Data Availability. Start and end dates of the sample period for each pool at a 7-day maturity, along with the corresponding number of daily observations (N).

5.2 Realized Data

5.2.1 Realized Impermanent Loss for Concentrated Liquidity

We obtain hourly spot data for each underlying from Amberdata. For each pool and each maturity T (in days), we compute a rolling measure of realized impermanent loss for Uniswap v3 pools (denoted as RIL^{v3}), which explicitly accounts for liquidity concentration within a finite price range (5.1.2).

For each hour t, we consider the price change from S_{t-1} to S_t and compute impermanent loss conditional on a liquidity range $[S_{\ell,t}, S_{u,t}]$. Liquidity is normalized to $\tilde{L} = 1$, so that impermanent loss depends only on relative prices and range boundaries. Given a range $[S_{\ell,t}, S_{u,t}]$, the instantaneous impermanent loss is computed as

$$\text{IL}_t = \text{IL}\Big(S_{t-1}, S_t, S_{\ell,t}, S_{u,t}, \tilde{L}\Big),$$

where $\text{IL}(\cdot)$ denotes the Uniswap v3 impermanent loss function as outlined in Heimbach et al. (2022a) or in Appendix C. We define realized impermanent loss at time t as $\text{RIL}_t^{\text{v3}} = -\text{IL}_t$ so that positive values correspond to losses borne by LPs.

For each maturity T, the realized impermanent loss is aggregated over a rolling window

of $T \cdot 24$ hourly observations using a rolling mean,

$$\mathrm{RIL}_t^{\mathrm{v3}}(T) = (24 \cdot 365) \cdot \frac{1}{(T \cdot 24)} \sum_{k=0}^{T \cdot 24 - 1} \mathrm{RIL}_{t-k}^{\mathrm{v3}},$$

where the window is evaluated using at least $T \cdot 24/2$ available observations. Finally, the measure is annualized. The resulting time series $\mathrm{RIL}_t^{\mathrm{v3},\alpha}(T)$ is computed for each pool, maturity, and liquidity concentration parameter α. The RIL for v2 is simply $1/8$ times the annualized variance of the relative price and is calculated following Appendix B.

5.2.2 Risk Premia

We calculate the (ex-ante) risk premium as the difference between the respective quantities under the risk-neutral (implied) and the real-world (realized) probability measures. The impermanent loss risk premia ($ILRP$) is defined as $ILRP := IIL - RIL$.

5.3 Liquidity Pool Data

We analyze daily data from Uniswap v3, the third version of the Uniswap DEX. We source the data through The Graph, which provides access to Ethereum blockchain data via GraphQL. We restrict the analysis to the relevant pool counterparts in our sample and exclude pools with average TVL below 10k or fewer than 50 daily observations. The final sample comprises 30 pools, reported in Table 5.3.

To characterize pool conditions, we retrieve daily pool-level snapshots (*poolDayDatas*) from the subgraph. These snapshots report total value locked in USD (*tvlUSD*), trading volume in USD (*volumeUSD*), fees in USD (*feesUSD*), aggregate liquidity, the active tick, and token USD prices (*token0_priceUSD*, *token1_priceUSD*). Token decimal precision (d_0, d_1) is reported directly and used to convert tick indices into prices.

Pool Name	Token 1	Token 2	Fee Tier (%)	Avg TVL (Mio USD)	Start	End
Volatile-Volatile Pools						
WBTC-WETH-0.01	BTC	ETH	0.01	0.65	2021-11-21	2026-01-15
WBTC-WETH-0.05	BTC	ETH	0.05	106.82	2021-05-05	2026-01-15
WBTC-WETH-0.30	BTC	ETH	0.30	293.34	2021-05-04	2026-01-15
WBTC-WETH-1.00	BTC	ETH	1.00	4.57	2021-05-05	2026-01-15
WETH-SOL-0.30	ETH	SOL	0.30	8.59	2021-11-10	2026-01-15
WXRP-WETH-1.00	XRP	ETH	1.00	0.10	2022-09-23	2026-01-15
BNB-WETH-0.30	BNB	ETH	0.30	0.03	2021-06-02	2026-01-12
BNB-WETH-1.00	BNB	ETH	1.00	0.36	2021-06-25	2026-01-14
WBNB-WETH-0.30	BNB	ETH	0.30	0.06	2021-11-18	2025-07-21
WBNB-WETH-1.00	BNB	ETH	1.00	0.05	2023-07-30	2026-01-15
Volatile-Stablecoin Pools						
WBTC-USDC-0.05	BTC	USDC	0.05	7.25	2021-06-03	2026-01-15
WBTC-USDC-0.30	BTC	USDC	0.30	113.58	2021-05-05	2026-01-15
WBTC-USDC-1.00	BTC	USDC	1.00	3.02	2021-06-09	2026-01-12
WBTC-USDT-0.01	BTC	USDT	0.01	0.03	2024-08-28	2026-01-15
WBTC-USDT-0.05	BTC	USDT	0.05	11.28	2021-06-09	2026-01-15
WBTC-USDT-0.30	BTC	USDT	0.30	33.61	2021-05-05	2026-01-15
WBTC-DAI-0.30	BTC	DAI	0.30	1.42	2021-05-05	2025-11-07
WBTC-DAI-1.00	BTC	DAI	1.00	0.15	2021-06-10	2025-04-28
WETH-USDT-0.01	ETH	USDT	0.01	9.65	2022-12-26	2026-01-15
WETH-USDT-0.05	ETH	USDT	0.05	66.87	2021-05-05	2026-01-15
WETH-USDT-0.30	ETH	USDT	0.30	178.32	2021-05-05	2026-01-15
WETH-USDT-1.00	ETH	USDT	1.00	6.39	2021-05-05	2026-01-16
USDC-WETH-0.01	USDC	ETH	0.01	5.18	2021-11-14	2026-01-15
USDC-WETH-0.05	USDC	ETH	0.05	344.59	2021-05-05	2026-01-15
USDC-WETH-0.30	USDC	ETH	0.30	327.24	2021-05-04	2026-01-15
USDC-WETH-1.00	USDC	ETH	1.00	14.59	2021-05-04	2026-01-14
DAI-WETH-0.05	DAI	ETH	0.05	19.59	2021-05-05	2026-01-16
DAI-WETH-0.30	DAI	ETH	0.30	57.65	2021-05-04	2026-01-16
DAI-WETH-1.00	DAI	ETH	1.00	0.58	2021-05-05	2026-01-16
SOL-USDT-0.30	SOL	USDT	0.30	0.06	2025-07-08	2025-12-30

Table 5.3: Uniswap Pools Considered. Uniswap V3 pools included in the analysis, grouped by volatile–volatile and volatile–stablecoin pairs. For each pool, we report the tokens (Token 1 and Token 2), the fee tier (in percentage), the average TVL (in million USD), and the sample start and end dates.

5.4 Uniswap Quantities

5.4.1 Tick-to-price mapping and tick intervals.

Let $\mathcal{T}_{p,t} = \{\tau_1 < \tau_2 < \cdots < \tau_{N_{p,t}}\} \subset \mathbb{Z}$ denote the ordered set of initialized ticks observed for pool p on day t. Given token decimals (d_0, d_1), we map each tick to the

decimal-adjusted price of token 0 in units of token 1 using the Uniswap v3 convention,

$$P_{01}(\tau) \;=\; \frac{1}{1.0001^{\tau}} \times 10^{-(d_0-d_1)}.$$

Consecutive initialized ticks define price intervals

$$I_{p,k,t} = [\tau_k, \tau_{k+1}), \qquad k = 1, \ldots, N_{p,t} - 1,$$

with associated price bounds $\big(P_{01}(\tau_k), P_{01}(\tau_{k+1})\big)$.

5.5 Tick-Level Liquidity and Band Construction

Our tick-level inputs are obtained from the Uniswap v3 subgraph. For each pool p, day t, and initialized tick τ, the endpoint reports the tick index τ (*tickIdx*), the gross liquidity associated with that tick (*liquidityGross*), and the net liquidity change at that tick (*liquidityNet*). The net change *liquidityNet* is the fundamental primitive governing liquidity activation: it represents the signed change in active liquidity when the pool price crosses tick τ.

At the pool-day level, the endpoint provides the active tick $\tau^*_{p,t}$, which identifies the tick corresponding to the prevailing pool price, and the pool's reported in-range liquidity $L^{\text{pool}}_{p,t}$ (*liquidity*), defined as the total liquidity currently active at the prevailing price.

5.5.1 Reconstructing active interval liquidity.

The Uniswap v3 subgraph does not report active liquidity directly at each price level. Instead, because liquidity is range-based, active liquidity changes discretely as the pool price crosses interval boundaries. Accordingly, the subgraph reports liquidity as *changes* at initialized ticks rather than as levels at each price

Specifically, for each initialized tick τ_k, the endpoint reports *liquidityNet*, denoted

$\Delta L_{p,t}(\tau_k)$. This variable measures the net change in active liquidity when the pool price crosses tick τ_k: positive values indicate that liquidity becomes active above τ_k, while negative values indicate that liquidity becomes inactive below τ_k. Thus, $\Delta L_{p,t}(\tau_k)$ is a flow variable and does not directly reveal the level of active liquidity at a given price.

To recover active liquidity as a function of price, we aggregate net liquidity changes across ticks. As price moves upward along the tick grid, active liquidity equals the cumulative sum of the changes encountered so far, which yields the cumulative net liquidity profile

$$C_{p,t}(\tau_k) = \sum_{j=1}^{k} \Delta L_{p,t}(\tau_j),$$

defined up to an additive constant.

We resolve this indeterminacy using the prevailing pool state. For each pool-day, the subgraph reports the active tick $\tau^*_{p,t}$ and the corresponding in-range liquidity $L^{\text{pool}}_{p,t}$. These provide an anchor for the cumulative profile. Specifically, we shift the cumulative net liquidity profile so that liquidity at the active tick matches the reported pool liquidity:

$$L_{p,t}(\tau_k) = C_{p,t}(\tau_k) - C_{p,t}(\tau^*_{p,t}) + L^{\text{pool}}_{p,t}.$$

Finally, because Uniswap v3 liquidity is constant between initialized ticks and changes only at tick boundaries, liquidity is defined over tick intervals rather than individual prices. Accordingly, the liquidity associated with interval $[\tau_k, \tau_{k+1})$ is given by the anchored level at τ_k. We use this interval-level measure to aggregate liquidity into price bands and construct the distribution measures used in the empirical analysis.

To illustrate the reconstruction of active liquidity from net liquidity changes, consider three initialized ticks, $\tau_1 < \tau_2 < \tau_3$, with reported net changes of $+50$, -20, and $+10$, respectively. These values describe how active liquidity changes when the price crosses each tick, but not the level of liquidity itself. Cumulative aggregation yields a profile of

50 at τ_1, 30 at τ_2, and 40 at τ_3, which identifies the shape of liquidity up to an additive constant. If the prevailing price lies in the interval starting at τ_2 and reported in-range liquidity is 100, we anchor the profile at τ_2. The implied liquidity levels are then 120 at τ_1, 100 at τ_2, and 110 at τ_3.

5.5.2 From tick intervals to price bands.

We aggregate interval-level liquidity into nested price bands indexed by α (Section 5.1.2), which capture distance from the prevailing pool price. Each interval $I_{p,k,t}$ is assigned to a band based on the overlap between its price support and the band. Let $\mathcal{K}_{p,t}(\alpha)$ denote the set of intervals contributing to band α. Liquidity inside the band α is then given by

$$L^{\text{inside}}_{p,\alpha,t} \equiv \sum_{k \in \mathcal{K}_{p,t}(\alpha)} L_{p,k,t},$$

which is weakly increasing in α because the bands are nested.

5.5.3 Liquidity measures and their visualization

We summarize the cross-price distribution of active liquidity using two complementary band-level measures: cumulative liquidity within a price band and incremental liquidity across successive price annuli.

Cumulative inside liquidity. For each pool p, day t, and band α, let $L^{\text{inside}}_{p,\alpha,t}$ denote total active liquidity within the band centered at the prevailing price. Because bands are nested, $L^{\text{inside}}_{p,\alpha,t}$ is weakly increasing in α and measures the liquidity available within $\pm\alpha$ of the current pool price.

Incremental (ring) liquidity. Cumulative inside liquidity captures the amount of liquidity available up to a given distance from the spot price, but not its marginal placement

across distances. To isolate this margin, we define *incremental ring liquidity* as the additional liquidity included when the band expands from α_{j-1} to α_j. Let $\{\alpha_1 < \cdots < \alpha_J\}$ denote the ordered set of finite bands. Ring liquidity is then

$$L^{\text{ring}}_{p,\alpha_j,t} = L^{\text{inside}}_{p,\alpha_j,t} - L^{\text{inside}}_{p,\alpha_{j-1},t},$$

which measures the liquidity in the annulus centered at the prevailing price, with a distance α_j.

Outside liquidity. We also construct a complementary measure of liquidity outside a given price band. Let total finite-band liquidity be

$$L^{\text{total}}_{p,t} \equiv \max_{\alpha} L^{\text{inside}}_{p,\alpha,t}.$$

Outside liquidity for band α is then

$$L^{\text{outside}}_{p,\alpha,t} = L^{\text{total}}_{p,t} - L^{\text{inside}}_{p,\alpha,t}.$$

This measure captures the liquidity that would become inactive if the pool price moved outside the $\pm\alpha$ range. While ring liquidity describes how liquidity is allocated across successive bands, outside liquidity provides a complementary measure of concentration by showing how much liquidity remains beyond a given band.

Share-based measures. To abstract from pool size, we use normalized versions of these liquidity measures. The ring share,

$$L^{\text{ring\%}}_{p,\alpha,t} = 100 \times \frac{L^{\text{ring}}_{p,\alpha,t}}{L^{\text{total}}_{p,t}},$$

measures the share of total liquidity allocated to the annulus at distance α. Similarly, the inside share,

$$L_{p,\alpha,t}^{\text{inside\%}} = 100 \times \frac{L_{p,\alpha,t}^{\text{inside}}}{L_{p,t}^{\text{total}}},$$

measures the cumulative share of liquidity within $\pm\alpha$ of the prevailing price. Thus, $L^{\text{ring\%}}$ captures marginal allocation across bands, while $L^{\text{inside\%}}$ summarizes overall concentration around the spot price.

5.5.4 Visualization of the tick-implied liquidity profile

Figure 5.1 illustrates the distribution of active liquidity across price bands α for the USDC–WETH 0.3 pool on January 14, 2025. Panel A plots incremental ring liquidity, L_{α}^{ring}, Panel B outside liquidity, $L_{\alpha}^{\text{outside}}$, Panel C ring liquidity shares, $L_{\alpha}^{\text{ring\%}}$, and Panel D cumulative inside liquidity shares, $L_{\alpha}^{\text{inside\%}}$. The figure shows that liquidity is concentrated near the prevailing price, although a nontrivial share remains distributed over wider price ranges.

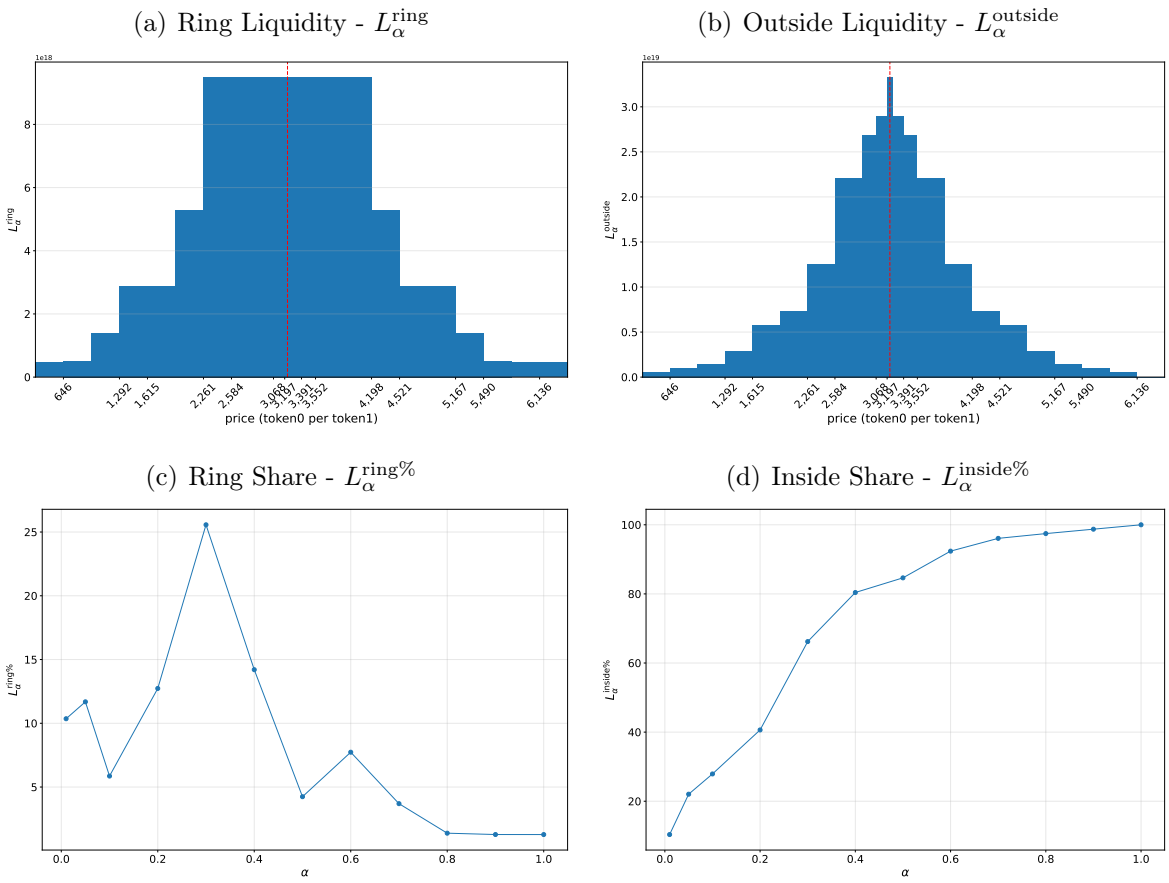

Figure 5.1: Liquidity Distribution Across Price Bands: USDC–WETH (0.3%) Pool on 2025–01–14. The figure visualizes the distribution of liquidity across price bands indexed by ticks or α. Panel (a) plots incremental ring liquidity L_α^{ring}, capturing liquidity added as bands expand. Panel (b) shows outside liquidity $L_\alpha^{\text{outside}}$, measuring liquidity remaining outside each band. The vertical dashed line displays the relative price of the tokens. Panel (c) reports ring liquidity shares $L_\alpha^{\text{ring\%}}$, which normalize incremental liquidity by total band liquidity. Panel (d) plots cumulative inside liquidity shares $L_\alpha^{\text{inside\%}}$, indicating the fraction of liquidity contained within each band.

5.6 Construction of Liquidity Provider Actions

Our unit of observation is an LP action at the pool–range–time level. For each pool, we recover the full on-chain history of liquidity events, including mints, which create or expand positions within a tick range, and burns, which partially or fully withdraw liquidity from a range. Event records include the timestamp, transaction identifiers, initiating address, liquidity and token amounts, tick bounds, and transaction-level gas usage. We use the externally owned account initiating the transaction (the *origin* address) as our baseline measure of LP identity, as it most closely captures the underlying decision-maker.

The final dataset is a pool–LP–event panel with one observation per LP action. Each record includes liquidity before and after the action, range-switch indicators, alpha-band classifications, pool conditions, and transaction costs. This structure supports high-frequency analysis of liquidity provision, rebalancing, and trading costs in concentrated liquidity markets.

5.6.1 Construction of LP action timelines

We reconstruct LP position states directly from transaction logs. For each pool, LP, and tick range (r), we define the signed liquidity change

$$\Delta L_{it} = \begin{cases} +\text{amount}_{it}, & \text{if event } i \text{ is a mint,} \\ -\text{amount}_{it}, & \text{if event } i \text{ is a burn,} \end{cases}$$

We then compute the running liquidity balance

$$L_{it}^{after} = \sum_{\tau \leqslant t} \Delta L_{i\tau}, \qquad L_{it}^{before} = L_{it}^{after} - \Delta L_{it},$$

separately for each $(pool, LP, tickLower, tickUpper)$ combination.

Because multiple events can occur within the same block, we impose a deterministic ordering of events based on event timestamp, transaction identifier, log index, and event identifier. This ensures correct liquidity accounting even when multiple actions share the same block timestamp.

5.6.2 Classification of LP actions

Using liquidity balances before and after each event, we classify LP actions into economically meaningful categories. We define an *opened range* as a mint that raises liquidity from zero to a positive level, and a *closed range* as a burn that reduces liquidity from a positive level to zero. Mint events that increase liquidity in an already active range are classified as *added liquidity*, while burn events that reduce liquidity without closing the position are classified as *removed liquidity*.

5.6.3 Range switches and Alpha-band classification

To capture active liquidity rebalancing, we define a *range switch* indicator. For a given pool and LP, a range switch occurs when an LP closes one range and opens another within a short window (one day in the baseline specification). We further classify switches by comparing the widths of the closing and opening ranges, defined as $tickUpper - tickLower$, as widening, narrowing, or unchanged. Finally, we classify each LP position by the concentration of its price range around the prevailing pool price (Section 5.1.2).

6 Empirical Analysis

This empirical analysis studies impermanent loss and liquidity provision in Uniswap v3 pools, focusing on volatile–volatile (e.g., BTC–ETH) and volatile–stablecoin (e.g., BTC–USD) pairs at a 7-day maturity. We document the time-series properties and

summary statistics of IIL, RIL, and the $ILRP$ across different concentration parameters and range designs, showing that tighter liquidity ranges produce higher and more volatile losses and risk premia, while wider ranges and the v2 benchmark are more stable. We then examine how these risk measures affect liquidity allocation across price bands and at the LP level. Higher expected impermanent loss induces precautionary widening away from the innermost bands, whereas higher risk premia lead LPs to re-center liquidity closer to the spot price. Overall, expected losses and risk compensation have distinct effects on liquidity concentration in concentrated AMMs.

6.1 Implied Impermanent Loss for v3

6.1.1 Volatile-Volatile Pools - Summary Statistics

Figure 6.1 Panel (a) plots the IIL for the BTC–ETH pool at a 7-day maturity across concentration parameters α. IIL displays strong time variation, with spikes concentrated in high-volatility periods. More concentrated liquidity (smaller α) generates higher and more volatile IIL, while wider ranges dampen both its level and variability. The v2 benchmark consistently lies below the v3 curves, highlighting the increase in impermanent loss caused by concentrated liquidity. After the 2021 peak, IIL declined and has remained relatively stable. Panel (b) compares asymmetric ranges and shows that the upward-only strategy yields substantially higher IIL than the downward-only and v2 benchmarks, particularly during sustained increases in the BTC–ETH price ratio, reflecting more continuous rebalancing during upward price movements.

Figure 6.1 Panel (c) reports RIL for the BTC–ETH pool at a 7-day maturity across range specifications. RIL closely mirrors IIL, with pronounced spikes during high-volatility periods, especially in 2020–2021. More concentrated liquidity (smaller α) leads to higher and more volatile realized losses, while wider ranges dampen both. Panel (d) shows that the upward-only strategy produces consistently higher RIL than the

downward-only and v2 benchmarks, which exhibit similar dynamics over time.

Figure 6.1 Panels (e) and (f) report the $ILRP$, defined as the difference between IIL and RIL, for the BTC–ETH pool at a 7-day maturity across different liquidity range specifications. Panel (e) shows that concentrated liquidity positions (smaller values of α) are associated with higher, more volatile risk premia, whereas wider ranges produce smaller, more stable differentials. Panel (f) compares asymmetric range designs and shows that the upward-only strategy has a markedly larger $ILRP$ than both the downward-only and v2 benchmarks, whereas the latter two exhibit comparatively muted and stable premia over time.

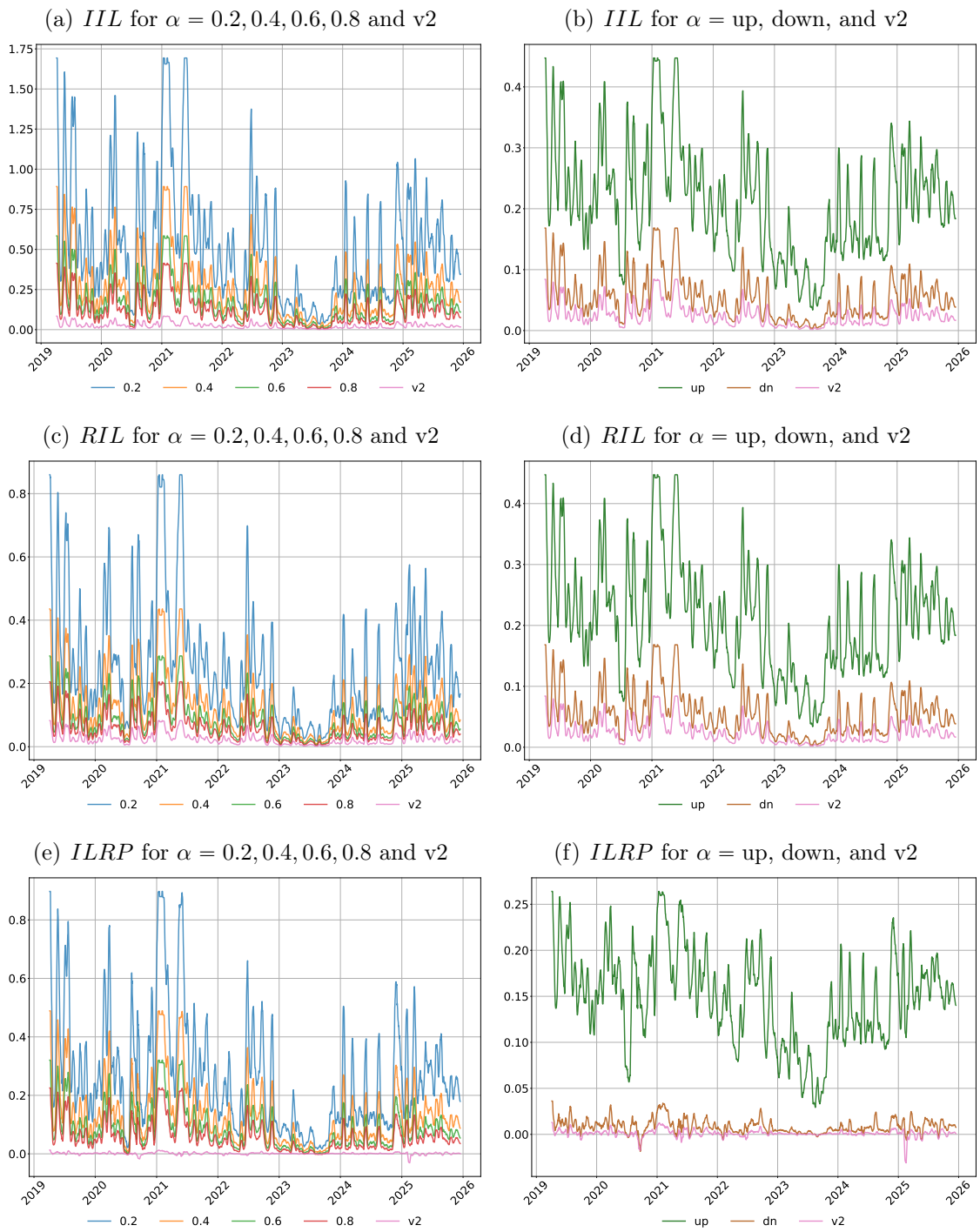

Figure 6.1: IIL, RIL, $ILRP$ **for BTC-ETH across Ranges.** The figure reports (top row) the implied impermanent loss IIL^{v3}, (middle row) the realized impermanent loss RIL^{v3}, and (bottom row) the impermanent loss risk premium $ILRP^{v3}$ for the BTC-ETH pool at a 7-day maturity. The left column shows $\alpha = 0.2, 0.4, 0.6, 0.8$ and the v2 benchmark, while the right column compares the up, down, and v2 ranges. The data are sampled daily over April 2019–December 2025 and smoothed using a 14-day rolling mean.

Table 6.1 reports summary statistics for IIL, RIL, and $ILRP$ for the BTC–ETH pool at a 7-day maturity across liquidity range specifications. Both IIL and RIL decline as liquidity ranges widen (higher α), while more concentrated positions exhibit higher average losses and greater dispersion. The v2 benchmark shows substantially lower means and volatilities for both IIL and RIL. The $ILRP$ is positive on average, largest for tightly concentrated liquidity, and decreases steadily with wider ranges, though it occasionally turns negative in the lower tail of the distribution.

Series	α	Mean	Std	Q(0.001)	Q1	Median	Q3	Q(0.999)	N	Maturity
IIL	0.2	0.57	0.62	0.03	0.21	0.38	0.67	5.30	2396	7
IIL	0.4	0.29	0.35	0.01	0.10	0.19	0.34	3.29	2396	7
IIL	0.6	0.19	0.23	0.00	0.06	0.12	0.22	2.24	2396	7
IIL	0.8	0.13	0.17	0.00	0.04	0.08	0.15	1.61	2396	7
IIL	up	0.22	0.13	0.03	0.14	0.20	0.27	1.06	2396	7
IIL	dn	0.06	0.06	0.00	0.02	0.04	0.07	0.50	2396	7
IIL	v2	0.03	0.03	0.00	0.01	0.02	0.03	0.31	2396	7
RIL	0.2	0.27	0.29	0.01	0.10	0.18	0.32	2.47	2396	7
RIL	0.4	0.14	0.15	0.01	0.05	0.09	0.16	1.25	2396	7
RIL	0.6	0.09	0.10	0.00	0.03	0.06	0.11	0.82	2396	7
RIL	0.8	0.06	0.07	0.00	0.02	0.04	0.08	0.59	2396	7
RIL	up	0.07	0.07	0.00	0.03	0.05	0.08	0.55	2396	7
RIL	dn	0.05	0.05	0.00	0.02	0.03	0.06	0.41	2396	7
RIL	v2	0.03	0.03	0.00	0.01	0.02	0.03	0.23	2396	7
ILRP	0.2	0.30	0.34	-0.01	0.11	0.20	0.34	2.97	2396	7
ILRP	0.4	0.16	0.21	-0.00	0.05	0.10	0.17	2.10	2396	7
ILRP	0.6	0.10	0.14	-0.00	0.03	0.06	0.11	1.46	2396	7
ILRP	0.8	0.07	0.10	-0.01	0.02	0.04	0.08	1.06	2396	7
ILRP	up	0.15	0.07	0.02	0.11	0.15	0.19	0.66	2396	7
ILRP	dn	0.01	0.02	-0.05	0.00	0.01	0.01	0.15	2396	7
ILRP	v2	0.00	0.01	-0.06	-0.00	0.00	0.00	0.11	2396	7

Table 6.1: Summary Statistics. IIL, RIL, $ILRP$ for BTC-ETH across Ranges. The table presents the summary statistics for the implied impermanent loss, IIL^{v3}, the realized impermanent loss RIL^{v3}, and the impermanent loss risk premium $ILRP^{v3}$, for the BTC–ETH pool at a 7-day maturity under different concentration parameters α $(0.2, 0.4, 0.6, 0.8$, the up, down, and v2 benchmark). The implied quantities are computed using the equations in Section 5.1.3. The realized quantities are computed using the equations in Section 5.2.1. The data are sampled daily over the period from April 2019 to December 2025.

6.1.2 Volatile-Stablecoin Pools - Summary Statistics

Table 6.2 reports summary statistics for IIL, RIL, and $ILRP$ at a 7-day maturity across liquidity range specifications. For both IIL and RIL, average losses and dispersion are highest for tightly concentrated liquidity ($\alpha = 0.2$) and decline monotonically as ranges widen (α increases to 0.8). Directional cases show asymmetry: the "up" scenario exhibits substantially higher mean IIL and $ILRP$ than the "dn" scenario, while RIL is closer across the two but remains slightly larger in "up". The v2 benchmark features markedly smaller means and volatilities for IIL and RIL, consistent with lower tail risk. The $ILRP$ is positive on average for all concentrated and directional specifications and decreases steadily with wider ranges; however, it displays sizable downside tail realizations (negative $Q(0.001)$) across all α settings and remains near zero for v2, indicating that improvements in average performance can coexist with occasional large adverse outcomes.

Figure 6.2 compares the evolution of the yearly average $IIL^{0.6}$ at a 7-day maturity across different liquidity pools.

Panel (a) reports results for Vola–Stable pools (quoted against USD). The $IIL^{0.6}$ is consistently highest for ETH–USD over most years, peaking around 2021, and then declining substantially in 2023. BTC–USD exhibits a similar pattern but at a lower level. SOL–USD appears only in the later period and shows a relatively high average $IIL^{0.6}$ in 2024–2025, exceeding BTC–USD and approaching ETH–USD in 2024.

Panel (b) presents Vola–Vola pools. Average $IIL^{0.6}$ is relatively moderate for BTC–ETH and declines sharply after 2021, becoming nearly negligible by 2023. Starting in 2024, several ETH-based cross-asset pools emerge, displaying larger losses than BTC–ETH. In particular, ETH–XRP shows the highest average $IIL^{0.6}$ in 2024, while ETH–SOL, ETH–BNB, and ETH–XRP remain elevated in 2025, indicating that impermanent loss is substantially larger for these more volatile cross-asset pairs.

Series	α	Mean	Std	Q(0.001)	Q1	Median	Q3	Q(0.999)	N	Maturity
IIL	0.2	1.10	0.81	0.19	0.57	0.88	1.42	6.22	2445	7
IIL	0.4	0.59	0.49	0.09	0.29	0.45	0.74	3.98	2445	7
IIL	0.6	0.38	0.33	0.06	0.19	0.29	0.48	2.71	2445	7
IIL	0.8	0.27	0.23	0.04	0.13	0.20	0.34	1.94	2445	7
IIL	up	0.38	0.17	0.13	0.26	0.34	0.46	1.42	2445	7
IIL	dn	0.13	0.10	0.02	0.07	0.10	0.16	0.86	2445	7
IIL	v2	0.06	0.05	0.01	0.03	0.04	0.07	0.39	2445	7
RIL	0.2	0.55	0.90	0.03	0.20	0.33	0.59	14.27	2445	7
RIL	0.4	0.28	0.45	0.02	0.10	0.17	0.30	7.22	2445	7
RIL	0.6	0.18	0.30	0.01	0.07	0.11	0.20	4.76	2445	7
RIL	0.8	0.13	0.21	0.01	0.05	0.08	0.14	3.39	2445	7
RIL	up	0.13	0.16	0.01	0.05	0.08	0.14	2.13	2445	7
RIL	dn	0.09	0.12	0.01	0.04	0.06	0.10	1.82	2445	7
RIL	v2	0.05	0.09	0.00	0.02	0.03	0.06	1.36	2445	7
ILRP	0.2	0.55	0.64	-6.92	0.28	0.48	0.81	3.10	2445	7
ILRP	0.4	0.31	0.33	-2.69	0.14	0.25	0.43	2.05	2445	7
ILRP	0.6	0.20	0.22	-1.71	0.09	0.16	0.28	1.39	2445	7
ILRP	0.8	0.14	0.16	-1.22	0.06	0.11	0.20	1.00	2445	7
ILRP	up	0.25	0.11	-0.62	0.19	0.24	0.31	0.72	2445	7
ILRP	dn	0.04	0.08	-0.85	0.01	0.03	0.06	0.37	2445	7
ILRP	v2	0.00	0.06	-0.87	-0.00	0.01	0.02	0.12	2445	7

Table 6.2: Summary Statistics. IIL, RIL, $ILRP$ for BTC-USD across Ranges. The table presents the summary statistics for the implied impermanent loss, IIL^{v3}, the realized impermanent loss RIL^{v3}, and the impermanent loss risk premium $ILRP^{v3}$, for the BTC–USD pool at a 7-day maturity under different concentration parameters α ($0.2, 0.4, 0.6, 0.8$, the up, down, and v2 benchmark). The implied quantities are computed using the equations in Section 5.1.3. The realized quantities are computed using the equations in Section 5.2.1. The data are sampled daily over the period from April 2019 to December 2025.

6.2 Concentrated Liquidity and the LP's Behavior

6.2.1 Liquidity Bands in v3

We study how risk conditions at time t affect the allocation of liquidity across price bands at time $t+1$. The unit of observation is a pool–band–day, indexed by pool p, distance band α, and day t. The dependent variable $y_{p,\alpha,t}$ captures band-level liquidity outcomes, and is alternatively measured as the ring share $L^{\text{ring}\%}_{p,\alpha,t}$, the cumulative inside share $L^{\text{inside}\%}_{p,\alpha,t}$, or other band-level liquidity objects.

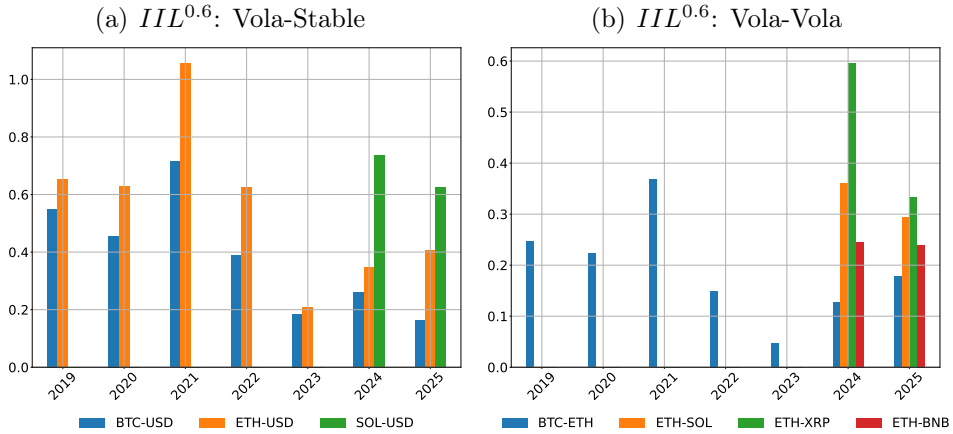

Figure 6.2: Comparison Across Pools over Time. The figure compares the yearly average of the IIL^{v3} at a 7-day maturity for the $\alpha = 0.6$ range across different pools. Panel (a) reports results for the Vola-Stable pools, and panel (b) compares the Vola-Vola pools.

Our baseline specification relates next-day liquidity allocation to contemporaneous risk through band-specific slopes:

$$y_{p,\alpha,t+1} = \beta_\alpha \, \text{Risk}_{p,t} + \gamma_p + \delta_\alpha + \mathbf{X}'_{p,t}\theta + \lambda_{y(t)} + \varepsilon_{p,\alpha,t},$$

where $\text{Risk}_{p,t}$ denotes either IIL or $ILRP$ at the pool–date level. Pool fixed effects γ_p absorb time-invariant differences across pools, band fixed effects δ_α capture average differences across distance bands, and $\lambda_{y(t)}$ denotes year fixed effects. The vector $\mathbf{X}_{p,t}$ includes pool-level controls, such as total value locked, trading volume, and token prices, typically in logs. Standard errors are clustered at the pool level to allow for arbitrary correlation across bands and over time within a pool. We consider dependent variables in levels, logs, and first differences, and focus on next-day outcomes to capture the predictive effect of risk on liquidity reallocation rather than contemporaneous mechanical responses.

Risk is fully interacted with band indicators, allowing its effect to vary flexibly with distance from the prevailing price. This specification estimates a separate coefficient β_α for each band, rather than imposing a common risk sensitivity. It identifies how changes

in risk affect liquidity allocated to each band, conditional on average differences across pools and bands. Economically, this specification allows risk to shift liquidity either away from or toward the spot price. The estimated coefficients $\{\beta_\alpha\}$ therefore trace how LPs rebalance liquidity across distance bands in response to changes in impermanent-loss risk.

This framework tests whether higher impermanent-loss risk shifts liquidity from narrow bands near the spot price to wider ranges, and whether this response varies with distance.

Figure 6.3 plots band-specific estimates of how risk at time t predicts next-day liquidity allocation. Each panel reports coefficients from regressions of next-day ring liquidity shares on contemporaneous risk interacted with band indicators. The horizontal axis indexes distance bands α, and the vertical axis reports the estimated marginal effect of risk on liquidity allocated to band α; shaded areas denote 95% confidence intervals.

Panels (a) and (b) use the IIL. Both show a negative or near-zero effect at the innermost band and positive effects over intermediate bands, with less precise estimates at large α. Panels (c) and (d) instead use $ILRP$ and display the opposite pattern: coefficients are generally positive at small and intermediate bands but turn sharply negative at the outermost band. Overall, the estimates suggest that higher IIL shifts liquidity away from the spot toward intermediate bands, whereas higher $ILRP$ is associated with a retrenchment from the farthest band.

Overall, a higher IIL is associated with less liquidity in the innermost band and more liquidity in intermediate bands, whereas a higher $ILRP$ is associated with more liquidity near the relative price but substantially less liquidity at the most distant band. These contrasting patterns underscore the different economic content of the two risk measures. The response to IIL is consistent with precautionary reallocation: as expected impermanent loss rises, LPs reduce exposure in narrow ranges near the spot price and shift liquidity toward wider ranges. By contrast, a higher $ILRP$ is associated with a re-centering of

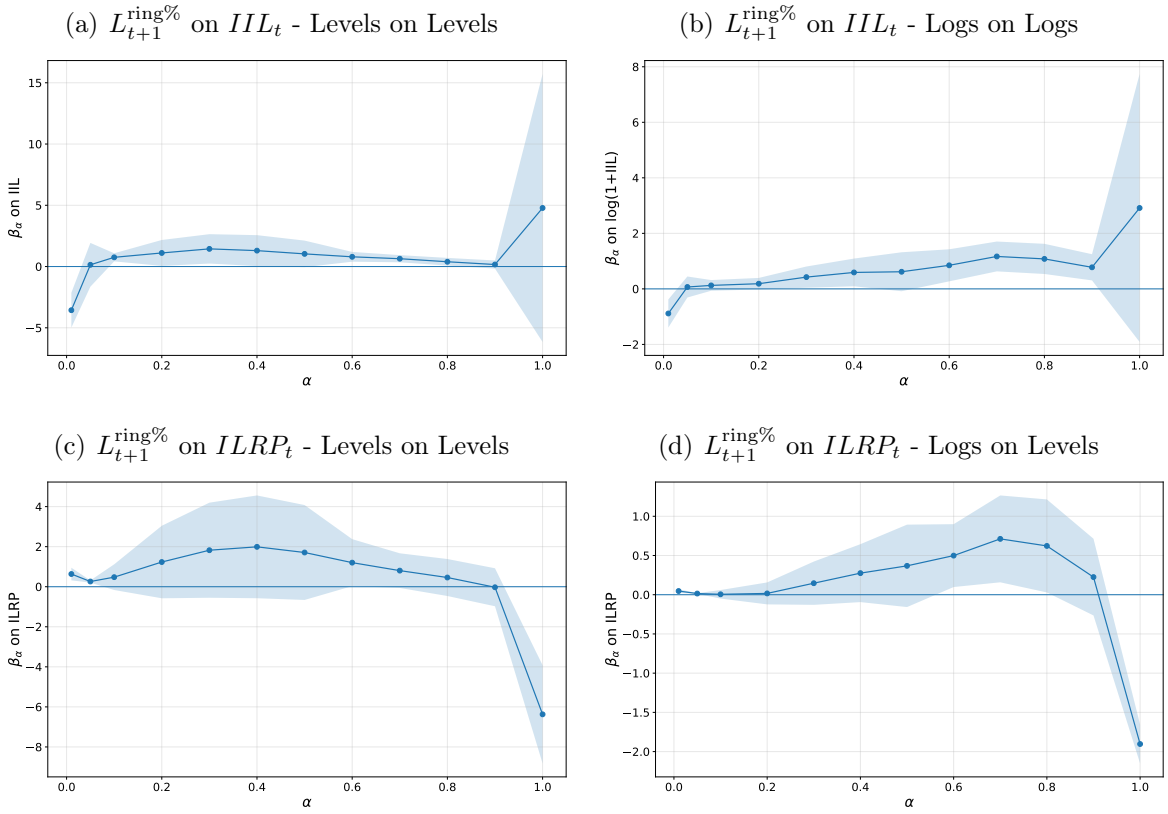

Figure 6.3: Band-Specific Risk Effects on Liquidity Allocation. This figure plots band-specific coefficients from panel regressions of next-day ring liquidity shares on contemporaneous risk interacted with price-band indicators. Points denote coefficient estimates and shaded areas 95% confidence intervals, with standard errors clustered at the pool level. Panels (a) and (b) use IIL_t, while Panels (c) and (d) use $ILRP_t$. Specifications differ by whether ring shares and risk are measured in levels or logs, as indicated in the panel titles. All regressions include pool, band, and year fixed effects, as well as controls for total value locked, trading volume, token prices, and fee tiers.

liquidity. When impermanent-loss risk is better compensated, LPs concentrate liquidity closer to the prevailing price to increase fee capture, while withdrawing liquidity from distant tail ranges that mainly provide insurance.

Taken together, the results suggest that higher risk leads LPs to widen their positions, whereas higher compensation for bearing that risk leads them to concentrate liquidity closer to the spot price and reduce exposure to the most distant bands.

6.2.2 LP Behavior for Symmetric Ranges

We collapse event-level LP actions into a daily LP pool panel. For each LP–day, we retain the last observed action, its tick-range bounds, and post-action liquidity. We complement these end-of-day state variables with daily measures of LP activity and flows constructed from intraday actions, including the α-band label and net liquidity change. We then merge the resulting daily LP panel with IIL or $ILRP$ measured at the pool–date–α level.

We estimate panel regressions on this daily entity-by-date panel to study how risk predicts subsequent changes in liquidity concentration and range placement. An *entity* i is an LP–pool pair, observed at the daily frequency. For each entity-day (i, t), we observe liquidity-provision outcomes that summarize the end-of-day characteristics of the LP's active position.

Our main outcome is liquidity concentration, denoted $\alpha_{i,t}$, which measures the end-of-day alpha-band classification of an LP's active range. We define the dependent variable as the one-day-ahead change in concentration,

$$\Delta\alpha_{i,t\to t+1} \;\equiv\; \alpha_{i,t+1} - \alpha_{i,t},$$

computed within entity by aligning the next available observation at $t+1$ with day t. This variable captures how the concentration of an LP's active range changes from day t to the next day.

We relate these forward-looking adjustments to contemporaneous risk conditions using the following panel specification:

$$\Delta Y_{i,t\to t+1} \;=\; \beta\,\mathrm{Risk}_{i,t} \;+\; \boldsymbol{\gamma}'\,\mathbf{X}_{i,t} \;+\; \mu_i \;+\; \lambda_{y(t)} \;+\; \varepsilon_{i,t}, \tag{6.1}$$

where $\Delta Y_{i,t\to t+1}$ denotes the $\Delta\alpha_{i,t\to t+1}$. Here, $Risk_{i,t}$ denotes the risk proxy at day t, and

$\mathbf{X}_{i,t}$ is a vector of time-varying pool-level controls including $\log(\text{Price}_{p(i),t})$, $\log(\text{TVL}_{p(i),t})$, and $\log(\text{Volume}_{p(i),t})$. The term μ_i denotes entity fixed effects, which absorb time-invariant heterogeneity across LP–pool pairs, and $\lambda_{y(t)}$ denotes year fixed effects. Standard errors are clustered at the entity level. We repeat the regression using $ILRP$ instead of IIL.

Table 6.3 shows sharply different forward-looking liquidity reallocation patterns for the two risk measures, underscoring their distinct economic content. Column (1) shows that higher IIL_t predicts subsequent reallocation away from the most concentrated liquidity positions. In particular, a higher IIL_t is associated with weaker allocation to the innermost band and stronger allocation to intermediate bands. This pattern is consistent with precautionary liquidity management: as expected impermanent loss rises, LPs reduce exposure in narrow ranges near the spot price and shift liquidity toward moderately wider ranges. Column (2) shows a contrasting response to $ILRP_t$. Higher $ILRP_t$ is associated with greater allocation to near and intermediate bands, but substantially lower allocation to the most distant band. This pattern suggests that when impermanent-loss risk is better compensated, LPs concentrate liquidity closer to the prevailing price to increase fee capture, while withdrawing liquidity from distant tail ranges. Thus, higher risk premia lead to a re-centering of liquidity rather than a general widening of positions.

Taken together, the results indicate that IIL_t and $ILRP_t$ reflect distinct economic forces: increases in expected impermanent loss prompt a precautionary widening of liquidity ranges, whereas increases in the impermanent loss risk premium encourage re-centering of liquidity toward the market price.

6.2.3 LP Behavior for up and Down Ranges

To analyze LP repositioning relative to the current price, we classify each LP position into three mutually exclusive states based on its position relative to the active price

	(1) $\Delta\alpha$	(2) $\Delta\alpha$
IIL_t	0.069***	
	(0.001)	
ILRP_t		-0.002***
		(0.000)
log(Price)	0.000***	0.000***
	(0.000)	(0.000)
log(TVL)	-0.002***	-0.005***
	(0.001)	(0.001)
log(Volume)	0.000	0.006***
	(0.000)	(0.000)
Observations	456675	456675
R^2 (within)	0.097	0.003
Entity FE	Yes	Yes
Year FE	Yes	Yes
SE	Clustered (entity)	Clustered (entity)

Table 6.3: Forward changes in LP outcomes, IIL and $ILRP$. The table reports panel regressions of one-period-ahead changes in α on IIL (Column 1) and $IRLP$ (Column 2). All specifications include pool–LP and year fixed effects, control variables, and standard errors clustered at the pool–LP level.

interval. Let (i) index the LP–pool pair and let (M_{it}) denote the position of liquidity relative to the current price range. We define

$$Up_{it} = \mathbf{1}(M_{it} = up), \quad Dn_{it} = \mathbf{1}(M_{it} = dn), \quad Range_{it} = \mathbf{1}(M_{it} \notin \{up, dn\})$$

where $\mathbf{1}(\cdot)$ denotes the indicator function. Using lagged state indicators, we construct transition variables that capture movements between states across consecutive days. For example, an *up-to-Range* transition occurs when liquidity moves from the upper region into the active range between days t and $t+1$:

$$UpToRange_{i,t+1} = \mathbf{1}(Up_{i,t} = 1 \wedge Range_{i,t+1} = 1).$$

Similarly, a $RangeToUp$ transition occurs when liquidity moves from the active range to the upper region, while $DnToRange$ and $RangeToDown$ transitions capture movements between the active range and the lower region. To study repositioning dynamics, we aggregate these transition indicators to the daily level. For each day, we compute the mean across LP–pool entities, producing a series for each transition type.

Figure 6.4 plots LP repositioning across price regions together with aggregate IIL. Transition measures are daily percentage shares of total transitions. Panel (a) reports transitions between the active range and the upper region. As expected, $UpToRange$ and $RangeToUp$ move in opposite directions and are strongly negatively correlated ($\rho = -0.94$). Higher IIL is associated with fewer transitions from the upper region into the range ($\rho = -0.37$) and more transitions from the range to the upper region ($\rho = 0.31$), consistent with liquidity moving out of the active range when impermanent loss is elevated. Since liquidity above the current price represents sell-side liquidity, this pattern suggests that LPs delay activating such liquidity when IIL rises. Panel (b) reports transitions between the range and the lower region. $DnToRange$ and $RangeToDn$ are positively correlated ($\rho = 0.57$), indicating more symmetric repositioning around the lower boundary. Their correlations with IIL are close to zero, ($\rho = 0.08$) and ($\rho = -0.09$), suggesting little systematic relation between impermanent loss and transitions involving the lower region.

We next estimate panel regressions of LP state transitions on IIL. We use the same controls, fixed effects, and clustering structure as in equation (6.1). Let i denote the LP–pool pair and t the day. We estimate

$$Transition_{i,t+1} = \beta\, \mathrm{IIL}_{i,t} + \boldsymbol{\gamma}'\mathbf{X}_{i,t} + \mu_i + \lambda_{y(t)} + \varepsilon_{i,t},$$

where i indexes the LP–pool pair (entity) and t denotes the day. The dependent variable $Transition_{i,t+1}$ is a binary indicator variable that indicates whether a specific reposi-

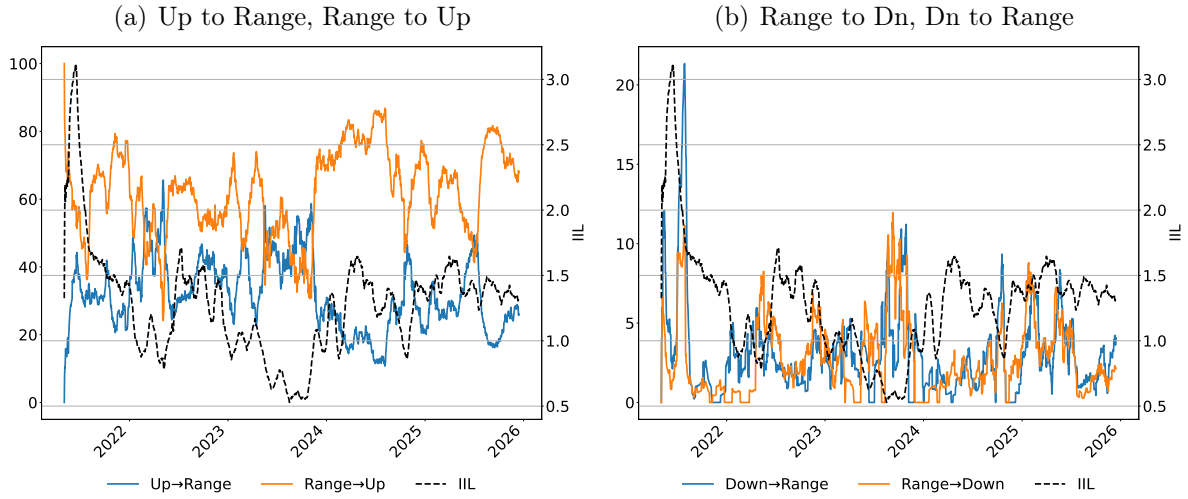

Figure 6.4: LP Repositioning – Up, Down and Ranges. The figure shows the dynamics of LP repositioning across price regions ($UpToRange$, $RangeToUp$, $DnToRange$, $RangeToDn$) and the aggregate IIL. Panel (a) reports transitions between $RangeToUp$ and $UpToRange$, while Panel (b) reports transitions between the $RangeToDn$ and $DnToRange$.

tioning event occurs between t and $t+1$. The dependent variable is forward-looking: transitions from t to $t+1$ are regressed on explanatory variables measured at t.

Table 6.4 examines how impermanent-loss conditions affect transitions from the upper region into the active range. The dependent variable $UpToRange_{i,t+1}$ equals one when an LP's position moves from *Up* at t to *Range* at $t+1$, so that liquidity previously above the current price becomes active around the spot. Column (1) shows that a higher IIL is associated with a significantly lower probability of such transitions, suggesting that LPs delay activating sell-side liquidity when impermanent-loss risk rises. Column (2) shows no significant relation between $ILRP$ and $UpToRange$ transitions.

Table 6.5 examines how impermanent-loss conditions affect transitions from the lower region into the active range. The dependent variable $DnToRange_{i,t+1}$ equals one when an LP's position moves from *Dn* at t to *Range* at $t+1$, so that liquidity previously below the market price becomes active around the spot. Column (1) shows that a higher IIL significantly lowers the probability of such transitions, suggesting that LPs delay

	(1) Up to Range	(2) Up to Range
IIL_t	-0.006***	
	(0.000)	
ILRP_t		0.000
		(0.000)
log(Price)	0.000	0.000
	(0.000)	(0.000)
log(TVL)	-0.000	-0.000
	(0.000)	(0.000)
log(Volume)	-0.002***	-0.002***
	(0.000)	(0.000)
Observations	464709	464709
R^2 (within)	0.001	0.000
Entity FE	Yes	Yes
Year FE	Yes	Yes
SE	Clustered (entity)	Clustered (entity)

Table 6.4: Up-to-Range transitions, IIL and $ILRP$. The table reports panel regressions of the one-period-ahead transition indicator $UpToRange$ on IIL (Column 1) and $ILRP$ (Column 2). $UpToRange_{i,t+1}$ equals one when an LP's position moves from *up* at t to *Range* at $t+1$. All specifications include pool–LP and year fixed effects, control variables, and standard errors clustered at the pool–LP level.

activating buy-side liquidity when impermanent-loss risk rises. Column (2) shows no significant relation between $ILRP$ and $DnToRange$ transitions.

Overall, the results suggest that LPs respond to impermanent loss by becoming more cautious about activating liquidity at current prices. A higher IIL is associated with a lower probability that liquidity positioned above or below the market price will move into the active range. Together with the earlier evidence on wider liquidity ranges, these findings indicate that LPs manage impermanent loss primarily by reducing the likelihood that liquidity becomes active near the spot price, rather than by aggressively reallocating liquidity across price regions.

	(1) Dn to Range	(2) Dn to Range
IIL_t	-0.001***	
	(0.000)	
ILRP_t		-0.000
		(0.000)
log(Price)	0.000	0.000
	(0.000)	(0.000)
log(TVL)	-0.000	-0.000
	(0.000)	(0.000)
log(Volume)	0.000	-0.000
	(0.000)	(0.000)
Observations	464709	464709
R^2 (within)	0.001	0.000
Entity FE	Yes	Yes
Year FE	Yes	Yes
SE	Clustered (entity)	Clustered (entity)

Table 6.5: Dn-to-Range transitions, IIL and $ILRP$. The table reports panel regressions of the one-period-ahead transition indicator $DnToRange$ on IIL (Column 1) and $ILRP$ (Column 2). $DnToRange_{i,t+1}$ equals one when an LP's position moves from *Dn* at t to *Range* at $t+1$. All specifications include pool–LP and year fixed effects, control variables, and standard errors clustered at the pool–LP level.

7 Conclusion

This paper interprets liquidity provision in concentrated AMMs as the supply of short-variance exposure. We develop measures of implied impermanent loss (IIL), realized impermanent loss (RIL), and the impermanent loss risk premium ($ILRP$), and use them to study how LPs adjust liquidity provision in concentrated AMMs.

We find that implied impermanent loss and compensation for bearing that risk have sharply different effects on liquidity allocation. Higher IIL predicts a precautionary widening of liquidity away from the spot price and reduces the probability that out-of-range liquidity is returned to the active range. Higher $ILRP$, by contrast, predicts a re-centering of liquidity toward the prevailing price and lower allocations to distant tail bands. These results show that LPs respond differently to risk and to risk premia, and

that concentrated liquidity makes the supply of variance exposure an endogenous choice.

More broadly, our findings suggest that decentralized market design shapes the allocation and pricing of risk in ways that parallel, but also differ from, traditional intermediary-based markets. Understanding impermanent loss through the joint behavior of expected losses and risk premia is therefore essential for understanding liquidity supply in modern on-chain exchanges.

References

Geert Bekaert and Marie Hoerova. The vix, the variance premium and stock market volatility. *Journal of Econometrics*, 183(2):181–192, 2014. ISSN 0304-4076. doi: https://doi.org/10.1016/j.jeconom.2014.05.008. URL `https://www.sciencedirect.com/science/article/pii/S0304407614001110`. Analysis of Financial Data.

Fischer Black and Myron Scholes. The pricing of options and corporate liabilities. *Journal of Political Economy*, 81(3):637–654, 1973. ISSN 0022-3808.

Tim Bollerslev, George Tauchen, and Hao Zhou. Expected stock returns and variance risk premia. *The Review of Financial Studies*, 22(11):4463–4492, 2009. ISSN 0893-9454.

Douglas T. Breeden and Robert H. Litzenberger. Prices of state-contingent claims implicit in option prices. *The Journal of Business*, 51(4):621–651, 1978. ISSN 0021-9398.

Agostino Capponi and Ruizhe Jia. Liquidity provision on blockchain-based decentralized exchanges. *The Review of Financial Studies*, 38(10):3040–3085, 07 2025. ISSN 0893-9454. doi: 10.1093/rfs/hhaf046. URL `https://doi.org/10.1093/rfs/hhaf046`.

Peter Carr and Roger Lee. Robust replication of volatility derivatives. In *MFA 2008 Annual Meeting*, 2008. URL `https://math.uchicago.edu/~rogerlee/rrvd.pdf`.

Peter Carr and Dilip Madan. *Volatility: New Estimation Techniques for Pricing Derivatives*, chapter 29 Towards a theory of volatility trading. Risk Books, 1998. ISBN 9781899332410.

Peter Carr and Liuren Wu. Variance risk premiums. *The Review of Financial Studies*, 22(3):1311–1341, 2009. ISSN 0893-9454.

Kresimir Demeterfi, Emanuel Derman, Michael Kamal, and Joseph Zou. A guide to volatility and variance swaps. *The Journal of Derivatives*, 6(4):9–32, 1999. ISSN 1074-1240.

Stephen Figlewski. Risk-neutral densities: A review. *Annual Review of Financial Economics*, 10:329–359, 2018. ISSN 1941-1367.

Masaaki Fukasawa, Basile Maire, and Marcus Wunsch. Weighted variance swaps hedge against impermanent loss. *Quantitative Finance*, 23(6):901–911, 2023. ISSN 1469-7688.

Paolo Guasoni and Eberhard Mayerhofer. Technical note—options portfolio selection. *Operations Research*, 68(3):733–740, 2020. ISSN 0030-364X.

Nicolae Gârleanu, Lasse Heje Pedersen, and Allen M. Poteshman. Demand-based option pricing. *The Review of Financial Studies*, 22(10):4259–4299, 02 2009. ISSN 0893-9454. doi: 10.1093/rfs/hhp005. URL `https://doi.org/10.1093/rfs/hhp005`.

Campbell R. Harvey, Joel Hasbrouck, and Fahad Saleh. The evolution of decentralized exchange: Risks, benefits, and oversight, 2024.

Lioba Heimbach, Eric Schertenleib, and Roger Wattenhofer. Risks and returns of uniswap V3 liquidity providers. In *4th ACM Conference on Advances in Financial Technologies*, Cambridge, Massachusetts, U.S.A., 2022a. ISBN 9781450398619.

Lioba Heimbach, Eric Schertenleib, and Roger Wattenhofer. Risks and returns of uniswap v3 liquidity providers. In *Proceedings of the 4th ACM Conference on Advances in Financial Technologies*, pages 89–101, 2022b.

Roger Lee. *Encyclopedia of Quantitative Finance*, chapter Corridor Variance Swap. John Wiley & Sons, 2010a. ISBN 9780470057568.

Roger Lee. *Encyclopedia of Quantitative Finance*, chapter Weighted variance swap. John Wiley & Sons, 2010b. ISBN 9780470057568.

Igor Makarov and Antoinette Schoar. Cryptocurrencies and decentralized finance. *Brookings Papers on Economic Activity*, Spring 2022:141–215, 2022. ISSN 0007-2303.

Jason Milionis, Ciamac C. Moallemi, Tim Roughgarden, and Anthony Lee Zhang. Automated market making and loss-versus-rebalancing. *arXiv Manuscript*, 2024. doi: https://doi.org/10.48550/arXiv.2208.06046.

Andrew Papanicolaou, Lorenzo Schönleber, and Thomas Nanfeng Li. The implied impermanent loss in decentralized liquidity provision. *SSRN Manuscript*, 2025. doi: https://dx.doi.org/10.2139/ssrn.4811111.

Peter Van Tassel. The law of one price in equity volatility markets. *FRB of New York Staff Report*, (953), 2020.

Appendix A Mathematics for Impermanent Loss

In this section, we briefly outline the application of our methodology, which is broadly applicable, for the valuation of impermanent loss in Uniswap v3—where liquidity providers can allocate tokens within specified price ranges—and to other adverse selection metrics, such as loss-versus-rebalancing (LVR), as discussed by Milionis et al. (2024).

A.1 Implied Impermanent Loss for Uniswap v3

The valuation formula in equation (4.5) applies to the Uniswap V2 protocol, but many pools now operate under the Uniswap v3 protocol, where LPs allocate tokens within a specific price range. Consider the ticks $(r_i)_{i=1,\,2,\,...,\,m}$ where $r_{i+1} = r_i \times 1.0001$, and let $C_i = [r_i,\, r_{i+1})$ denote the band. If $R(t) \in C_i$ then the LP earns a reward but is also exposed to impermanent loss, in particular, it can be shown that the v3 analog to equation (3.6) is

$$dIL_i(t) = -\frac{\sigma_R^2(t)\sqrt{R(t)}}{4\left(2\sqrt{R(t)} - \sqrt{r_i} - \frac{R(t)}{\sqrt{r_{i+1}}}\right)}\mathbf{1}_{\{R(t)\in C_i\}}dt.$$

This increment of impermanent loss can be derived using Itô's lemma as done in deriving equation (3.6). Integrating over time yields the total impermanent loss, which is equivalent to a corridor variance swap (Lee (2010a) and Lee (2010b)),

$$\begin{aligned}\widetilde{\mathbb{E}}^Q\left[IL_i(T)\right] &= -\frac{1}{4}\widetilde{\mathbb{E}}^Q\left[\int_0^T \frac{\sigma_R^2(t)\sqrt{R(t)}}{2\sqrt{R(t)} - \sqrt{r_i} - \frac{R(t)}{\sqrt{r_{i+1}}}}\mathbf{1}_{\{R(t)\in C_i\}}(t)\,dt\right], \qquad \text{(A.1)}\\ &= -\frac{1}{2}\int_{K\in C_i} \frac{\widetilde{\mathbb{E}}^Q\left[(K - R(T))^+\right]\mathbf{1}_{\{K<R(0)\}} + \widetilde{\mathbb{E}}^Q\left[(R(T) - K)^+\right]\mathbf{1}_{\{K\geqslant R(0)\}}}{\sqrt{K^3}\left(2\sqrt{K} - \sqrt{r_i} - \frac{K}{\sqrt{r_{i+1}}}\right)}dK.\end{aligned}$$

The pool-wide impermanent loss is a weighted sum of individual corridor variance swaps, with weights proportional to the TVL in each band: $\sum_i \frac{TVL_i\widetilde{\mathbb{E}}^Q[IL_i(T)]}{\sum_i TVL_i}$, where TVL_i is the TVL in band i.

A.2 Implied Loss-Versus-Rebalancing

Our framework can be used to assess loss-versus-rebalancing (LVR) **?**, with the advantage of valuing LVR under the probability measure $\mathbb{Q}$ introduced in Section 4.

We define the TVL of a liquidity pool at time t is $TVL(t) := N_1(t)\,P_1(t) + N_2(t)\,P_2(t)$. In our continuous-time framework, an increment of LVR under the Uniswap V2 protocol

is

$$dLVR\left(t\right) = \frac{1}{8} TVL\left(t\right) \sigma_R^2\left(t\right) dt,$$

where $N_i\left(t\right)$ and $P_i\left(t\right)$ for $i = 1,\ 2$ are the notation from Section 3.1 for the number of tokens in the pool and the market prices. Consider the constant product rule as given in equation (3.1), where the parameter L remains constant. We can express the N_i in terms of L and $R\left(t\right)$, namely $N_1\left(t\right) = \frac{L}{\sqrt{R(t)}}$ and $N_2\left(t\right) = L\sqrt{R\left(t\right)}$, and from Assumption 3.1 it follows that

$$TVL\left(t\right) = 2L\sqrt{P_1\left(t\right) P_2\left(t\right)}.$$

Then the valuation of LVR under $\mathbb{Q}$ is computed using the change of numéraire introduced in Section **??**,

$$\mathbb{E}^Q\left[LVR\left(T\right)\right] = \frac{e^{rT} L P_2\left(0\right)}{4} \int_0^T \widetilde{\mathbb{E}}^Q\left[\sqrt{R\left(t\right)} \sigma_R^2\left(t\right)\right] dt.$$

Using the weighted variance swap framework of Lee (2010b), it follows that

$$\mathbb{E}^Q\left[LVR\left(T\right)\right] = -2L\left(\mathbb{E}^Q\sqrt{P_1\left(T\right) P_2\left(T\right)} - e^{rT}\sqrt{P_1\left(0\right) P_2\left(0\right)}\right) \tag{A.2}$$

Equation (A.2) can be computed using the estimated RND obtained by minimizing the HJ bound, as proposed in Section 4.3.

Implied LVR for non-constant L can be managed under assumptions such as L being uncorrelated with $R\left(t\right)$ and behaving as a martingale. In Uniswap v3, implied LVR can be computed as a portfolio of options, similar to equation (A.1) for IL. Like the implied LVR of Uniswap V2, the implied LVR under Uniswap v3 is expressed in units of the original numéraire.

A.2.1 Non-Constant L

Let the constant product rule in equation (3.1) have a dynamic parameter $L(t)$, which we assume to be $\mathcal{F}_t$-adapted (recall the probability space introduced in Section 3). If we attempt to repeat the step taken for constant L, we find

$$\mathbb{E}^Q\Big[\text{LVR}(T)\Big] = \frac{P_2(0)e^{rT}}{4}\int_0^T \widetilde{\mathbb{E}}^Q\Big[L(t)\sqrt{R(t)}\sigma_R^2(t)\Big]dt \ ,$$

which requires more information about the $L(t)$'s distribution. In particular, changes in $L(t)$ will depend on how LPs respond to the market. Per the rules on staking of new liquidity to the pool, the LP does not move the relative price, and hence

$$dL(t)dR(t) = 0 \ .$$

Without any particular specification of the SDE for $L(t)$, if we assume (i) that $L(t)$ is a $\widetilde{\mathbb{Q}}$-martingale so that $\widetilde{\mathbb{E}}^Q\int_0^T \sqrt{R(t)}dL(t) = 0$, and (ii) that $L(t)$ and $\sqrt{R(t)}$ are uncorrelated under $\widetilde{\mathbb{Q}}$ so that $\widetilde{\mathbb{E}}^Q\Big[L(T)\sqrt{R(T)}\Big] = \widetilde{\mathbb{E}}^Q\Big[L(T)\Big]\widetilde{\mathbb{E}}^Q\Big[\sqrt{R(T)}\Big]$, then we can move forward with the calculations to obtain an expression similar to equation (A.2),

$$\mathbb{E}^Q\Big[\text{LVR}(T)\Big] = -2L(0)\left(\mathbb{E}^Q\sqrt{P_1(T)P_2(T)} - e^{rT}\sqrt{P_1(0)P_2(0)}\right) \ . \tag{A.3}$$

Certainly there are other ways to model $L(t)$ for LVR valuation, but assuming $L(t)$ to be an uncorrelated martingale is perhaps the simplest way to arrive at a formula like (A.3) that is convenient for implementation.

A.2.2 LVR in v3

The LVR calculations shown thus far are for V2. For a v3 band C_i with constant L_i, the value locked in the band is $V_i(t) = P_2(t)\left(2\sqrt{R(t)} - \sqrt{r_i} - R(t)/\sqrt{r_{i+1}}\right)$, and the

LVR valuation is

$$\mathbb{E}^Q\Big[\mathrm{LVR}_i(T)\Big] = \frac{LP_2(0)e^{rT}}{4}\int_0^T \widetilde{\mathbb{E}}^Q\Big[\sqrt{R(t)}\sigma_R^2(t)\mathbf{1}_{\{R(t)\in C_i\}}\Big]dt\ ,$$

and again using the weighted variance swap framework of Lee (2010b)the v3 valuation of LVR is

$$\mathbb{E}^Q\Big[\mathrm{LVR}_i(T)\Big] = \frac{LP_2(0)e^{rT}}{2}\Bigg(\int_{K\in C_i} K^{-3/2}\widetilde{\mathbb{E}}^Q\Big[(K-R(T))^+\Big]\mathbf{1}_{\{K<R(0)\}}dK + \int_{K\in C_i} K^{-3/2}\widetilde{\mathbb{E}}^Q\Big[(R(T)-K)^+\Big]\mathbf{1}_{\{K\geqslant R(0)\}}dK\Bigg)\ . \tag{A.4}$$

Equation (A.4) can be implemented on data using the estimated risk-neutral density from Section 4.3.

Appendix B Realized Impermanent Loss for V2

For each pool and each maturity T (in days), we compute a rolling measure (denoted as RIL) from the log price ratio (P_1/P_1). Let $P_{1,t}$ and $P_{2,t}$ be the spot prices of tokens 1 and 2 at time t (hourly frequency). Define the log ratio

$$x_t = \log\left(\frac{P_{1,t}}{P_{2,t}}\right),$$

and its hourly increment $\Delta x_t = x_t - x_{t-1}$. For a window length of T days, i.e. $T\cdot 24$ hourly observations, the pairwise RIL is computed as

$$\mathrm{RIL}_t(T) = \frac{1}{8}\cdot(24\cdot 365)\cdot\frac{1}{(T\cdot 24)}, \left(\sum_{k=0}^{T\cdot 24-1}\left(\Delta x_{t-k}^{(i,j)}\right)^2\right)$$

where this sum is evaluated using at least $T \cdot 24/2$ available observations within the window. The resulting time series $\mathrm{RIL}_t(T)$ is calculated for each pair and maturity.

Appendix C Uniswap v3 Arithmetics

Let $\tilde{L}$ denote normalized liquidity and let S_0, S_1 denote the initial and final prices, respectively, with liquidity provided over the range $[S_\ell, S_u]$. Define the value of a Uniswap v3 liquidity position evaluated at price S_1 as

$$V_{\mathrm{pos}}(\tilde{L}, S_1, S_\ell, S_u) = \begin{cases} \tilde{L}\, S_1 \left(\dfrac{1}{\sqrt{S_\ell}} - \dfrac{1}{\sqrt{S_u}} \right), & \text{if } S_1 < S_\ell, \\ \tilde{L} \left(2\sqrt{S_1} - \sqrt{S_\ell} - \dfrac{S_1}{\sqrt{S_u}} \right), & \text{if } S_\ell \leqslant S_1 < S_u, \\ \tilde{L} \left(\sqrt{S_u} - \sqrt{S_\ell} \right), & \text{if } S_1 \geqslant S_u. \end{cases}$$

The corresponding buy-and-hold benchmark value is defined as

$$V_{\mathrm{hold}}(\tilde{L}, S_0, S_1, S_\ell, S_u) = \begin{cases} \tilde{L}\, S_1 \left(\dfrac{1}{\sqrt{S_\ell}} - \dfrac{1}{\sqrt{S_u}} \right), & \text{if } S_0 < S_\ell, \\ \tilde{L} \left(\dfrac{S_0 + S_1}{\sqrt{S_0}} - \sqrt{S_\ell} - \dfrac{S_1}{\sqrt{S_u}} \right), & \text{if } S_\ell \leqslant S_0 < S_u, \\ \tilde{L} \left(\sqrt{S_u} - \sqrt{S_\ell} \right), & \text{if } S_0 \geqslant S_u. \end{cases}$$

The impermanent loss is defined as the relative difference between the value of the liquidity position and the corresponding buy-and-hold benchmark

$$\mathrm{IL}(S_0, S_1, S_\ell, S_u, \tilde{L}) = \frac{V_{\mathrm{pos}}(\tilde{L}, S_1, S_\ell, S_u) - V_{\mathrm{hold}}(\tilde{L}, S_0, S_1, S_\ell, S_u)}{V_{\mathrm{hold}}(\tilde{L}, S_0, S_1, S_\ell, S_u)}.$$

Appendix D Risk-Neutral Densities (RND)

To ensure the estimated density captures the tail behavior more realistically, we append log-normal tails to both ends of the strike support. To the right, we extrapolate the density using a log-normal approximation based on the last observed IV $\sigma(k_{\max})$, generating a right tail over an extended grid $k > k_{\max}$ and scaling it as

$$p_{\text{right}}(k) = \frac{p(k_{\max})}{C_{KK}(S, k_{\max}, T, \sigma(k_{\max}))} \cdot C_{KK}(S, k, T, \sigma(k_{\max})),$$

where $C_{KK}(\cdot)$ denotes the second derivative of the Black–Scholes call price with respect to strike. Similarly, the left tail is constructed for $k < k_{\min}$ using

$$p_{\text{left}}(k) = \frac{p(k_{\min})}{C_{KK}(S, k_{\min}, T, \sigma(k_{\min}))} \cdot C_{KK}(S, k, T, \sigma(k_{\min})).$$

Finally, we concatenate the left tail, core, and right tail densities to obtain the full strike grid $\{k_i\}$ and corresponding density values. The resulting density is normalized so that it integrates to one.

Internet Appendix

I Additional Figures and Tables

I.1 Trading Volume on Deribit

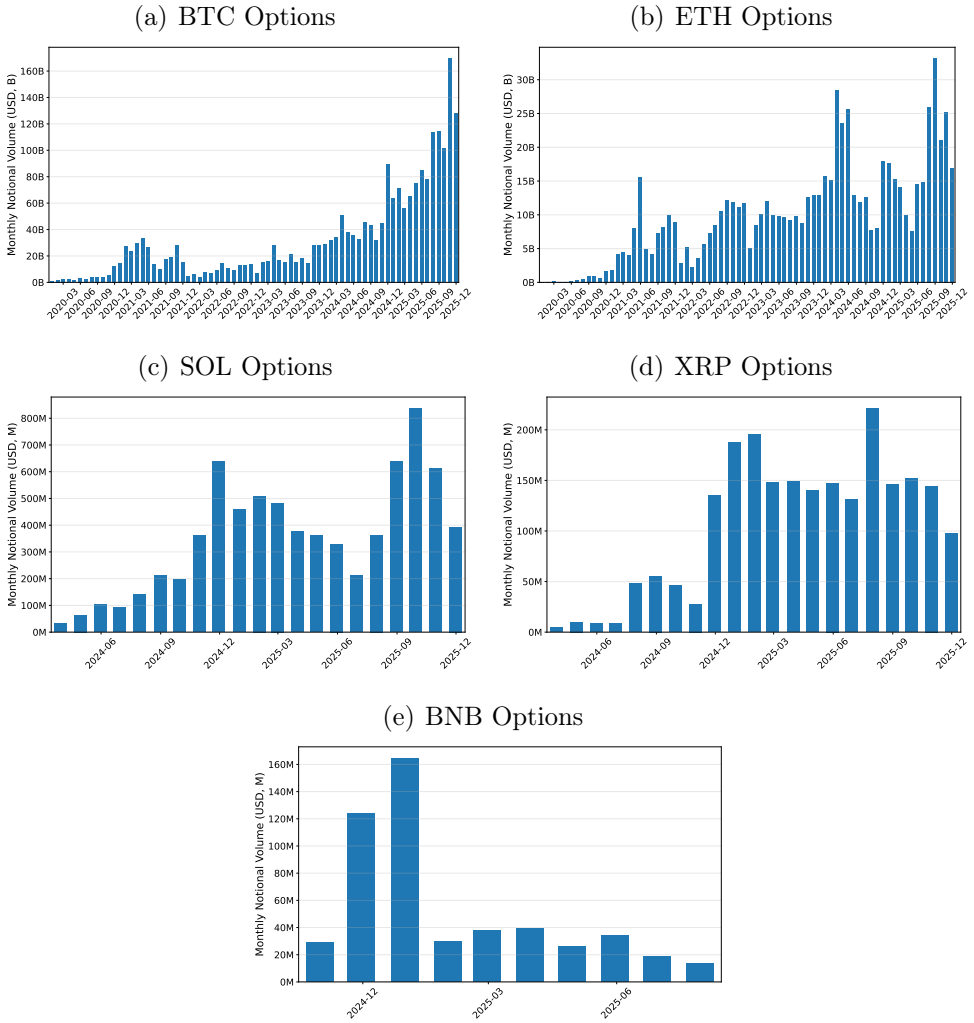

Figure I.1: Monthly Option Volumes on Deribit. The figure reports the monthly total option trading volume on Deribit, measured in notional value (USD). Notional volume is defined as the total value of option contracts traded, including both on-screen trades executed directly on the exchange and block trades executed through third-party platforms. The data are sourced from Amberdata.

I.1.1 The Term Structure of Implied Impermanent Loss

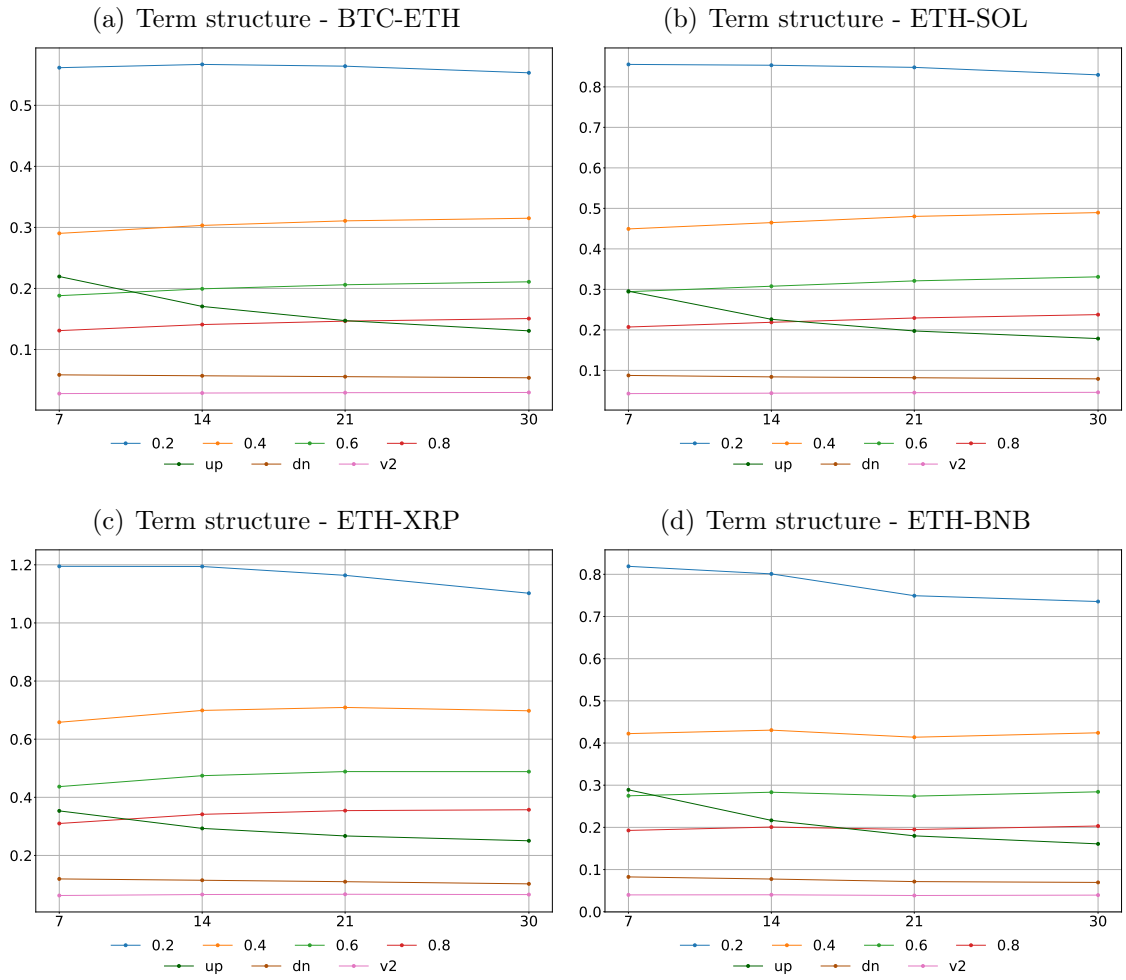

Figure I.2: Term Structure of IIL for Vola-Vola Pools. The figure reports the term structure of the implied impermanent loss IIL^{v3} across maturities (7, 14, 21, and 30 days) for different ranges. Panel (a) shows BTC-ETH, panel (b) ETH-SOL, panel (c) ETH-XRP, and panel (d) ETH-BNB. For each pool, we compare $\alpha = 0.2, 0.4, 0.6, 0.8$ with the v2 benchmark, as well as the up and down ranges.

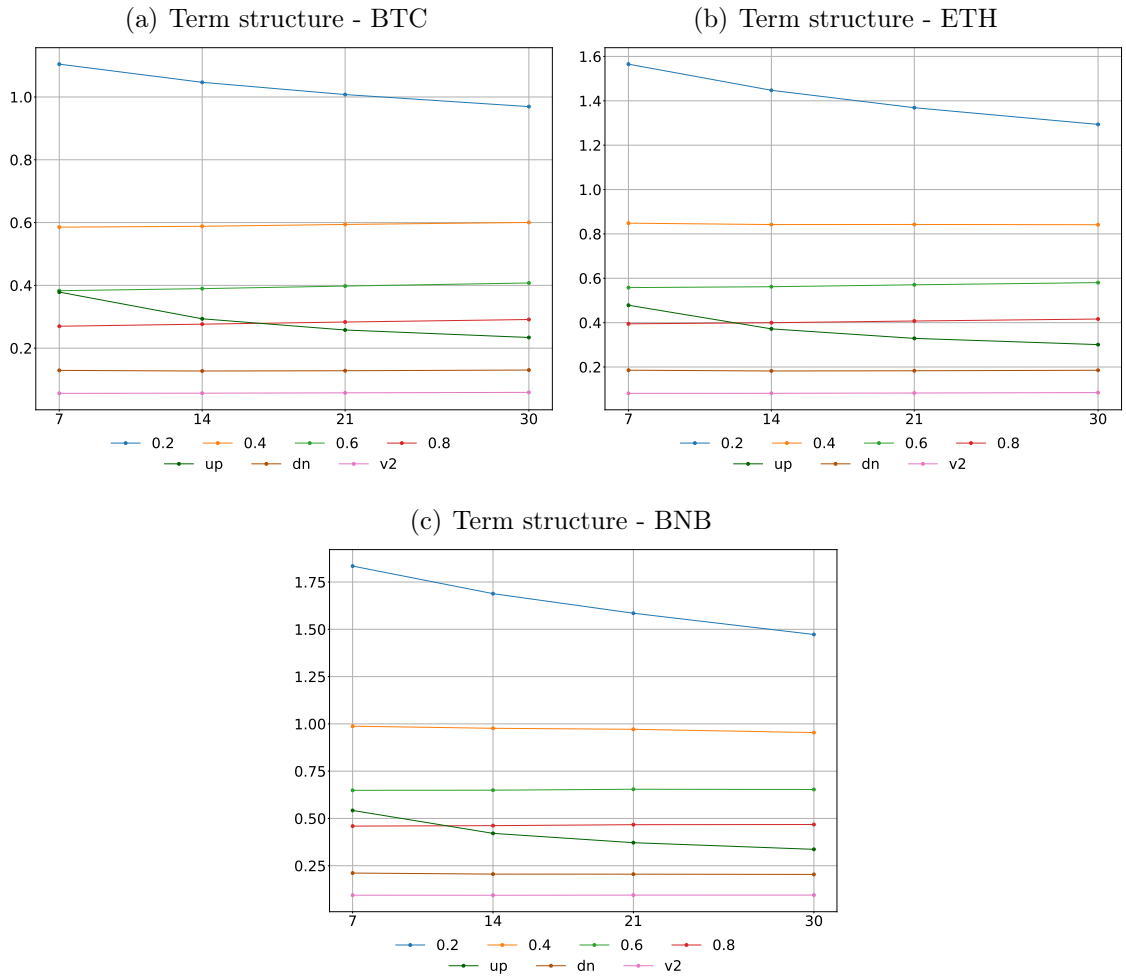

Figure I.3: Term Structure of IIL for Vola-Stable Pools. The figure reports the term structure of the implied impermanent loss IIL^{v3} across maturities (7, 14, 21, and 30 days) for different ranges. Panel (a) shows BTC-USD, panel (b) ETH-USD and panel (c) BNB-USD. For each pool, we compare $\alpha = 0.2, 0.4, 0.6, 0.8$ with the v2 benchmark, as well as the up and down ranges.

Panel A: Volatile–Volatile Pools

Pool	TTM	0.2	0.4	0.6	0.8	up	dn	v2	N
BTC-ETH	7	0.5617	0.2903	0.1882	0.1310	0.2196	0.0585	0.0278	2383
	14	0.5671	0.3033	0.1994	0.1409	0.1706	0.0569	0.0287	2383
	21	0.5642	0.3108	0.2061	0.1465	0.1473	0.0555	0.0293	2383
	30	0.5533	0.3151	0.2109	0.1507	0.1306	0.0537	0.0296	2383
ETH-SOL	7	0.8554	0.4493	0.2944	0.2071	0.2954	0.0875	0.0427	479
	14	0.8534	0.4649	0.3078	0.2187	0.2261	0.0840	0.0438	479
	21	0.8481	0.4802	0.3210	0.2294	0.1973	0.0819	0.0450	479
	30	0.8297	0.4896	0.3310	0.2377	0.1785	0.0791	0.0458	479
ETH-XRP	7	1.1948	0.6583	0.4368	0.3100	0.3533	0.1193	0.0622	484
	14	1.1942	0.6990	0.4745	0.3415	0.2931	0.1147	0.0656	484
	21	1.1637	0.7092	0.4886	0.3543	0.2671	0.1097	0.0665	484
	30	1.1022	0.6978	0.4884	0.3573	0.2505	0.1023	0.0654	484
ETH-BNB	7	0.8190	0.4223	0.2748	0.1928	0.2890	0.0826	0.0399	182
	14	0.8010	0.4306	0.2834	0.2008	0.2166	0.0775	0.0402	182
	21	0.7493	0.4138	0.2741	0.1949	0.1799	0.0715	0.0385	182
	30	0.7355	0.4242	0.2843	0.2032	0.1609	0.0695	0.0394	182

Panel B: Volatile–Stable Pools

Pool	TTM	0.2	0.4	0.6	0.8	up	dn	v2	N
BTC-USD	7	1.1045	0.5854	0.3830	0.2698	0.3786	0.1292	0.0561	2450
	14	1.0467	0.5882	0.3896	0.2765	0.2935	0.1272	0.0566	2450
	21	1.0077	0.5940	0.3978	0.2832	0.2578	0.1281	0.0577	2450
	30	0.9693	0.6004	0.4076	0.2912	0.2340	0.1303	0.0592	2450
ETH-USD	7	1.5652	0.8485	0.5580	0.3947	0.4785	0.1857	0.0813	2450
	14	1.4474	0.8422	0.5619	0.3997	0.3719	0.1821	0.0815	2450
	21	1.3689	0.8426	0.5706	0.4074	0.3290	0.1831	0.0828	2450
	30	1.2936	0.8414	0.5804	0.4163	0.3010	0.1853	0.0846	2450
SOL-USD	7	1.8344	0.9877	0.6487	0.4595	0.5423	0.2112	0.0943	486
	14	1.6885	0.9766	0.6493	0.4620	0.4211	0.2057	0.0939	486
	21	1.5850	0.9713	0.6543	0.4670	0.3718	0.2054	0.0947	486
	30	1.4726	0.9539	0.6531	0.4679	0.3367	0.2040	0.0948	486

Table I.1: Term Structure of Implied Impermanent Loss Across Uniswap v3 Pools. The table reports average implied impermanent loss IIL^{v3} at maturities TTM $\in \{7, 14, 21, 30\}$ days for each pool and for different price ranges $\alpha \in \{0.2, 0.4, 0.6, 0.8\}$, as well as the up, dn, and v2 benchmarks. N indicates the number of daily observations used in the estimation. Panel A reports results for pools composed of two volatile tokens, while Panel B reports results for pools pairing a volatile token with a stablecoin.

I.2 7-Day Maturity

I.2.1 BTC-ETH

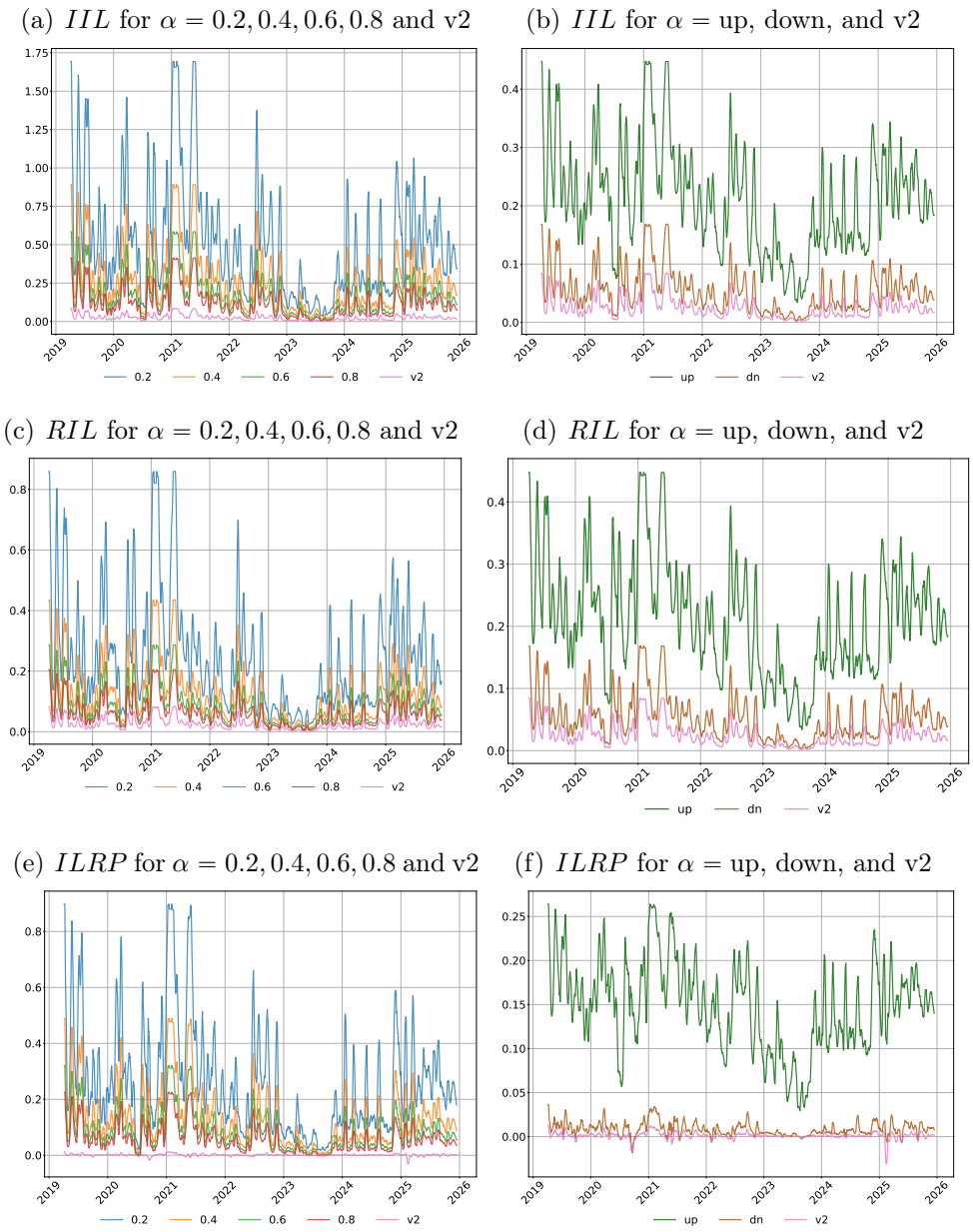

Figure I.4: IIL, RIL, ILRP for BTC-ETH across Ranges. The figure reports (top row) the implied impermanent loss IIL^{v3}, (middle row) the realized impermanent loss RIL^{v3}, and (bottom row) the impermanent loss risk premium $ILRP^{v3}$ for the BTC-ETH pool at a 7-day maturity. The left column shows $\alpha = 0.2, 0.4, 0.6, 0.8$ and the v2 benchmark, while the right column compares the up, down, and v2 ranges. The data are sampled daily over April 2019–December 2025 and smoothed using a 14-day rolling mean.

Series	α	Mean	Std	Q(0.001)	Q1	Median	Q3	Q(0.999)	N	Maturity
IIL	0.2	0.57	0.62	0.03	0.21	0.38	0.67	5.30	2396	7
IIL	0.4	0.29	0.35	0.01	0.10	0.19	0.34	3.29	2396	7
IIL	0.6	0.19	0.23	0.00	0.06	0.12	0.22	2.24	2396	7
IIL	0.8	0.13	0.17	0.00	0.04	0.08	0.15	1.61	2396	7
IIL	up	0.22	0.13	0.03	0.14	0.20	0.27	1.06	2396	7
IIL	dn	0.06	0.06	0.00	0.02	0.04	0.07	0.50	2396	7
IIL	v2	0.03	0.03	0.00	0.01	0.02	0.03	0.31	2396	7
RIL	0.2	0.27	0.29	0.01	0.10	0.18	0.32	2.47	2396	7
RIL	0.4	0.14	0.15	0.01	0.05	0.09	0.16	1.25	2396	7
RIL	0.6	0.09	0.10	0.00	0.03	0.06	0.11	0.82	2396	7
RIL	0.8	0.06	0.07	0.00	0.02	0.04	0.08	0.59	2396	7
RIL	up	0.07	0.07	0.00	0.03	0.05	0.08	0.55	2396	7
RIL	dn	0.05	0.05	0.00	0.02	0.03	0.06	0.41	2396	7
RIL	v2	0.03	0.03	0.00	0.01	0.02	0.03	0.23	2396	7
ILRP	0.2	0.30	0.34	-0.01	0.11	0.20	0.34	2.97	2396	7
ILRP	0.4	0.16	0.21	-0.00	0.05	0.10	0.17	2.10	2396	7
ILRP	0.6	0.10	0.14	-0.00	0.03	0.06	0.11	1.46	2396	7
ILRP	0.8	0.07	0.10	-0.01	0.02	0.04	0.08	1.06	2396	7
ILRP	up	0.15	0.07	0.02	0.11	0.15	0.19	0.66	2396	7
ILRP	dn	0.01	0.02	-0.05	0.00	0.01	0.01	0.15	2396	7
ILRP	v2	0.00	0.01	-0.06	-0.00	0.00	0.00	0.11	2396	7

Table I.2: Summary Statistics. IIL, RIL, ILRP for BTC-ETH across Ranges. The table presents the summary statistics for the implied impermanent loss, IIL^{v3}, the realized impermanent loss RIL^{v3}, and the impermanent loss risk premium $ILRP^{v3}$, for the BTC–SOL pool at a 7-day maturity under different concentration parameters α $(0.2, 0.4, 0.6, 0.8$, the up, down, and v2 benchmark). The implied quantities are computed using the equations in Section 5.1.3. The realized quantities are computed using the equations in Section 5.2.1. The data are sampled daily over the period from April 2019 to December 2025.

I.2.2 ETH-SOL

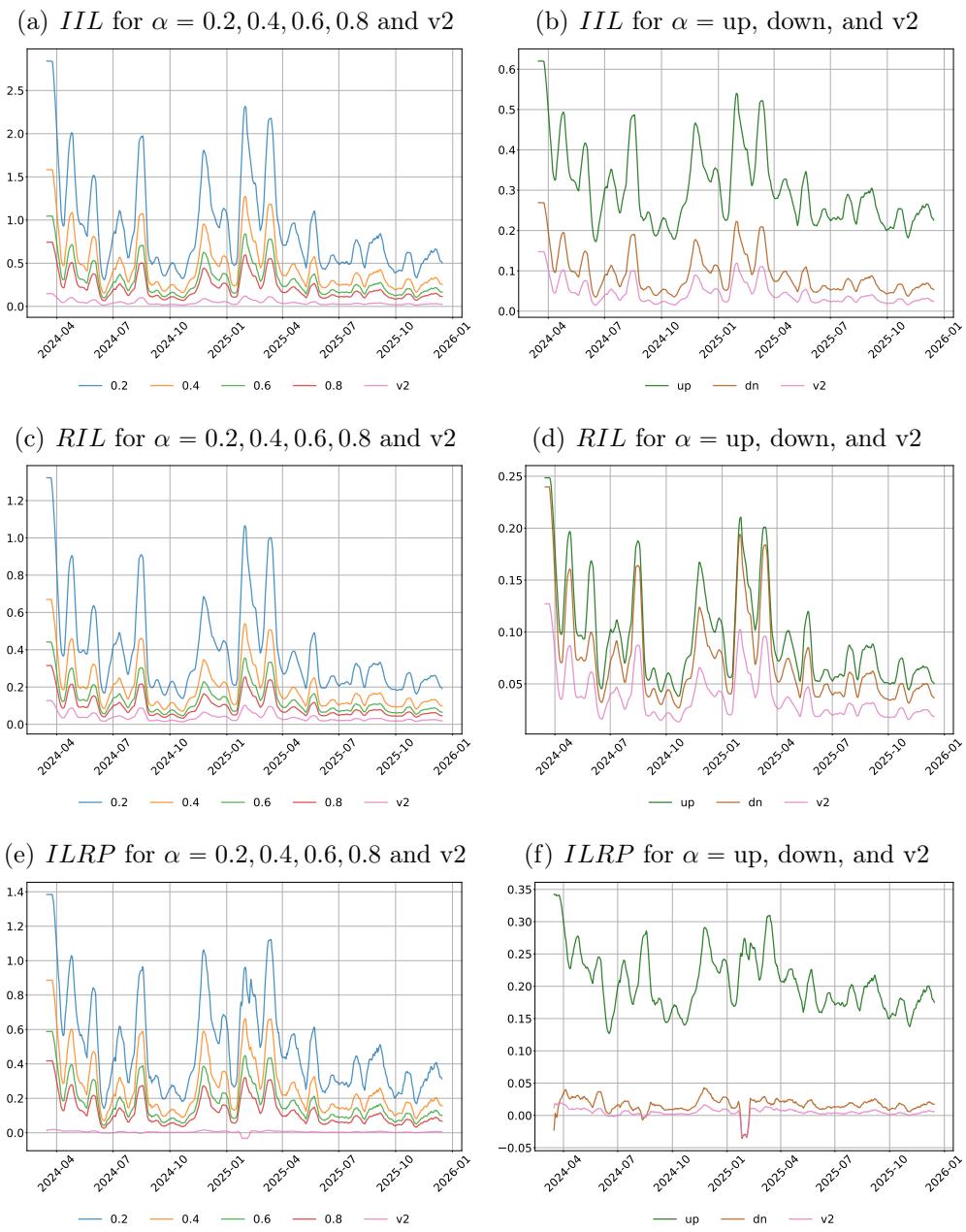

Figure I.5: IIL, RIL, ILRP for ETH-SOL across Ranges. The figure reports (top row) the implied impermanent loss IIL^{v3}, (middle row) the realized impermanent loss RIL^{v3}, and (bottom row) the impermanent loss risk premium $ILRP^{v3}$ for the ETH-SOL pool at a 7-day maturity. The left column shows $\alpha = 0.2, 0.4, 0.6, 0.8$ and the v2 benchmark, while the right column compares the up, down, and v2 ranges. The data are sampled daily over April 2019–December 2025 and smoothed using a 14-day rolling mean.

Series	α	Mean	Std	Q(0.001)	Q1	Median	Q3	Q(0.999)	N	Maturity
IIL	0.2	0.94	0.82	0.22	0.46	0.69	1.04	5.95	640	7
IIL	0.4	0.49	0.49	0.11	0.23	0.34	0.53	3.81	640	7
IIL	0.6	0.32	0.34	0.07	0.15	0.22	0.35	2.64	640	7
IIL	0.8	0.23	0.24	0.04	0.10	0.16	0.24	1.91	640	7
IIL	up	0.31	0.15	0.14	0.22	0.27	0.34	1.22	640	7
IIL	dn	0.09	0.08	0.02	0.05	0.07	0.11	0.56	640	7
IIL	v2	0.05	0.05	0.01	0.02	0.03	0.05	0.36	640	7
RIL	0.2	0.43	0.50	0.11	0.20	0.29	0.44	4.37	640	7
RIL	0.4	0.22	0.25	0.06	0.10	0.15	0.23	2.21	640	7
RIL	0.6	0.14	0.17	0.04	0.07	0.10	0.15	1.46	640	7
RIL	0.8	0.10	0.12	0.03	0.05	0.07	0.11	1.04	640	7
RIL	up	0.10	0.09	0.03	0.06	0.08	0.11	0.84	640	7
RIL	dn	0.08	0.08	0.02	0.04	0.05	0.08	0.65	640	7
RIL	v2	0.04	0.05	0.01	0.02	0.03	0.04	0.42	640	7
ILRP	0.2	0.51	0.39	0.01	0.25	0.38	0.61	2.45	640	7
ILRP	0.4	0.28	0.26	0.03	0.12	0.19	0.31	1.85	640	7
ILRP	0.6	0.18	0.18	0.02	0.08	0.12	0.20	1.34	640	7
ILRP	0.8	0.13	0.13	0.01	0.05	0.08	0.14	0.98	640	7
ILRP	up	0.21	0.07	0.10	0.16	0.19	0.23	0.53	640	7
ILRP	dn	0.02	0.02	-0.18	0.01	0.01	0.02	0.13	640	7
ILRP	v2	0.01	0.01	-0.13	0.00	0.00	0.01	0.06	640	7

Table I.3: Summary Statistics. IIL, RIL, ILRP for ETH-SOL across Ranges. The table presents the summary statistics for the implied impermanent loss, IIL^{v3}, the realized impermanent loss RIL^{v3}, and the impermanent loss risk premium $ILRP^{v3}$, for the ETH–SOL pool at a 7-day maturity under different concentration parameters α $(0.2, 0.4, 0.6, 0.8$, the up, down, and v2 benchmark). The implied quantities are computed using the equations in Section 5.1.3. The realized quantities are computed using the equations in Section 5.2.1. The data are sampled daily over the period from April 2019 to December 2025.

I.2.3 ETH-XRP

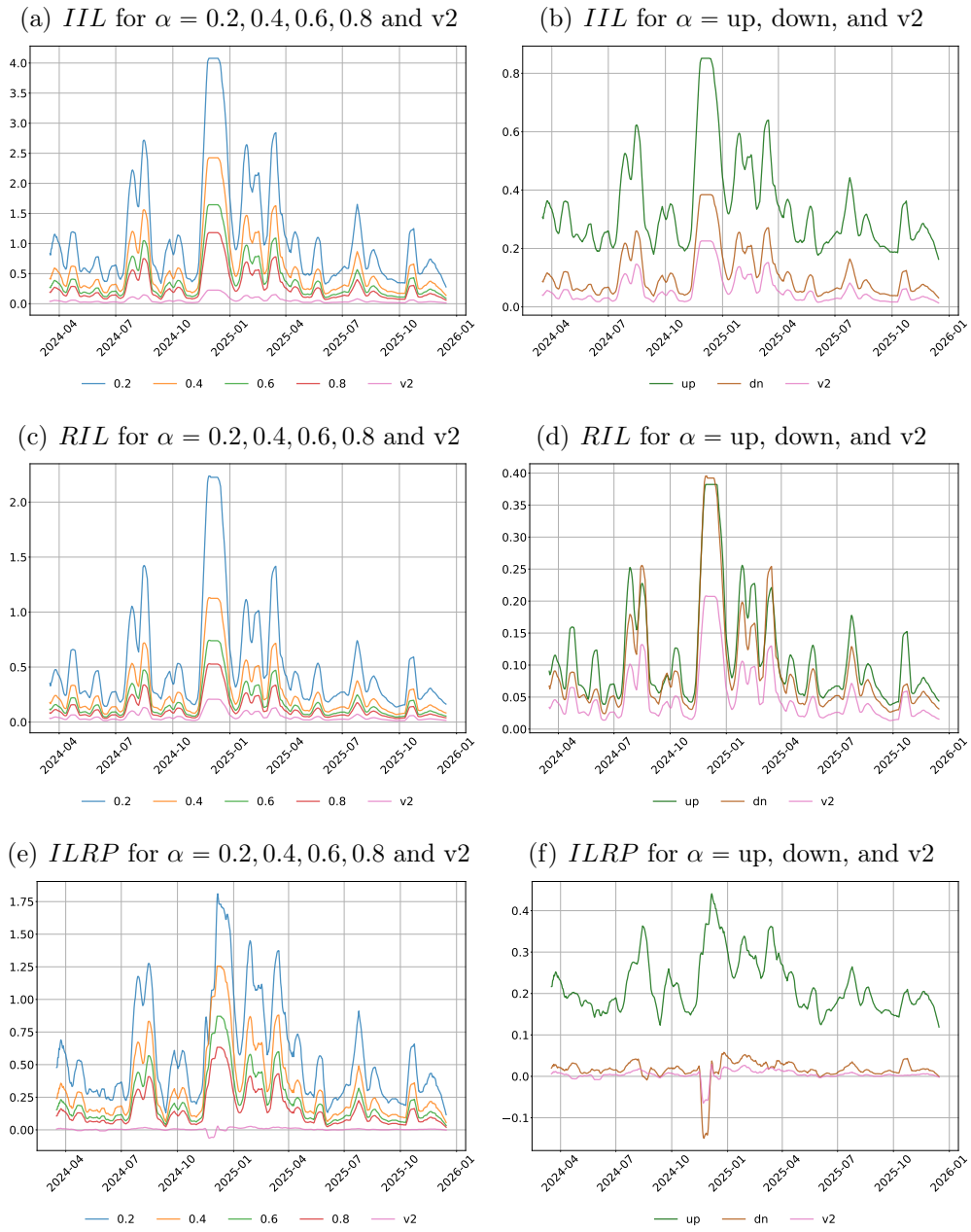

Figure I.6: IIL, RIL, ILRP for ETH-XRP across Ranges. The figure reports (top row) the implied impermanent loss IIL^{v3}, (middle row) the realized impermanent loss RIL^{v3}, and (bottom row) the impermanent loss risk premium $ILRP^{v3}$ for the ETH-XRP pool at a 7-day maturity. The left column shows $\alpha = 0.2, 0.4, 0.6, 0.8$ and the v2 benchmark, while the right column compares the up, down, and v2 ranges. The data are sampled daily over April 2019–December 2025 and smoothed using a 14-day rolling mean.

Series	α	Mean	Std	Q(0.001)	Q1	Median	Q3	Q(0.999)	N	Maturity
IIL	0.2	1.23	1.38	0.17	0.45	0.69	1.45	8.32	639	7
IIL	0.4	0.68	0.88	0.08	0.22	0.35	0.76	5.60	639	7
IIL	0.6	0.45	0.61	0.05	0.14	0.23	0.49	3.95	639	7
IIL	0.8	0.32	0.44	0.03	0.10	0.16	0.35	2.90	639	7
IIL	up	0.36	0.25	0.12	0.22	0.28	0.41	1.78	639	7
IIL	dn	0.12	0.13	0.02	0.05	0.07	0.15	0.79	639	7
IIL	v2	0.06	0.08	0.01	0.02	0.03	0.07	0.52	639	7
RIL	0.2	0.61	0.86	0.09	0.20	0.30	0.61	5.67	639	7
RIL	0.4	0.31	0.44	0.05	0.10	0.15	0.31	2.87	639	7
RIL	0.6	0.20	0.29	0.03	0.07	0.10	0.20	1.89	639	7
RIL	0.8	0.14	0.21	0.02	0.05	0.07	0.14	1.35	639	7
RIL	up	0.13	0.15	0.02	0.05	0.08	0.14	1.02	639	7
RIL	dn	0.10	0.14	0.02	0.04	0.06	0.11	0.95	639	7
RIL	v2	0.06	0.08	0.01	0.02	0.03	0.06	0.54	639	7
ILRP	0.2	0.62	0.65	-0.52	0.23	0.39	0.79	4.62	639	7
ILRP	0.4	0.37	0.49	0.02	0.12	0.20	0.42	3.61	639	7
ILRP	0.6	0.25	0.35	0.01	0.07	0.13	0.27	2.59	639	7
ILRP	0.8	0.18	0.26	0.00	0.05	0.09	0.19	1.90	639	7
ILRP	up	0.23	0.12	0.08	0.16	0.20	0.26	1.00	639	7
ILRP	dn	0.02	0.05	-0.45	0.01	0.01	0.03	0.20	639	7
ILRP	v2	0.01	0.03	-0.22	0.00	0.00	0.01	0.18	639	7

Table I.4: Summary Statistics. IIL, RIL, ILRP for ETH-XRP across Ranges. The table presents the summary statistics for the implied impermanent loss, IIL^{v3}, the realized impermanent loss RIL^{v3}, and the impermanent loss risk premium $ILRP^{v3}$, for the ETH–XRP pool at a 7-day maturity under different concentration parameters α $(0.2, 0.4, 0.6, 0.8$, the up, down, and v2 benchmark). The implied quantities are computed using the equations in Section 5.1.3. The realized quantities are computed using the equations in Section 5.2.1. The data are sampled daily over the period from April 2019 to December 2025.

I.2.4 ETH-BNB

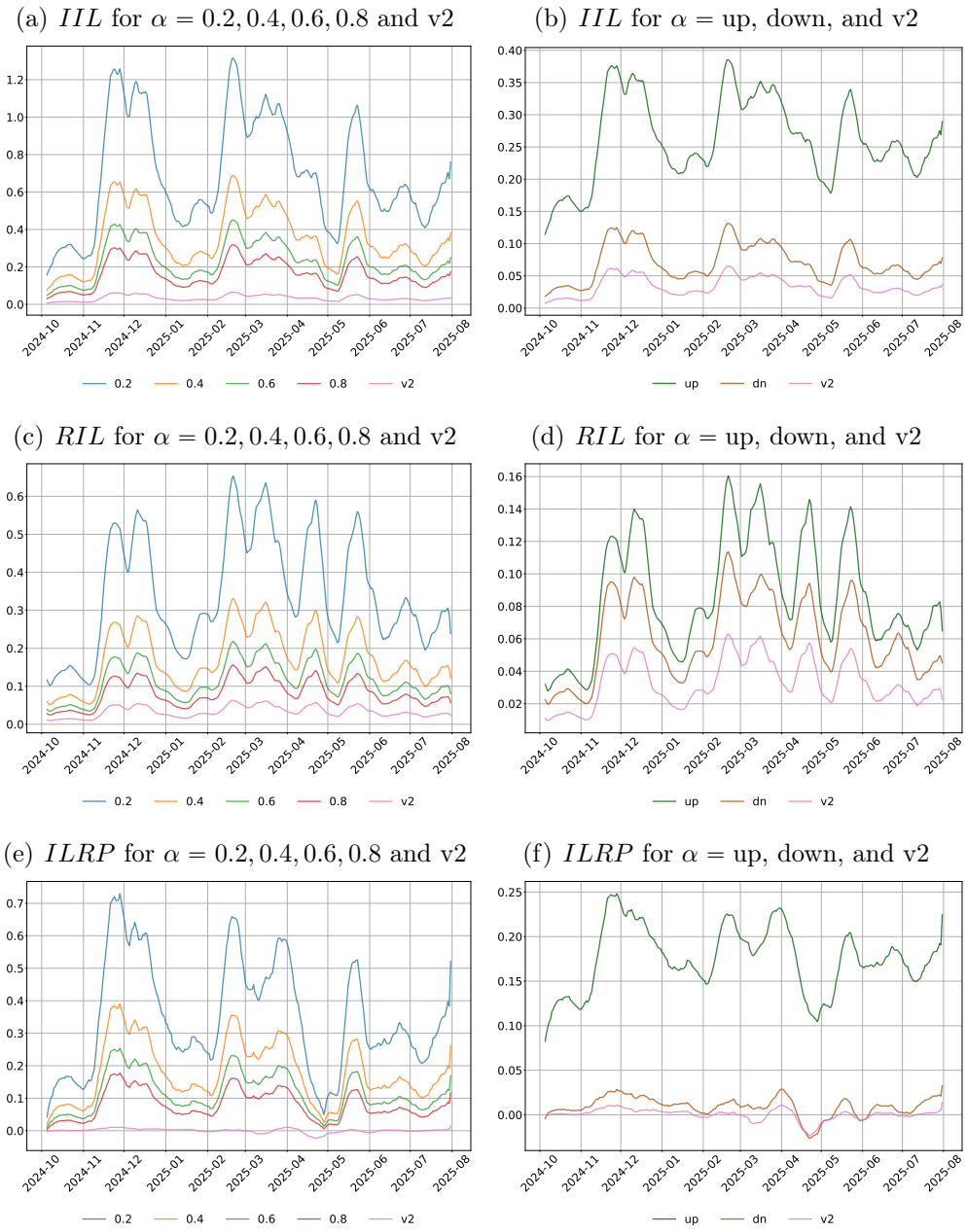

Figure I.7: IIL, RIL, ILRP for ETH-BNB across Ranges. The figure reports (top row) the implied impermanent loss IIL^{v3}, (middle row) the realized impermanent loss RIL^{v3}, and (bottom row) the impermanent loss risk premium $ILRP^{v3}$ for the ETH-BNB pool at a 7-day maturity. The left column shows $\alpha = 0.2, 0.4, 0.6, 0.8$ and the v2 benchmark, while the right column compares the up, down, and v2 ranges. The data are sampled daily over April 2019–December 2025 and smoothed using a 14-day rolling mean.

Series	α	Mean	Std	Q(0.001)	Q1	Median	Q3	Q(0.999)	N	Maturity
IIL	0.2	0.72	0.41	0.17	0.42	0.61	0.92	2.08	278	7
IIL	0.4	0.37	0.22	0.08	0.21	0.31	0.47	1.13	278	7
IIL	0.6	0.24	0.14	0.05	0.13	0.20	0.30	0.74	278	7
IIL	0.8	0.17	0.10	0.03	0.09	0.14	0.21	0.53	278	7
IIL	up	0.27	0.08	0.12	0.21	0.25	0.32	0.50	278	7
IIL	dn	0.07	0.04	0.02	0.04	0.06	0.09	0.21	278	7
IIL	v2	0.04	0.02	0.01	0.02	0.03	0.04	0.11	278	7
RIL	0.2	0.36	0.20	0.09	0.20	0.30	0.44	0.93	278	7
RIL	0.4	0.18	0.10	0.04	0.10	0.15	0.22	0.47	278	7
RIL	0.6	0.12	0.07	0.03	0.07	0.10	0.15	0.31	278	7
RIL	0.8	0.09	0.05	0.02	0.05	0.07	0.10	0.22	278	7
RIL	up	0.09	0.05	0.02	0.05	0.08	0.11	0.22	278	7
RIL	dn	0.06	0.03	0.02	0.04	0.06	0.08	0.16	278	7
RIL	v2	0.03	0.02	0.01	0.02	0.03	0.04	0.09	278	7
ILRP	0.2	0.37	0.24	-0.05	0.20	0.29	0.51	1.31	278	7
ILRP	0.4	0.19	0.13	-0.01	0.10	0.15	0.26	0.73	278	7
ILRP	0.6	0.12	0.09	-0.01	0.06	0.09	0.17	0.48	278	7
ILRP	0.8	0.08	0.06	-0.01	0.04	0.06	0.12	0.34	278	7
ILRP	up	0.18	0.05	0.08	0.15	0.17	0.21	0.32	278	7
ILRP	dn	0.01	0.02	-0.04	0.00	0.01	0.02	0.08	278	7
ILRP	v2	0.00	0.01	-0.04	-0.00	0.00	0.00	0.04	278	7

Table I.5: Summary Statistics. IIL, RIL, ILRP for ETH-BNB across Ranges. The table presents the summary statistics for the implied impermanent loss, IIL^{v3}, the realized impermanent loss RIL^{v3}, and the impermanent loss risk premium $ILRP^{v3}$, for the ETH–BNB pool at a 7-day maturity under different concentration parameters α $(0.2, 0.4, 0.6, 0.8$, the up, down, and v2 benchmark). The implied quantities are computed using the equations in Section 5.1.3. The realized quantities are computed using the equations in Section 5.2.1. The data are sampled daily over the period from April 2019 to December 2025.

I.2.5 BTC-USD

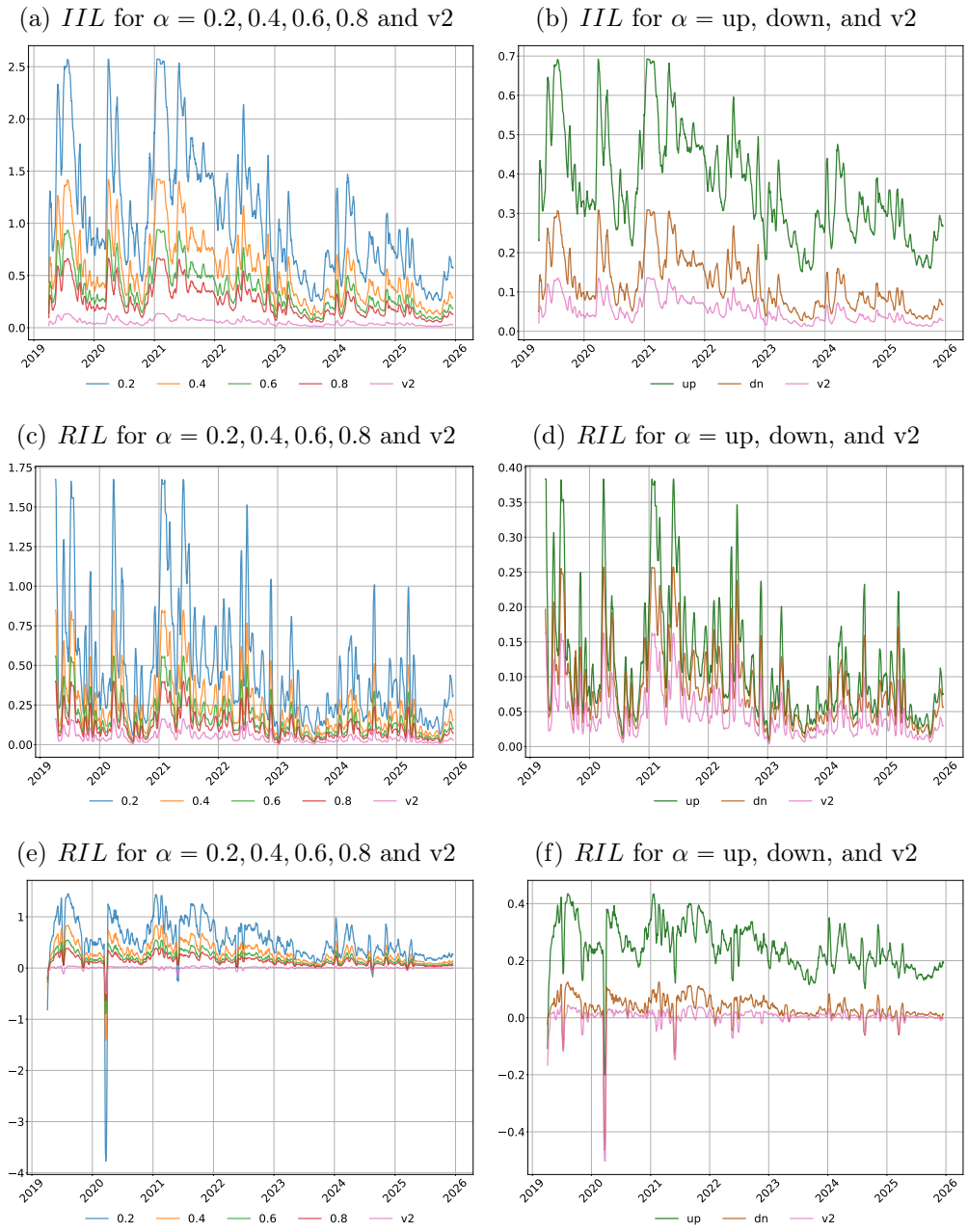

Figure I.8: IIL, RIL, ILRP for BTC-USD across Ranges. The figure reports (top row) the implied impermanent loss IIL^{v3}, (middle row) the realized impermanent loss RIL^{v3}, and (bottom row) the impermanent loss risk premium $ILRP^{v3}$ for the BTC-USD pool at a 7-day maturity. The left column shows $\alpha = 0.2, 0.4, 0.6, 0.8$ and the v2 benchmark, while the right column compares the up, down, and v2 ranges. The data are sampled daily over April 2019–December 2025 and smoothed using a 14-day rolling mean.

Series	α	Mean	Std	Q(0.001)	Q1	Median	Q3	Q(0.999)	N	Maturity
IIL	0.2	1.10	0.81	0.19	0.57	0.88	1.42	6.22	2445	7
IIL	0.4	0.59	0.49	0.09	0.29	0.45	0.74	3.98	2445	7
IIL	0.6	0.38	0.33	0.06	0.19	0.29	0.48	2.71	2445	7
IIL	0.8	0.27	0.23	0.04	0.13	0.20	0.34	1.94	2445	7
IIL	up	0.38	0.17	0.13	0.26	0.34	0.46	1.42	2445	7
IIL	dn	0.13	0.10	0.02	0.07	0.10	0.16	0.86	2445	7
IIL	v2	0.06	0.05	0.01	0.03	0.04	0.07	0.39	2445	7
RIL	0.2	0.55	0.90	0.03	0.20	0.33	0.59	14.27	2445	7
RIL	0.4	0.28	0.45	0.02	0.10	0.17	0.30	7.22	2445	7
RIL	0.6	0.18	0.30	0.01	0.07	0.11	0.20	4.76	2445	7
RIL	0.8	0.13	0.21	0.01	0.05	0.08	0.14	3.39	2445	7
RIL	up	0.13	0.16	0.01	0.05	0.08	0.14	2.13	2445	7
RIL	dn	0.09	0.12	0.01	0.04	0.06	0.10	1.82	2445	7
RIL	v2	0.05	0.09	0.00	0.02	0.03	0.06	1.36	2445	7
ILRP	0.2	0.55	0.64	-6.92	0.28	0.48	0.81	3.10	2445	7
ILRP	0.4	0.31	0.33	-2.69	0.14	0.25	0.43	2.05	2445	7
ILRP	0.6	0.20	0.22	-1.71	0.09	0.16	0.28	1.39	2445	7
ILRP	0.8	0.14	0.16	-1.22	0.06	0.11	0.20	1.00	2445	7
ILRP	up	0.25	0.11	-0.62	0.19	0.24	0.31	0.72	2445	7
ILRP	dn	0.04	0.08	-0.85	0.01	0.03	0.06	0.37	2445	7
ILRP	v2	0.00	0.06	-0.87	-0.00	0.01	0.02	0.12	2445	7

Table I.6: Summary Statistics. IIL, RIL, ILRP for BTC-USD across Ranges. The table presents the summary statistics for the implied impermanent loss, IIL^{v3}, the realized impermanent loss RIL^{v3}, and the impermanent loss risk premium $ILRP^{v3}$, for the BTC–USD pool at a 7-day maturity under different concentration parameters α $(0.2, 0.4, 0.6, 0.8$, the up, down, and v2 benchmark). The implied quantities are computed using the equations in Section 5.1.3. The realized quantities are computed using the equations in Section 5.2.1. The data are sampled daily over the period from April 2019 to December 2025.

I.2.6 ETH-USD

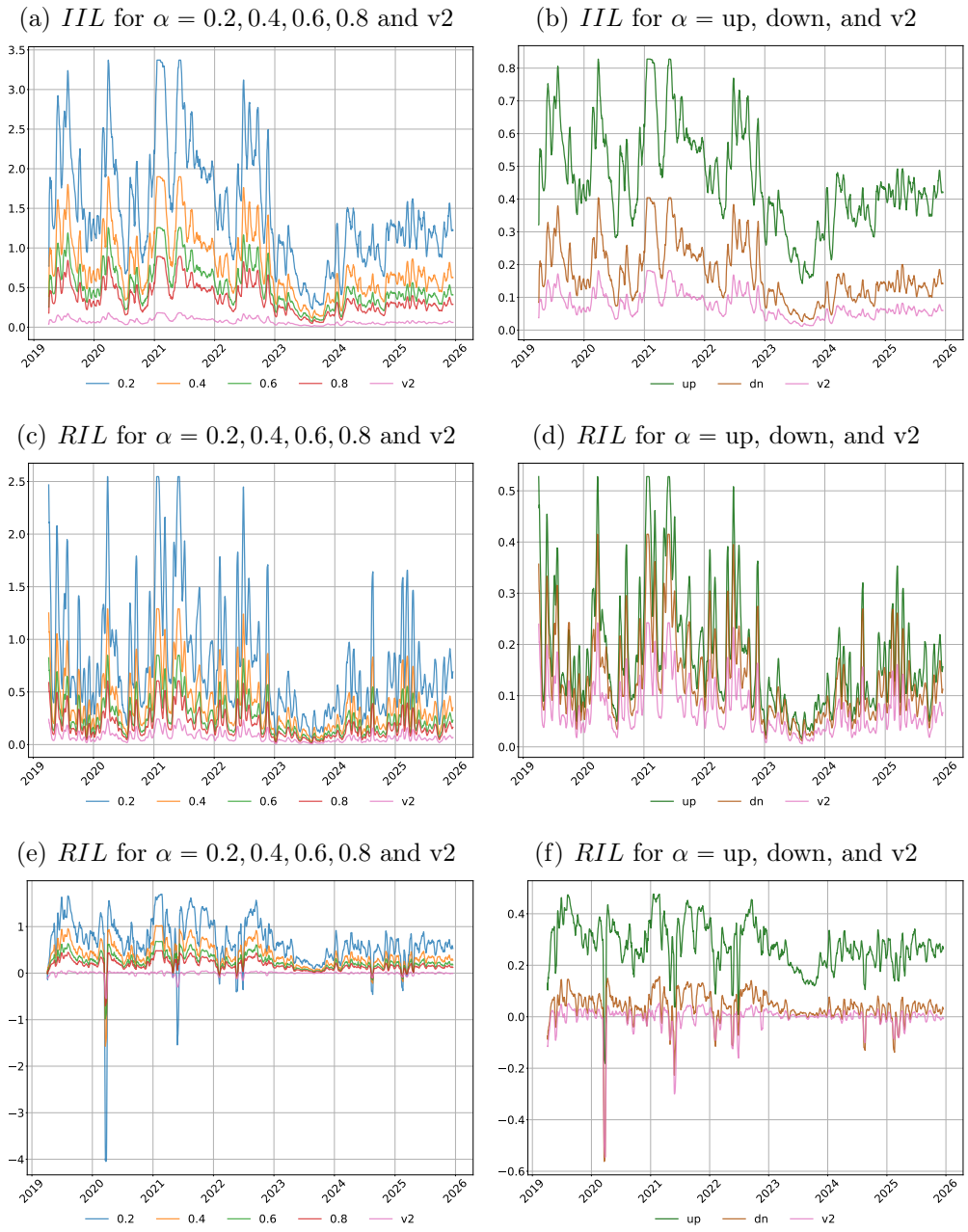

Figure I.9: IIL, RIL, ILRP for ETH-USD across Ranges. The figure reports (top row) the implied impermanent loss IIL^{v3}, (middle row) the realized impermanent loss RIL^{v3}, and (bottom row) the impermanent loss risk premium $ILRP^{v3}$ for the ETH-USD pool at a 7-day maturity. The left column shows $\alpha = 0.2, 0.4, 0.6, 0.8$ and the v2 benchmark, while the right column compares the up, down, and v2 ranges. The data are sampled daily over April 2019–December 2025 and smoothed using a 14-day rolling mean.

Series	α	Mean	Std	Q(0.001)	Q1	Median	Q3	Q(0.999)	N	Maturity
IIL	0.2	1.57	1.04	0.19	0.94	1.30	1.94	8.03	2445	7
IIL	0.4	0.85	0.66	0.10	0.48	0.67	1.03	5.63	2445	7
IIL	0.6	0.56	0.45	0.06	0.31	0.44	0.68	3.99	2445	7
IIL	0.8	0.39	0.32	0.04	0.22	0.31	0.48	2.85	2445	7
IIL	up	0.48	0.21	0.13	0.36	0.44	0.56	1.71	2445	7
IIL	dn	0.19	0.15	0.02	0.11	0.15	0.23	1.41	2445	7
IIL	v2	0.08	0.06	0.01	0.05	0.06	0.10	0.58	2445	7
RIL	0.2	0.87	1.18	0.04	0.36	0.57	0.97	15.36	2445	7
RIL	0.4	0.44	0.60	0.02	0.18	0.29	0.49	7.77	2445	7
RIL	0.6	0.29	0.39	0.01	0.12	0.19	0.33	5.11	2445	7
RIL	0.8	0.21	0.28	0.01	0.09	0.14	0.23	3.64	2445	7
RIL	up	0.19	0.20	0.01	0.09	0.14	0.23	2.10	2445	7
RIL	dn	0.14	0.17	0.01	0.06	0.10	0.16	2.05	2445	7
RIL	v2	0.08	0.11	0.00	0.03	0.05	0.09	1.43	2445	7
ILRP	0.2	0.70	0.80	-8.13	0.39	0.66	1.01	3.63	2445	7
ILRP	0.4	0.41	0.43	-3.26	0.21	0.35	0.56	2.75	2445	7
ILRP	0.6	0.27	0.29	-2.08	0.14	0.23	0.37	1.93	2445	7
ILRP	0.8	0.19	0.21	-1.48	0.09	0.16	0.26	1.38	2445	7
ILRP	up	0.28	0.13	-0.57	0.22	0.28	0.35	0.83	2445	7
ILRP	dn	0.04	0.10	-1.09	0.01	0.04	0.08	0.51	2445	7
ILRP	v2	-0.00	0.07	-0.93	-0.01	0.01	0.02	0.16	2445	7

Table I.7: Summary Statistics. IIL, RIL, ILRP for ETH-USD across Ranges. The table presents the summary statistics for the implied impermanent loss, IIL^{v3}, the realized impermanent loss RIL^{v3}, and the impermanent loss risk premium $ILRP^{v3}$, for the ETH–USD pool at a 7-day maturity under different concentration parameters α $(0.2, 0.4, 0.6, 0.8$, the up, down, and v2 benchmark). The implied quantities are computed using the equations in Section 5.1.3. The realized quantities are computed using the equations in Section 5.2.1. The data are sampled daily over the period from April 2019 to December 2025.

I.2.7 SOL-USD

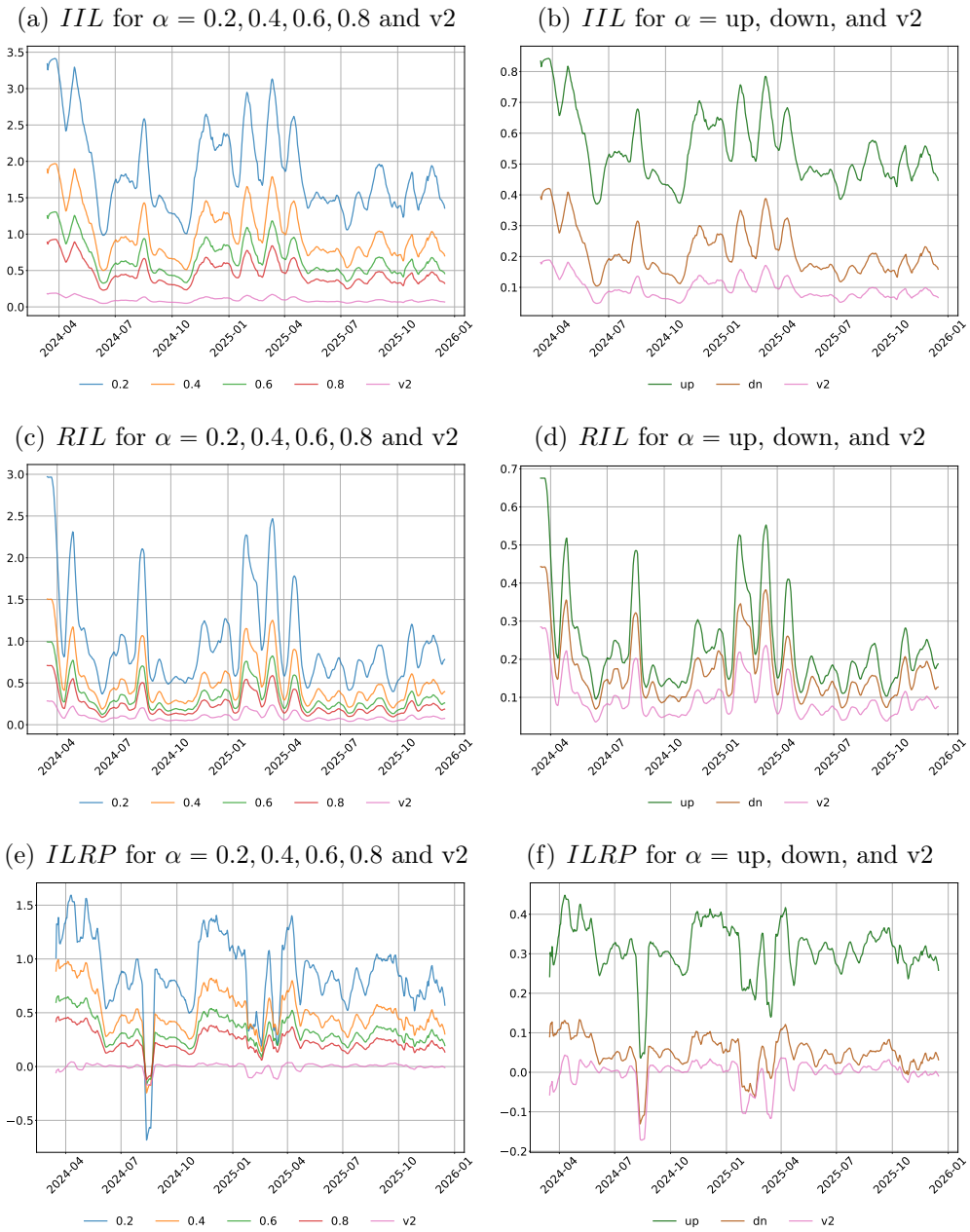

Figure I.10: IIL, RIL, ILRP for SOL-USD across Ranges. The figure reports (top row) the implied impermanent loss IIL^{v3}, (middle row) the realized impermanent loss RIL^{v3}, and (bottom row) the impermanent loss risk premium $ILRP^{v3}$ for the SOL-USD pool at a 7-day maturity. The left column shows $\alpha = 0.2, 0.4, 0.6, 0.8$ and the v2 benchmark, while the right column compares the up, down, and v2 ranges. The data are sampled daily over April 2019–December 2025 and smoothed using a 14-day rolling mean.

Series	α	Mean	Std	Q(0.001)	Q1	Median	Q3	Q(0.999)	N	Maturity
IIL	0.2	1.90	0.77	0.83	1.36	1.69	2.21	5.15	640	7
IIL	0.4	1.03	0.48	0.42	0.71	0.89	1.20	3.16	640	7
IIL	0.6	0.67	0.32	0.27	0.46	0.58	0.79	2.13	640	7
IIL	0.8	0.48	0.23	0.19	0.33	0.41	0.56	1.51	640	7
IIL	up	0.55	0.15	0.33	0.45	0.52	0.62	1.17	640	7
IIL	dn	0.22	0.10	0.09	0.15	0.19	0.25	0.70	640	7
IIL	v2	0.10	0.05	0.04	0.07	0.08	0.11	0.31	640	7
RIL	0.2	1.04	0.87	0.26	0.58	0.80	1.04	5.36	640	7
RIL	0.4	0.53	0.44	0.13	0.30	0.40	0.53	2.72	640	7
RIL	0.6	0.35	0.29	0.09	0.20	0.27	0.35	1.79	640	7
RIL	0.8	0.25	0.21	0.06	0.14	0.19	0.25	1.28	640	7
RIL	up	0.24	0.17	0.07	0.15	0.20	0.25	1.04	640	7
RIL	dn	0.17	0.12	0.05	0.10	0.14	0.18	0.70	640	7
RIL	v2	0.10	0.08	0.02	0.06	0.08	0.10	0.52	640	7
ILRP	0.2	0.86	0.55	-2.50	0.62	0.87	1.15	2.14	640	7
ILRP	0.4	0.50	0.30	-1.15	0.34	0.48	0.65	1.65	640	7
ILRP	0.6	0.33	0.20	-0.76	0.22	0.31	0.42	1.13	640	7
ILRP	0.8	0.23	0.14	-0.55	0.15	0.22	0.30	0.80	640	7
ILRP	up	0.31	0.11	-0.31	0.27	0.31	0.37	0.57	640	7
ILRP	dn	0.05	0.07	-0.35	0.02	0.05	0.08	0.24	640	7
ILRP	v2	-0.00	0.06	-0.37	-0.01	0.01	0.02	0.07	640	7

Table I.8: Summary Statistics. IIL, RIL, ILRP for SOL-USD across Ranges. The table presents the summary statistics for the implied impermanent loss, IIL^{v3}, the realized impermanent loss RIL^{v3}, and the impermanent loss risk premium $ILRP^{v3}$, for the SOL–USD pool at a 7-day maturity under different concentration parameters α $(0.2, 0.4, 0.6, 0.8$, the up, down, and v2 benchmark). The implied quantities are computed using the equations in Section 5.1.3. The realized quantities are computed using the equations in Section 5.2.1. The data are sampled daily over the period from April 2019 to December 2025.

I.3 30-Day Maturity

Pool	Start date	End date	N
BTC-ETH	2019-04-16	2025-12-15	2434
ETH-SOL	2024-04-13	2025-12-15	479
ETH-XRP	2024-04-13	2025-12-15	484
ETH-BNB	2024-10-17	2025-06-25	188
BTC-USD	2019-04-01	2025-12-16	2450
ETH-USD	2019-04-01	2025-12-16	2450
SOL-USD	2024-03-22	2025-12-16	486

Table I.9: Data Availability. Start and end dates of the sample period for each pool at a 30-day maturity, along with the corresponding number of daily observations (N).

I.3.1 BTC-ETH

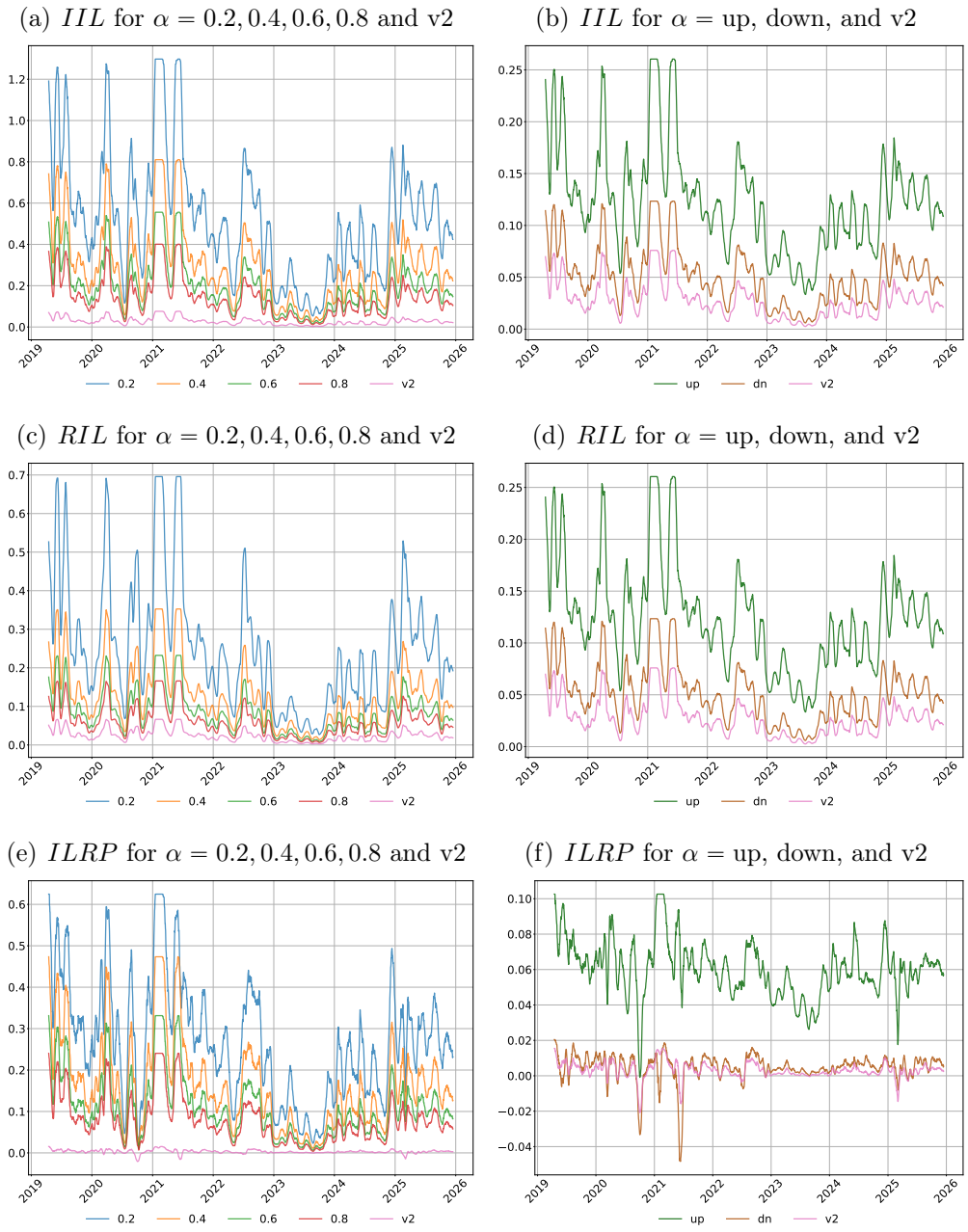

Figure I.11: IIL, RIL, ILRP for BTC-ETH across Ranges. The figure reports (top row) the implied impermanent loss IIL^{v3}, (middle row) the realized impermanent loss RIL^{v3}, and (bottom row) the impermanent loss risk premium $ILRP^{v3}$ for the BTC-ETH pool at a 30-day maturity. The left column shows $\alpha = 0.2, 0.4, 0.6, 0.8$ and the v2 benchmark, while the right column compares the up, down, and v2 ranges. The data are sampled daily over April 2019–December 2025 and smoothed using a 14-day rolling mean.

Series	α	Mean	Std	Q(0.001)	Q1	Median	Q3	Q(0.999)	N	Maturity
IIL	0.2	0.55	0.39	0.04	0.29	0.49	0.67	2.63	2434	30
IIL	0.4	0.31	0.26	0.02	0.15	0.26	0.37	1.89	2434	30
IIL	0.6	0.21	0.18	0.01	0.10	0.17	0.24	1.39	2434	30
IIL	0.8	0.15	0.13	0.01	0.07	0.12	0.17	1.03	2434	30
IIL	up	0.13	0.07	0.03	0.09	0.12	0.14	0.61	2434	30
IIL	dn	0.05	0.04	0.00	0.03	0.05	0.06	0.25	2434	30
IIL	v2	0.03	0.02	0.00	0.01	0.02	0.03	0.18	2434	30
RIL	0.2	0.27	0.22	0.02	0.13	0.23	0.32	1.36	2434	30
RIL	0.4	0.14	0.11	0.01	0.06	0.12	0.16	0.69	2434	30
RIL	0.6	0.09	0.07	0.01	0.04	0.08	0.11	0.45	2434	30
RIL	0.8	0.06	0.05	0.00	0.03	0.06	0.08	0.32	2434	30
RIL	up	0.07	0.05	0.00	0.03	0.06	0.08	0.31	2434	30
RIL	dn	0.05	0.04	0.00	0.02	0.04	0.06	0.23	2434	30
RIL	v2	0.03	0.02	0.00	0.01	0.02	0.03	0.13	2434	30
ILRP	0.2	0.28	0.19	-0.05	0.16	0.25	0.35	1.49	2434	30
ILRP	0.4	0.18	0.16	-0.02	0.08	0.14	0.21	1.28	2434	30
ILRP	0.6	0.12	0.12	-0.01	0.05	0.09	0.14	0.98	2434	30
ILRP	0.8	0.09	0.09	-0.01	0.04	0.07	0.10	0.74	2434	30
ILRP	up	0.06	0.03	-0.01	0.05	0.06	0.07	0.36	2434	30
ILRP	dn	0.01	0.01	-0.06	0.00	0.00	0.01	0.07	2434	30
ILRP	v2	0.00	0.01	-0.03	0.00	0.00	0.01	0.07	2434	30

Table I.10: Summary Statistics. IIL, RIL, ILRP for BTC-ETH across Ranges. The table presents the summary statistics for the implied impermanent loss, IIL^{v3}, the realized impermanent loss RIL^{v3}, and the impermanent loss risk premium $ILRP^{v3}$, for the BTC–SOL pool at a 30-day maturity under different concentration parameters α $(0.2, 0.4, 0.6, 0.8$, the up, down, and v2 benchmark). The implied quantities are computed using the equations in Section 5.1.3. The realized quantities are computed using the equations in Section 5.2.1. The data are sampled daily over the period from April 2019 to December 2025.

I.3.2 ETH-SOL

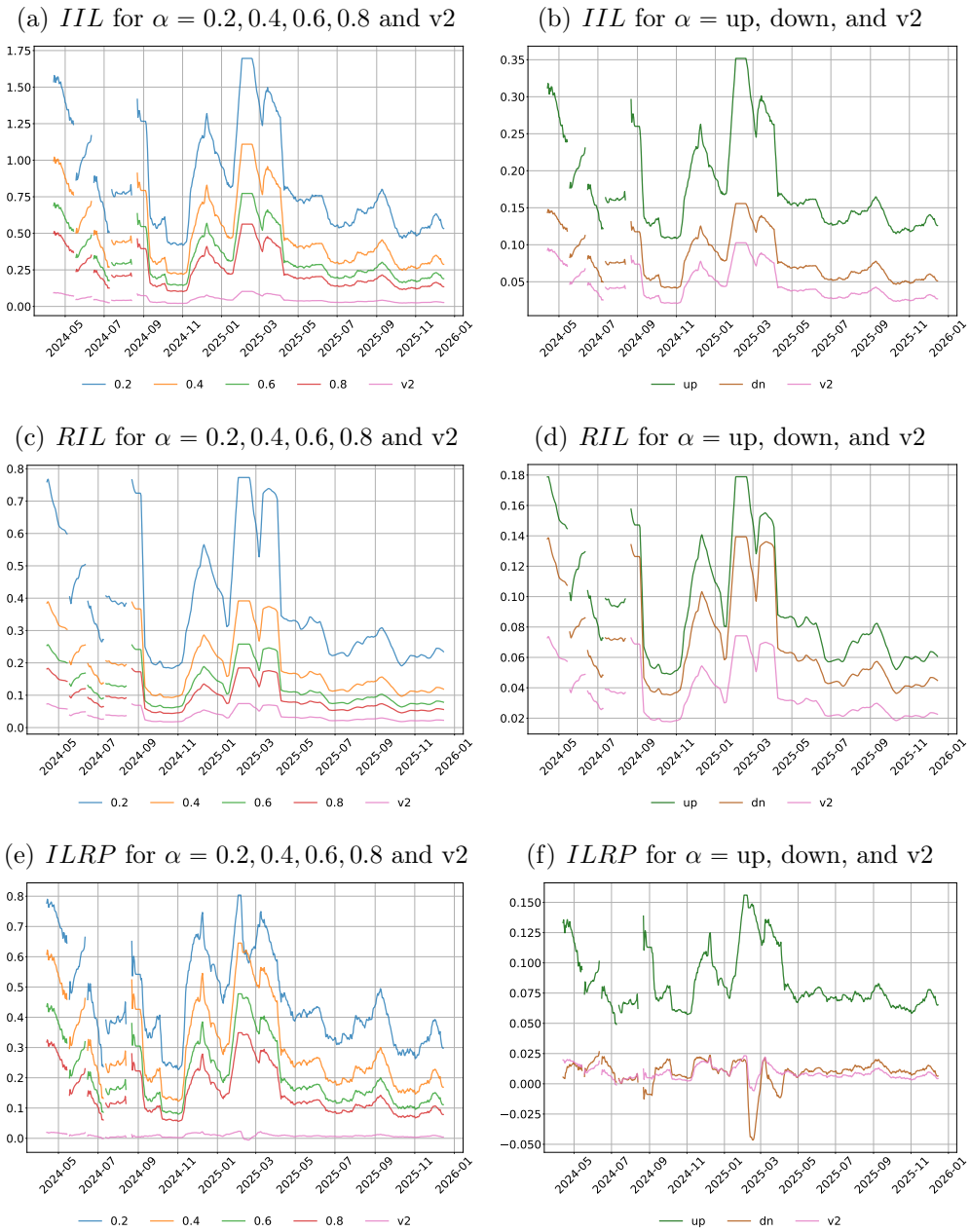

Figure I.12: IIL, RIL, ILRP for ETH-SOL across Ranges. The figure reports (top row) the implied impermanent loss IIL^{v3}, (middle row) the realized impermanent loss RIL^{v3}, and (bottom row) the impermanent loss risk premium $ILRP^{v3}$ for the ETH-SOL pool at a 30-day maturity. The left column shows $\alpha = 0.2, 0.4, 0.6, 0.8$ and the v2 benchmark, while the right column compares the up, down, and v2 ranges. The data are sampled daily over April 2019–December 2025 and smoothed using a 14-day rolling mean.

Series	α	Mean	Std	Q(0.001)	Q1	Median	Q3	Q(0.999)	N	Maturity
IIL	0.2	0.83	0.41	0.36	0.55	0.71	0.98	2.51	479	30
IIL	0.4	0.49	0.29	0.18	0.30	0.40	0.57	1.79	479	30
IIL	0.6	0.33	0.21	0.12	0.20	0.26	0.38	1.31	479	30
IIL	0.8	0.24	0.16	0.09	0.14	0.19	0.27	0.98	479	30
IIL	up	0.18	0.08	0.10	0.13	0.15	0.19	0.60	479	30
IIL	dn	0.08	0.04	0.04	0.05	0.07	0.09	0.23	479	30
IIL	v2	0.05	0.03	0.02	0.03	0.04	0.05	0.17	479	30
RIL	0.2	0.38	0.25	0.17	0.23	0.30	0.41	1.46	479	30
RIL	0.4	0.19	0.13	0.09	0.11	0.15	0.21	0.74	479	30
RIL	0.6	0.13	0.08	0.06	0.08	0.10	0.14	0.49	479	30
RIL	0.8	0.09	0.06	0.04	0.05	0.07	0.10	0.35	479	30
RIL	up	0.09	0.05	0.05	0.06	0.08	0.10	0.30	479	30
RIL	dn	0.07	0.04	0.03	0.04	0.06	0.08	0.23	479	30
RIL	v2	0.04	0.02	0.02	0.02	0.03	0.04	0.14	479	30
ILRP	0.2	0.45	0.19	0.18	0.32	0.41	0.54	1.29	479	30
ILRP	0.4	0.30	0.17	0.09	0.18	0.24	0.36	1.16	479	30
ILRP	0.6	0.20	0.13	0.06	0.12	0.16	0.24	0.90	479	30
ILRP	0.8	0.15	0.10	0.04	0.08	0.11	0.17	0.68	479	30
ILRP	up	0.09	0.04	0.05	0.06	0.07	0.09	0.35	479	30
ILRP	dn	0.01	0.01	-0.06	0.00	0.01	0.02	0.04	479	30
ILRP	v2	0.01	0.01	-0.02	0.00	0.01	0.01	0.06	479	30

Table I.11: Summary Statistics. IIL, RIL, ILRP for ETH-SOL across Ranges. The table presents the summary statistics for the implied impermanent loss, IIL^{v3}, the realized impermanent loss RIL^{v3}, and the impermanent loss risk premium $ILRP^{v3}$, for the ETH–SOL pool at a 30-day maturity under different concentration parameters α $(0.2, 0.4, 0.6, 0.8$, the up, down, and v2 benchmark). The implied quantities are computed using the equations in Section 5.1.3. The realized quantities are computed using the equations in Section 5.2.1. The data are sampled daily over the period from April 2019 to December 2025.

I.3.3 ETH-XRP

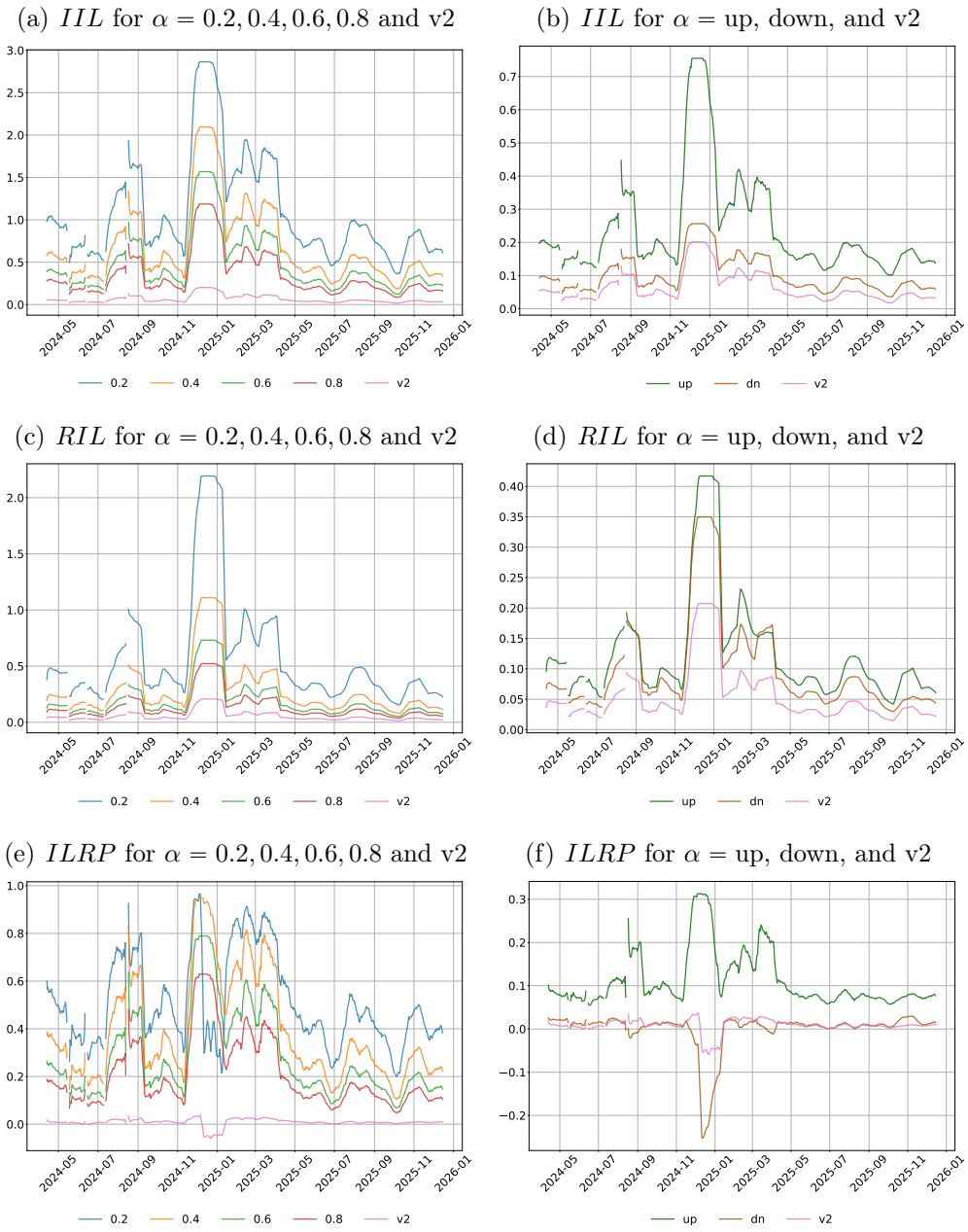

Figure I.13: IIL, RIL, ILRP for ETH-XRP across Ranges. The figure reports (top row) the implied impermanent loss IIL^{v3}, (middle row) the realized impermanent loss RIL^{v3}, and (bottom row) the impermanent loss risk premium $ILRP^{v3}$ for the ETH-XRP pool at a 30-day maturity. The left column shows $\alpha = 0.2, 0.4, 0.6, 0.8$ and the v2 benchmark, while the right column compares the up, down, and v2 ranges. The data are sampled daily over April 2019–December 2025 and smoothed using a 14-day rolling mean.

Series	α	Mean	Std	Q(0.001)	Q1	Median	Q3	Q(0.999)	N	Maturity
IIL	0.2	1.10	0.78	0.32	0.66	0.84	1.25	4.65	484	30
IIL	0.4	0.70	0.61	0.16	0.37	0.48	0.77	3.63	484	30
IIL	0.6	0.49	0.47	0.11	0.24	0.32	0.52	2.83	484	30
IIL	0.8	0.36	0.36	0.08	0.17	0.23	0.38	2.20	484	30
IIL	up	0.25	0.23	0.09	0.15	0.17	0.24	1.53	484	30
IIL	dn	0.10	0.07	0.03	0.06	0.08	0.12	0.39	484	30
IIL	v2	0.07	0.06	0.02	0.03	0.04	0.07	0.35	484	30
RIL	0.2	0.59	0.67	0.14	0.28	0.36	0.56	3.94	484	30
RIL	0.4	0.30	0.34	0.07	0.14	0.18	0.28	2.00	484	30
RIL	0.6	0.20	0.22	0.05	0.09	0.12	0.19	1.32	484	30
RIL	0.8	0.14	0.16	0.03	0.07	0.09	0.13	0.94	484	30
RIL	up	0.13	0.12	0.04	0.07	0.09	0.13	0.72	484	30
RIL	dn	0.10	0.11	0.03	0.05	0.06	0.10	0.63	484	30
RIL	v2	0.06	0.06	0.01	0.03	0.03	0.05	0.37	484	30
ILRP	0.2	0.51	0.26	-0.16	0.35	0.45	0.60	1.76	484	30
ILRP	0.4	0.40	0.30	0.09	0.21	0.29	0.49	2.03	484	30
ILRP	0.6	0.29	0.26	0.06	0.14	0.20	0.34	1.77	484	30
ILRP	0.8	0.22	0.21	0.04	0.10	0.14	0.25	1.44	484	30
ILRP	up	0.12	0.12	0.03	0.07	0.08	0.12	0.95	484	30
ILRP	dn	0.00	0.05	-0.29	0.00	0.01	0.02	0.05	484	30
ILRP	v2	0.01	0.02	-0.10	0.00	0.01	0.02	0.08	484	30

Table I.12: Summary Statistics. IIL, RIL, ILRP for ETH-XRP across Ranges. The table presents the summary statistics for the implied impermanent loss, IIL^{v3}, the realized impermanent loss RIL^{v3}, and the impermanent loss risk premium $ILRP^{v3}$, for the ETH–XRP pool at a 30-day maturity under different concentration parameters α ($0.2, 0.4, 0.6, 0.8$, the up, down, and v2 benchmark). The implied quantities are computed using the equations in Section 5.1.3. The realized quantities are computed using the equations in Section 5.2.1. The data are sampled daily over the period from April 2019 to December 2025.

I.3.4 ETH-BNB

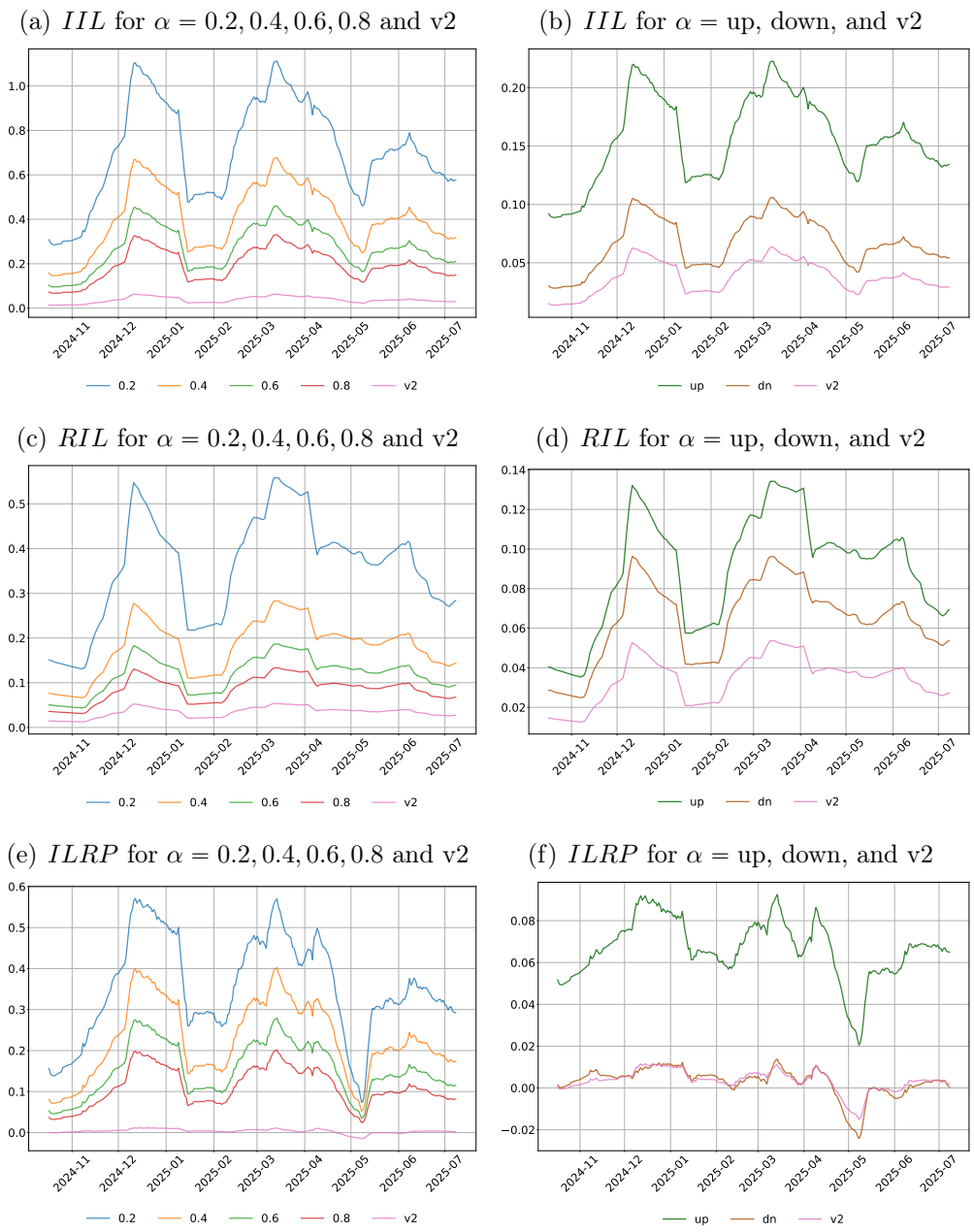

Figure I.14: IIL, RIL, ILRP for ETH-BNB across Ranges. The figure reports (top row) the implied impermanent loss IIL^{v3}, (middle row) the realized impermanent loss RIL^{v3}, and (bottom row) the impermanent loss risk premium $ILRP^{v3}$ for the ETH-BNB pool at a 30-day maturity. The left column shows $\alpha = 0.2, 0.4, 0.6, 0.8$ and the v2 benchmark, while the right column compares the up, down, and v2 ranges. The data are sampled daily over April 2019–December 2025 and smoothed using a 14-day rolling mean.

Series	α	Mean	Std	Q(0.001)	Q1	Median	Q3	Q(0.999)	N	Maturity
IIL	0.2	0.73	0.24	0.28	0.54	0.71	0.90	1.30	188	30
IIL	0.4	0.42	0.16	0.14	0.30	0.40	0.53	0.82	188	30
IIL	0.6	0.28	0.11	0.09	0.20	0.27	0.35	0.57	188	30
IIL	0.8	0.20	0.08	0.06	0.14	0.19	0.25	0.41	188	30
IIL	up	0.16	0.04	0.09	0.13	0.16	0.19	0.26	188	30
IIL	dn	0.07	0.02	0.03	0.05	0.07	0.09	0.13	188	30
IIL	v2	0.04	0.01	0.01	0.03	0.04	0.05	0.08	188	30
RIL	0.2	0.37	0.12	0.13	0.29	0.38	0.44	0.60	188	30
RIL	0.4	0.19	0.06	0.06	0.14	0.19	0.22	0.30	188	30
RIL	0.6	0.12	0.04	0.04	0.10	0.13	0.15	0.20	188	30
RIL	0.8	0.09	0.03	0.03	0.07	0.09	0.11	0.14	188	30
RIL	up	0.09	0.03	0.03	0.07	0.10	0.11	0.15	188	30
RIL	dn	0.07	0.02	0.02	0.05	0.07	0.08	0.10	188	30
RIL	v2	0.04	0.01	0.01	0.03	0.04	0.04	0.06	188	30
ILRP	0.2	0.36	0.14	0.05	0.27	0.35	0.46	0.71	188	30
ILRP	0.4	0.23	0.11	0.04	0.16	0.22	0.31	0.53	188	30
ILRP	0.6	0.16	0.08	0.03	0.11	0.15	0.21	0.37	188	30
ILRP	0.8	0.11	0.06	0.02	0.08	0.10	0.15	0.27	188	30
ILRP	up	0.07	0.02	0.02	0.06	0.07	0.08	0.12	188	30
ILRP	dn	0.00	0.01	-0.03	-0.00	0.00	0.01	0.03	188	30
ILRP	v2	0.00	0.01	-0.02	0.00	0.00	0.01	0.02	188	30

Table I.13: Summary Statistics. IIL, RIL, ILRP for ETH-BNB across Ranges. The table presents the summary statistics for the implied impermanent loss, IIL^{v3}, the realized impermanent loss RIL^{v3}, and the impermanent loss risk premium $ILRP^{v3}$, for the ETH–BNB pool at a 30-day maturity under different concentration parameters α $(0.2, 0.4, 0.6, 0.8$, the up, down, and v2 benchmark). The implied quantities are computed using the equations in Section 5.1.3. The realized quantities are computed using the equations in Section 5.2.1. The data are sampled daily over the period from April 2019 to December 2025.

I.3.5 BTC-USD

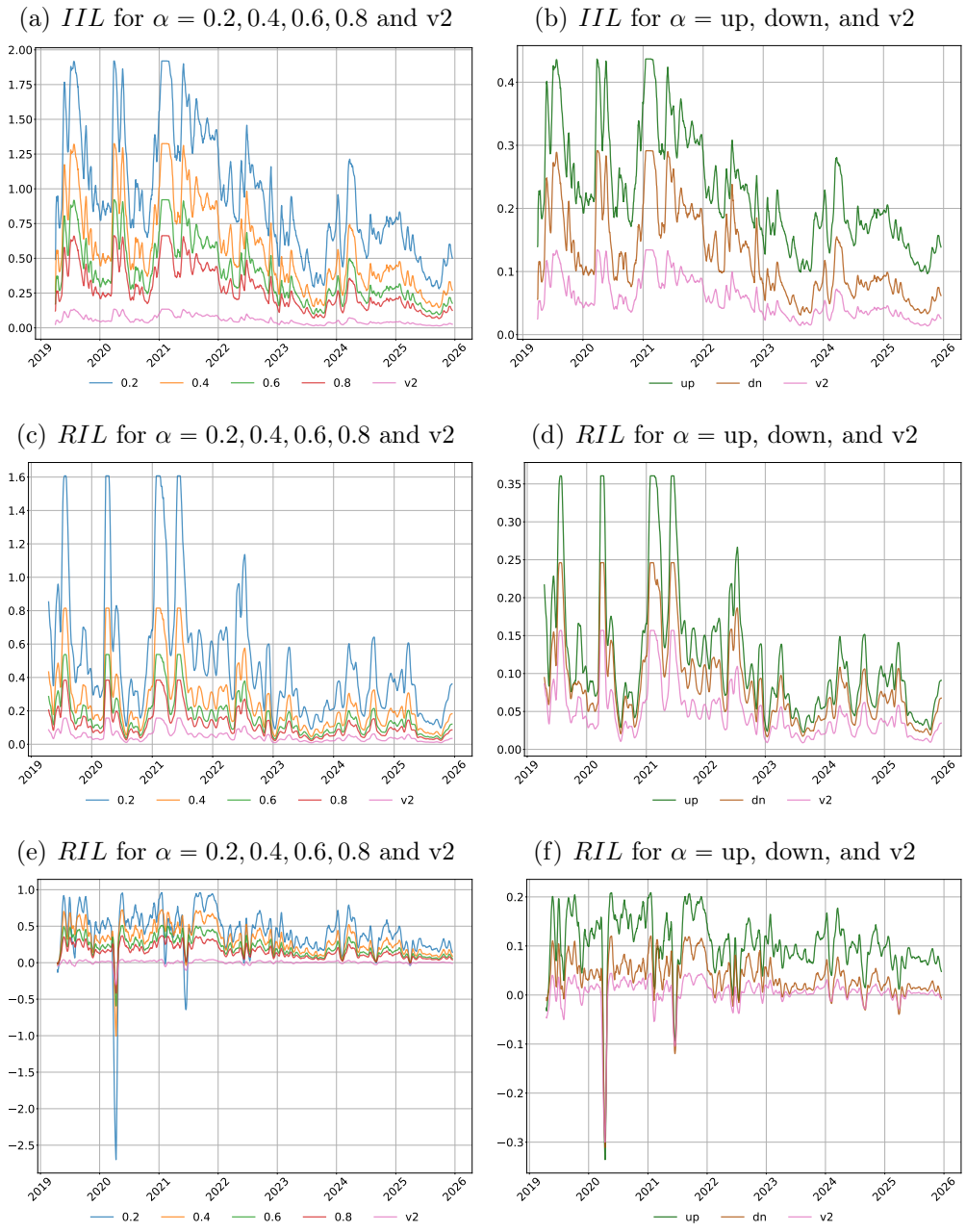

Figure I.15: IIL, RIL, ILRP for BTC-USD across Ranges. The figure reports (top row) the implied impermanent loss IIL^{v3}, (middle row) the realized impermanent loss RIL^{v3}, and (bottom row) the impermanent loss risk premium $ILRP^{v3}$ for the BTC-USD pool at a 30-day maturity. The left column shows $\alpha = 0.2, 0.4, 0.6, 0.8$ and the v2 benchmark, while the right column compares the up, down, and v2 ranges. The data are sampled daily over April 2019–December 2025 and smoothed using a 14-day rolling mean.

Series	α	Mean	Std	Q(0.001)	Q1	Median	Q3	Q(0.999)	N	Maturity
IIL	0.2	0.97	0.51	0.26	0.62	0.83	1.24	3.31	2434	30
IIL	0.4	0.60	0.38	0.13	0.34	0.49	0.78	2.57	2434	30
IIL	0.6	0.41	0.28	0.09	0.23	0.32	0.52	1.93	2434	30
IIL	0.8	0.29	0.20	0.06	0.16	0.23	0.37	1.42	2434	30
IIL	up	0.23	0.11	0.09	0.16	0.21	0.28	0.82	2434	30
IIL	dn	0.13	0.09	0.03	0.07	0.10	0.17	0.62	2434	30
IIL	v2	0.06	0.04	0.01	0.03	0.05	0.08	0.29	2434	30
RIL	0.2	0.55	0.58	0.07	0.25	0.39	0.63	4.58	2434	30
RIL	0.4	0.28	0.29	0.04	0.13	0.20	0.32	2.32	2434	30
RIL	0.6	0.18	0.19	0.02	0.08	0.13	0.21	1.53	2434	30
RIL	0.8	0.13	0.14	0.02	0.06	0.09	0.15	1.09	2434	30
RIL	up	0.13	0.11	0.02	0.06	0.10	0.15	0.76	2434	30
RIL	dn	0.09	0.08	0.01	0.04	0.07	0.11	0.62	2434	30
RIL	v2	0.05	0.06	0.01	0.02	0.04	0.06	0.44	2434	30
ILRP	0.2	0.42	0.40	-2.86	0.24	0.42	0.60	1.76	2434	30
ILRP	0.4	0.32	0.25	-1.13	0.17	0.28	0.44	1.67	2434	30
ILRP	0.6	0.22	0.18	-0.69	0.11	0.19	0.30	1.38	2434	30
ILRP	0.8	0.16	0.13	-0.49	0.08	0.13	0.21	1.01	2434	30
ILRP	up	0.11	0.07	-0.37	0.07	0.10	0.14	0.44	2434	30
ILRP	dn	0.04	0.05	-0.35	0.01	0.03	0.06	0.36	2434	30
ILRP	v2	0.01	0.04	-0.32	-0.00	0.01	0.02	0.14	2434	30

Table I.14: Summary Statistics. IIL, RIL, ILRP for BTC-USD across Ranges. The table presents the summary statistics for the implied impermanent loss, IIL^{v3}, the realized impermanent loss RIL^{v3}, and the impermanent loss risk premium $ILRP^{v3}$, for the BTC–USD pool at a 30-day maturity under different concentration parameters α $(0.2, 0.4, 0.6, 0.8$, the up, down, and v2 benchmark). The implied quantities are computed using the equations in Section 5.1.3. The realized quantities are computed using the equations in Section 5.2.1. The data are sampled daily over the period from April 2019 to December 2025.

I.3.6 ETH-USD

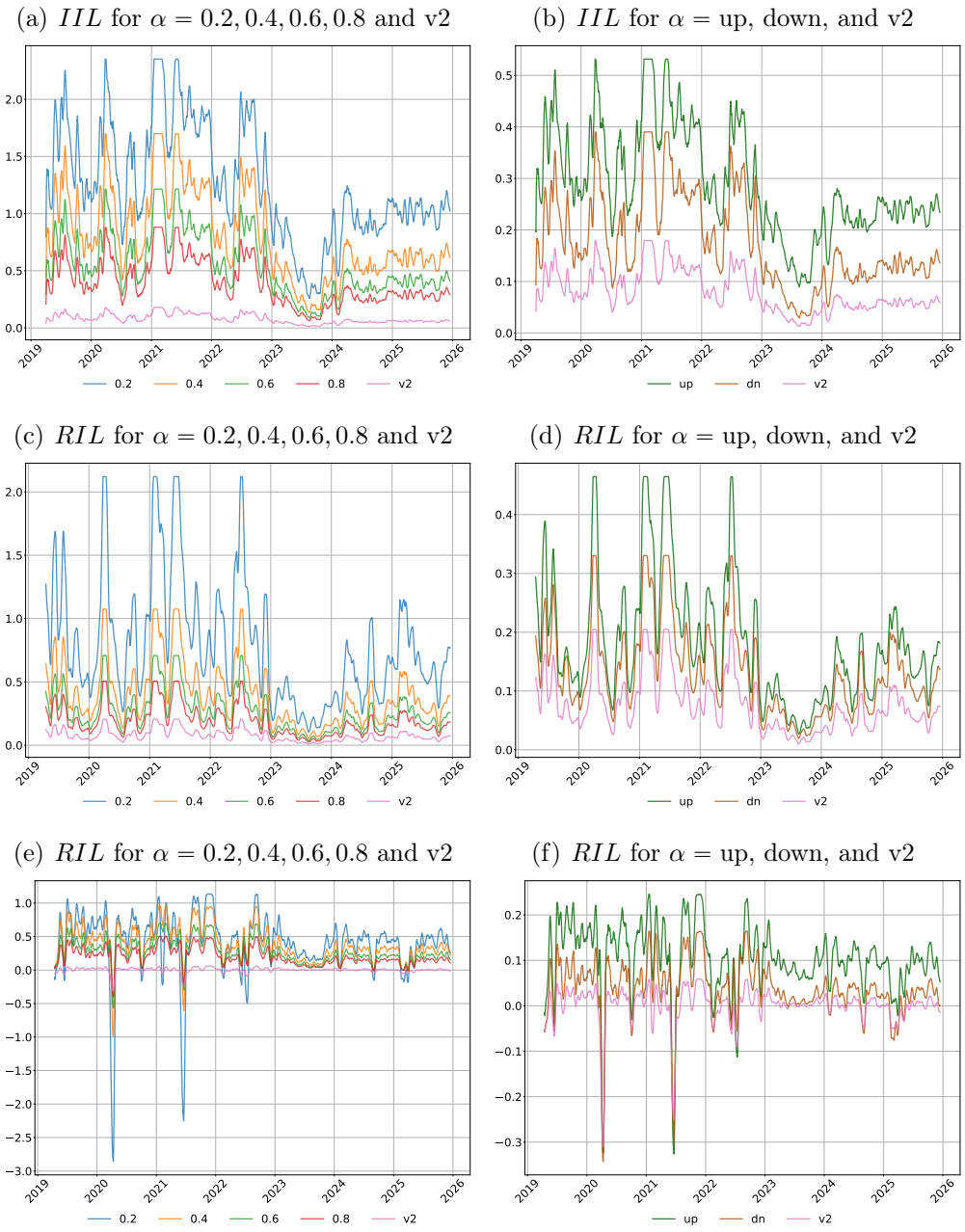

Figure I.16: IIL, RIL, ILRP for ETH-USD across Ranges. The figure reports (top row) the implied impermanent loss IIL^{v3}, (middle row) the realized impermanent loss RIL^{v3}, and (bottom row) the impermanent loss risk premium $ILRP^{v3}$ for the ETH-USD pool at a 30-day maturity. The left column shows $\alpha = 0.2, 0.4, 0.6, 0.8$ and the v2 benchmark, while the right column compares the up, down, and v2 ranges. The data are sampled daily over April 2019–December 2025 and smoothed using a 14-day rolling mean.

Series	α	Mean	Std	Q(0.001)	Q1	Median	Q3	Q(0.999)	N	Maturity
IIL	0.2	1.29	0.61	0.23	0.91	1.14	1.67	4.12	2434	30
IIL	0.4	0.84	0.49	0.12	0.53	0.69	1.10	3.40	2434	30
IIL	0.6	0.58	0.37	0.08	0.35	0.47	0.76	2.70	2434	30
IIL	0.8	0.42	0.27	0.05	0.25	0.33	0.54	2.03	2434	30
IIL	up	0.30	0.14	0.08	0.22	0.26	0.37	1.00	2434	30
IIL	dn	0.19	0.12	0.03	0.11	0.15	0.24	0.97	2434	30
IIL	v2	0.08	0.06	0.01	0.05	0.07	0.11	0.42	2434	30
RIL	0.2	0.87	0.79	0.07	0.42	0.65	1.01	5.13	2434	30
RIL	0.4	0.44	0.40	0.04	0.21	0.33	0.51	2.60	2434	30
RIL	0.6	0.29	0.26	0.02	0.14	0.22	0.34	1.71	2434	30
RIL	0.8	0.21	0.19	0.02	0.10	0.16	0.24	1.22	2434	30
RIL	up	0.19	0.14	0.02	0.10	0.16	0.23	0.88	2434	30
RIL	dn	0.14	0.12	0.01	0.07	0.12	0.17	0.76	2434	30
RIL	v2	0.08	0.07	0.01	0.04	0.06	0.10	0.48	2434	30
ILRP	0.2	0.42	0.53	-3.08	0.26	0.47	0.65	1.94	2434	30
ILRP	0.4	0.40	0.32	-1.20	0.23	0.35	0.54	2.04	2434	30
ILRP	0.6	0.29	0.24	-0.73	0.16	0.24	0.39	1.66	2434	30
ILRP	0.8	0.21	0.18	-0.51	0.11	0.17	0.28	1.25	2434	30
ILRP	up	0.11	0.09	-0.38	0.07	0.11	0.15	0.51	2434	30
ILRP	dn	0.04	0.08	-0.40	0.01	0.04	0.07	0.49	2434	30
ILRP	v2	0.00	0.05	-0.33	-0.01	0.01	0.02	0.18	2434	30

Table I.15: Summary Statistics. IIL, RIL, ILRP for ETH-USD across Ranges. The table presents the summary statistics for the implied impermanent loss, IIL^{v3}, the realized impermanent loss RIL^{v3}, and the impermanent loss risk premium $ILRP^{v3}$, for the ETH–USD pool at a 30-day maturity under different concentration parameters α $(0.2, 0.4, 0.6, 0.8$, the up, down, and v2 benchmark). The implied quantities are computed using the equations in Section 5.1.3. The realized quantities are computed using the equations in Section 5.2.1. The data are sampled daily over the period from April 2019 to December 2025.

I.3.7 SOL-USD

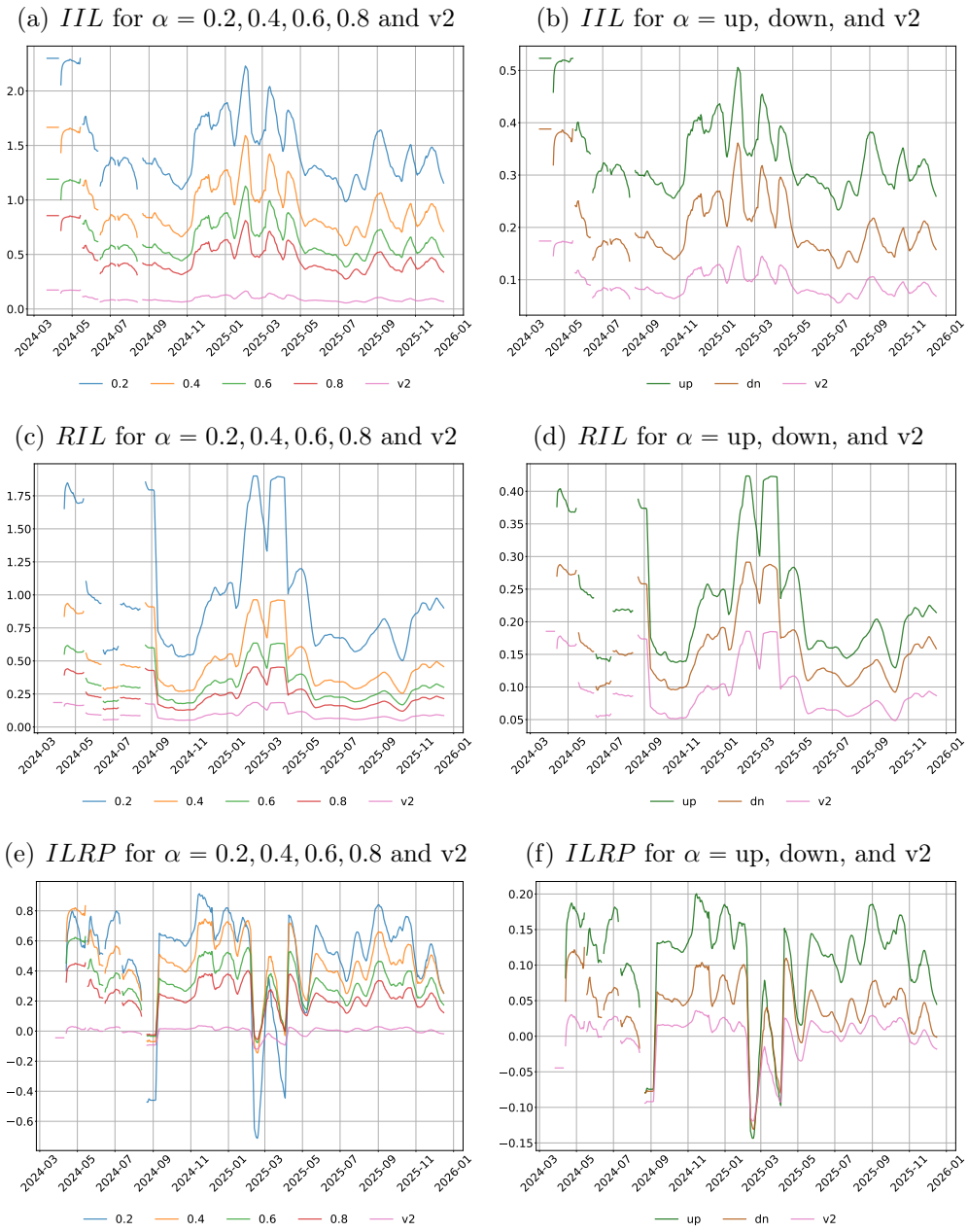

Figure I.17: IIL, RIL, ILRP for SOL-USD across Ranges. The figure reports (top row) the implied impermanent loss IIL^{v3}, (middle row) the realized impermanent loss RIL^{v3}, and (bottom row) the impermanent loss risk premium $ILRP^{v3}$ for the SOL-USD pool at a 30-day maturity. The left column shows $\alpha = 0.2, 0.4, 0.6, 0.8$ and the v2 benchmark, while the right column compares the up, down, and v2 ranges. The data are sampled daily over April 2019–December 2025 and smoothed using a 14-day rolling mean.

Series	α	Mean	Std	Q(0.001)	Q1	Median	Q3	Q(0.999)	N	Maturity
IIL	0.2	1.46	0.35	0.93	1.21	1.38	1.63	2.76	479	30
IIL	0.4	0.94	0.29	0.54	0.74	0.87	1.06	2.08	479	30
IIL	0.6	0.65	0.22	0.36	0.50	0.59	0.73	1.53	479	30
IIL	0.8	0.46	0.16	0.26	0.36	0.42	0.52	1.11	479	30
IIL	up	0.33	0.08	0.22	0.28	0.31	0.37	0.63	479	30
IIL	dn	0.20	0.07	0.11	0.16	0.18	0.23	0.51	479	30
IIL	v2	0.09	0.03	0.05	0.07	0.09	0.11	0.23	480	30
RIL	0.2	0.95	0.43	0.48	0.64	0.84	1.05	2.29	479	30
RIL	0.4	0.48	0.22	0.24	0.32	0.43	0.53	1.16	479	30
RIL	0.6	0.32	0.14	0.16	0.21	0.28	0.35	0.76	479	30
RIL	0.8	0.23	0.10	0.11	0.15	0.20	0.25	0.55	479	30
RIL	up	0.22	0.09	0.12	0.16	0.20	0.25	0.49	479	30
RIL	dn	0.16	0.06	0.09	0.11	0.15	0.18	0.35	479	30
RIL	v2	0.09	0.04	0.05	0.06	0.08	0.10	0.23	480	30
ILRP	0.2	0.51	0.34	-0.84	0.39	0.58	0.70	1.15	479	30
ILRP	0.4	0.46	0.23	-0.24	0.35	0.45	0.58	1.17	479	30
ILRP	0.6	0.33	0.17	-0.14	0.24	0.31	0.40	0.93	479	30
ILRP	0.8	0.24	0.12	-0.10	0.17	0.22	0.29	0.68	479	30
ILRP	up	0.11	0.07	-0.17	0.08	0.12	0.15	0.27	479	30
ILRP	dn	0.04	0.05	-0.16	0.02	0.05	0.06	0.22	479	30
ILRP	v2	0.00	0.03	-0.13	-0.01	0.01	0.02	0.06	480	30

Table I.16: Summary Statistics. IIL, RIL, ILRP for SOL-USD across Ranges. The table presents the summary statistics for the implied impermanent loss, IIL^{v3}, the realized impermanent loss RIL^{v3}, and the impermanent loss risk premium $ILRP^{v3}$, for the SOL–USD pool at a 30-day maturity under different concentration parameters α $(0.2, 0.4, 0.6, 0.8$, the up, down, and v2 benchmark). The implied quantities are computed using the equations in Section 5.1.3. The realized quantities are computed using the equations in Section 5.2.1. The data are sampled daily over the period from April 2019 to December 2025.

	(1) Range to Up	(2) Range to Up
IIL_t	-0.002***	
	(0.000)	
ILRP_t		-0.000*
		(0.000)
log(Price)	-0.000	-0.000
	(0.000)	(0.000)
log(TVL)	0.001***	0.001***
	(0.000)	(0.000)
log(Volume)	-0.000	-0.000
	(0.000)	(0.000)
Observations	464709	464709
R^2 (within)	0.001	0.000
Entity FE	Yes	Yes
Year FE	Yes	Yes
SE	Clustered (entity)	Clustered (entity)

Table I.17: Range-to-Up transitions, IIL and $ILRP$. The table reports panel regressions of the one-period-ahead transition indicator $RangeToUp$ on IIL (Column 1) and $ILRP$ (Column 2). $RangeToUpi, t+1$ equals one when an LP's position moves from *Range* at t to *Up* at $t+1$. All specifications include pool–LP and year fixed effects, control variables, and standard errors clustered at the pool–LP level.

	(1) Range to Dn	(2) Range to Dn
IIL_t	0.000	
	(0.000)	
ILRP_t		0.000
		(0.000)
log(Price)	-0.000	-0.000
	(0.000)	(0.000)
log(TVL)	-0.000	-0.000
	(0.000)	(0.000)
log(Volume)	-0.000	-0.000
	(0.000)	(0.000)
Observations	464709	464709
R^2 (within)	0.000	0.000
Entity FE	Yes	Yes
Year FE	Yes	Yes
SE	Clustered (entity)	Clustered (entity)

Table I.18: Range-to-Down transitions, IIL and $ILRP$. The table reports panel regressions of the one-period-ahead transition indicator *RangeToDown* on IIL (Column 1) and $ILRP$ (Column 2). $RangeToDowni, t+1$ equals one when an LP's position moves from *Range* at t to *Down* at $t+1$. All specifications include pool–LP and year fixed effects, control variables, and standard errors clustered at the pool–LP level.

	(1) Switch	(2) Switch	(3) Switch widened	(4) Switch widened
IIL_t	0.020***		0.030***	
	(0.001)		(0.001)	
ILRP_t		-0.001***		-0.001***
		(0.000)		(0.000)
log(Price)	-0.001***	-0.001***	-0.001***	-0.000***
	(0.000)	(0.000)	(0.000)	(0.000)
log(TVL)	0.004***	0.004***	0.003***	0.002***
	(0.001)	(0.001)	(0.001)	(0.001)
log(Volume)	-0.001	0.000	-0.001*	0.001
	(0.001)	(0.001)	(0.000)	(0.000)
Observations	456844	456844	456844	456844
R^2 (within)	0.001	0.000	0.003	0.000
Entity FE	Yes	Yes	Yes	Yes
Year FE	Yes	Yes	Yes	Yes
SE	Clustered (entity)	Clustered (entity)	Clustered (entity)	Clustered (entity)

Table I.19: The table reports panel regressions of forward-looking liquidity provider (LP) behavior on IIL and the $ILRP$. Columns (1)–(2) use an indicator for whether an LP switches its price range in the next period, while Columns (3)–(4) use an indicator for whether, conditional on switching, the LP widens its price range. All specifications include pool–LP and time fixed effects, control variables, and standard errors clustered at the pool–LP level.